Diacylated SH4 domain proteins: studies on their lipid and protein environment at the plasma membrane and intracellular transport

DISSERTATION

submitted to the
Combined Faculties for the Natural Sciences and for Mathematics
of the Ruperto-Carola University of Heidelberg, Germany
for the degree of Doctor of Natural Sciences

Paulina Turcza

2013

DISSERTATION

submitted to the

Combined Faculties for the Natural Sciences and for Mathematics

of the Ruperto-Carola University of Heidelberg, Germany

for the degree of Doctor of Natural Sciences

presented by

Master of Science in Biotechnology

Paulina Turcza

born in Kraków, Poland

oral examination:

Diacylated SH4 domain proteins: studies on their lipid and protein environment at the plasma membrane and intracellular transport

Referees:

Prof. Dr. Walter Nickel

Prof. Dr. Thomas Söllner

Summary

Several members of the Src family of non-receptor protein tyrosine kinases (e.g. Yes), as well as *Leishmania* hydrophilic acylated surface protein B (HASPB) harbor a short N-terminal motif called the Src homology 4 (SH4) domain, which undergoes tandem modification with the saturated acyl chains myristate and palmitate. SH4 domains are responsible for stable anchoring of these otherwise soluble proteins to the cytoplasmic leaflet of cellular membranes, mediate their targeting to the plasma membrane, and moreover, confer affinity for cholesterol- and sphingolipid-enriched membrane microdomains, that is lipid rafts. N-terminal myristoylation occurs in the cytosol, concurrently with translation of the protein, and is a prerequisite for subsequent palmitoylation. The latter is thought to occur at perinuclear (most probably Golgi) membranes. It has been hypothesized that doubly acylated SH4 domain proteins partition into lipid rafts soon after being palmitoylated at the Golgi, and that these microdomains are necessary for the transport of SH4 proteins to the plasma membrane, by playing a role in their sorting and/or formation of transport carriers at the *trans*-Golgi network.

The aim of the first part of this study was to characterize membrane (both lipid and protein) environment of diacylated SH4 domain proteins residing in lipid rafts. The approach was to analyze lipid and protein components of immunoaffinity-purified detergent-resistant membranes (DRMs) containing SH4 domain reporter fusion proteins. DRMs immunoisolated using a HASPB SH4 domain fusion protein as bait differed in lipid composition from the total DRM pool, being enriched in sphingomyelin, and depleted in phosphatidylcholine and phosphatidylethanolamine, and therefore seem to be a subset of total DRMs. This may suggest that *in vivo*, the protein associates with a specific subset of lipid rafts, thus indicating that the heterogeneity of lipid rafts can be appreciated also using the detergent method. Our immunoaffinity purification approach seemed to enrich for *bona fide* raft proteins, as suggested by an increase compared to total DRMs in the proportion of plasma membrane and lipid-anchored proteins, as well as proteins whose association with DRMs is sensitive to cholesterol depletion. We estimated relative amounts of proteins in immunoisolated SH4 DRMs and total DRMs, with the use

of label-free mass spectrometry-based quantification, which was validated for a subset of proteins by quantitative Western blotting. We could observe a lack of enrichment of endogenous Yes kinase in immunoisolated SH4 DRMs, which may indicate that the identity of lipid rafts into which SH4 domain proteins partition, is determined not only by the dual fatty acylation with myristate and palmitate, but also by interactions conferred by domains distal from the SH4 domain.

In the second part of this study, we intended to investigate the previously reported role of the COPI coatomer complex, as well as of the secretory pathway in general, in the plasma membrane transport of diacylated SH4 domain proteins. Conditions that disrupted the structure and function of the Golgi apparatus, i.e. siRNA-mediated knockdown of the β subunit of the COPI complex, expression of constitutively active mutant (Q71L) of the small GTPase Arf1, as well as brefeldin A treatment, resulted in increased intracellular accumulation of a HASPB SH4 fluorescent fusion protein, pointing out to the role of the Golgi in its transport to the plasma membrane. None of the above treatments, however, blocked the appearance of the SH4 reporter protein at the plasma membrane, suggesting the existence of an alternative trafficking pathway that does not require the Golgi complex.

Zusammenfassung

Mehrere Mitglieder der Src-Familie der Nicht-Rezeptor-Tyrosinkinasen (z.B. Yes), wie auch das hydrophile acylierte Oberflächenprotein B (HASPB) von *Leishmania* besitzen ein kurzes aminoterminales Motiv, die Src-Homologiedomäne 4 (SH4), die mit den beiden gesättigten Acylketten Myristinsäure und Palmitinsäure modifiziert ist. SH4-Domänen sind für die stabile Verankerung dieser ansonsten löslichen Proteine in der zytoplasmatischen Lipidschicht zellulärer Membranen verantwortlich, bewirken den gerichteten Transport zur Plasmamembran und vermitteln Affinität zu mit Cholesterin und Sphingolipid angereicherten Membranmikrodomänen, den sogenannten „lipid rafts“. Aminoterminale Myristoylierung geschieht während der Translation im Zytosol und ist Voraussetzung für die nachfolgende Palmitoylierung an perinukleären Membranen (wahrscheinlich am Golgi-Apparat). Vermutlich segregieren diacylierte SH4-Domäne-Proteine sofort nach der Palmitoylierung noch am Golgi in „lipid rafts“. Diese Mikrodomänen sind wahrscheinlich für den Transport der SH4-Proteine zur Plasmamembran verantwortlich, wobei sie eine Rolle beim Sortieren und/oder der Bildung von Transportmodulen am *trans*-Golgi-Netzwerk spielen.

Das Ziel des ersten Teils dieser Arbeit war die Charakterisierung der Membranumgebung (Lipide und Proteine) von in „lipid rafts“ residierenden diacylierten SH4-Domäne-Proteinen. Der experimentelle Ansatz bestand in der Analyse von Lipid- und Proteinkomponenten immunaffinitätsgereinigter detergensresistenter Membranen (DRMs), welche SH4-Domäne-Reporter-Fusionsproteine enthalten. Die mittels des HASPB SH4-Fusionsproteins immunaffinitätsgereinigten DRMs unterschieden sich hinsichtlich ihrer Lipidzusammensetzung von der DRM-Ausgangszusammensetzung dahingehend, dass sie Sphingomyelin-angereichert und Phosphatidylcholin- sowie Phosphatidylethanolamin-abgereichert waren. Dies deutet darauf hin, dass das Protein *in vivo* mit einer spezifischen „lipid raft“ Subpopulation assoziiert ist, was wiederum darauf schließen lässt, dass die Heterogenität von „lipid rafts“ mit der Detergens-Methode abgebildet werden kann. Unser Immunaffinitätsreinigungsansatz führt offensichtlich zur Anreicherung von *bona fide* Raft-Proteinen, da im Vergleich zu gesamt-DRMs der Anteil von Plasmamembran- und Lipidanker-Proteinen anstieg, wie

auch von Proteinen deren Assoziierung mit DRMs gegen Cholesterin-Abreicherung empfindlich ist. Wir bestimmten die relativen Proteinmengen in gesamt-DRMs und in immungereinigten SH4-DRMs mittels markierungsfreier Massenspektrometrie-basierter Quantifizierung. Diese Ergebnisse wurden für eine Reihe ausgewählter Proteine mittels quantitativem Western Blot validiert. Wir sahen allerdings keine Anreicherung endogener Yes Kinase in immungereinigten SH4-DRMs. Das mag daran liegen, dass die Identität von „lipid rafts“, in welche die SH4-Domäne-Proteine segregieren, nicht nur durch die duale Fettsäureacylierung mit Myristat und Palmitat bestimmt wird, sondern auch durch Interaktionen, welche von Domänen distal von den SH4-Domänen vermittelt werden.

Im zweiten Teil dieser Arbeit wollten wir die Rolle des COPI-Coatomer-Komplexes, sowie des sekretorischen Weges im Allgemeinen beim Plasmamembrantransport diacylierter SH4-Domäne-Proteine studieren. Bedingungen die zur Zerstörung von Struktur und Funktion des Golgi-Apparates führten, d. h. siRNA-vermitteltes Knockdown der β-Untereinheit des COPI-Komplexes oder Expression der konstitutiv aktiven (Q71L) Mutante der kleinen GTPase Arf1, wie auch die Behandlung mit brefeldin A, führten zur intrazellulären Anhäufung des fluoreszierenden HASPB SH4-Fusionsproteins, was auf eine Rolle des Golgi-Apparates beim Transport zur Plasmamembran hinweist. Allerdings konnte mit keiner dieser Behandlungen das Auftauchen des SH4-Reporterproteins an der Plasmamembran blockiert werden, was auf alternative, Golgi-Komplex-unabhängige Transportwege hindeutet.

1 Introduction

1.1 The secretory pathway

All eukaryotic cells use the secretory pathway for synthesizing and sorting proteins destined for secretion or membrane insertion. In mammalian cells, most of the proteins are targeted to the endoplasmic reticulum (ER) cotranslationally (Jungnickel *et al.,* 1994). During synthesis of a secretory protein on free ribosomes in the cytosol, an N-terminal 7- to 20-residue hydrophobic ER signal sequence (Schatz *et al.*, 1996), as soon as it emerges from the ribosome, is recognized by the signal recognition particle (SRP). SRP is a complex of six proteins and an RNA, which binds not only to the ER signal sequence, but also to the ribosome, leading to arrest of polypeptide chain elongation (Walter *et al.*, 1994; Halic *et al*., 2005). SRP targets the ribosome/nascent chain complex to the ER membrane by interaction with the SRP receptor (SR), a heterodimer formed by an SRα, and a smaller SRβ subunit. Formation of the SRP/SR complex requires GTP binding to both SRP and SR (Rapiejko *et al.*, 1992; Miller *et al.*, 1993). The ribosome/nascent chain complex is then transferred to the translocon (the Sec61 complex), a protein-conducting channel within the ER membrane (Johnson *et al.,* 1999). The SRP/SR complex dissociates from the ribosome and upon GTP hydrolysis, SRP is released from the SR to the cytosol (Connolly *et al.,* 1991). Translation elongation resumes, and the nascent chain passes through the central pore of the translocon into the ER lumen, where the signal sequence is cleaved by a transmembrane signal peptidase (Dalbey *et al.*, 1992). Afterwards, the polypeptide is released into the ER lumen (in the case of secreted proteins, and soluble luminal proteins of the ER, Golgi or lysosome) or transferred into the ER membrane (membrane proteins of the ER, Golgi, lysosome or the plasma membrane). In the ER, formation and rearrangement of disulfide bonds, folding of polypeptide chains and assembly of multimers take place (Zapun *et al.*, 1999; Sevier *et al.*, 2002). Moreover, here occurs the attachment and initial processing of N-linked glycans (Kornfeld *et al.*, 1985). Export of newly synthesized proteins from the ER is mediated by COPII vesicles (Lee *et al.*, 2004; Hughes *et al.*, 2008). In mammalian cells, COPII vesicles fuse with each other, generating the vesicular-tubular clusters (VTCs), also known as the ER-Golgi intermediate compartment (ERGIC). ERGIC is

subsequently delivered in a microtubule-dependent manner to the *cis*-side of the Golgi apparatus (Klumperman, 2000; Duden, 2003). Retrograde transport from the *cis*-Golgi/ERGIC back to the ER is mediated by COPI vesicles (Barlowe, 2000; Lee *et al.*, 2004).

Formation of coated vesicles is initiated through activation of small GTP-binding proteins, Sar1 for COPII and ADP-ribosylation factor 1 (Arf1) for COPI vesicles (Barlowe, 2000; Lee *et al.*, 2004). Both proteins cycle between inactive GDP-bound cytosolic and active GTP-bound membrane-associated forms. The exchange of bound GDP for GTP is catalyzed by guanine nucleotide exchange factors (GEFs). Upon exchange of bound GDP for GTP, catalyzed by an ER membrane GEF Sec12, Sar1 exposes an N-terminal amphipathic α-helix, which inserts into the lipid bilayer (Bielli *et al.*, 2005). Membrane-associated Sar1 recruits the Sec23/Sec24 heterodimeric coat complex. Sec24 interacts with transmembrane cargo proteins carrying di-acidic or di-hydrophobic/di-aromatic sorting signals in their cytoplasmic domains (Barlowe, 2003). Subsequently, the heterotetrameric Sec13/Sec31 coat complex is recruited, which is responsible for coat polymerization and membrane deformation, yielding a COPII vesicle (Lee *et al.*, 2004; Hughes *et al.*, 2008). Upon budding, Sec23 acts as the GTPase-activating protein (GAP) for Sar1, stimulating Sar1-mediated GTP hydrolysis, which results in uncoating of vesicles (Duden, 2003). COPI coat formation is initiated by the exchange of bound GDP for GTP on Arf1, catalyzed by an Arf GEF. GBF1 is the GEF involved in COPI vesicle biogenesis at the *cis*-Golgi/ERGIC (Zhao *et al.*, 2002). GTP binding by Arf1 exposes its myristoylated N-terminal amphipathic α-helix that provides stable membrane anchorage (Antonny *et al.*, 1997). Membrane-associated Arf1 recruits the heptameric COPI coatomer complex, composed of α, β, β', γ, δ, ε and ζ subunits (Palmer *et al*., 1993). This recruitment seems to be assisted by members of the p24 family membrane proteins, which bind directly to coatomer, stimulating vesicle formation (Bremser *et al.*, 1999). Uptake of cargo membrane proteins into COPI vesicles involves a direct interaction of di-lysine or arginine-based sorting signals on their cytoplasmic domains with subunits of the COPI coat, whereas soluble ER-resident proteins contain a C-terminal KDEL sequence, recognized by transmembrane adaptors, KDEL receptors, which in turn harbor a di-lysine motif (Beck *et al.*, 2009; Popoff *et al.*,

2011). Recruitment of cargo by COPI vesicles was proposed to be regulated by a cycle of GTP exchange on Arf1 and Arf1-mediated GTP hydrolysis stimulated by Arf GTPase-activating proteins, Arf GAPs (Malsam *et al.*, 1999; Pepperkok *et al.,* 2000). Fusion of COPI vesicles with the target compartment requires uncoating, which also depends on GTP hydrolysis by Arf1 (Tanigawa *et al.*, 1993).

Delivery of secretory proteins to the *cis*-side of the Golgi apparatus is followed by their passage across the Golgi stack of cisternae, which contains enzymes involved in sequential processing of oligosaccharide chains on glycoproteins, and in proteolytic cleavage (Mellman *et al.*, 2000). The favored model of anterograde intra-Golgi transport is the cisternal maturation and progression (Glick *et al.*, 1998). It assumes that new cisternae form at the *cis*-Golgi, progress through the stack carrying anterograde cargo, and disassemble at the *trans*-Golgi. The cisternae would mature by retrograde transport of Golgi-resident proteins mediated by COPI vesicles. However, current evidence suggests that COPI vesicles may mediate also anterograde cargo transport between Golgi cisternae (Orci *et al.*, 1997). Proteins are exported from the *trans*-Golgi network (TGN), a tubular network that emanates from the last two *trans*-Golgi cisternae (De Matteis *et al.*, 2008). The TGN is the main sorting hub in the secretory pathway (Griffiths *et al.*, 1986) that segregates cargo molecules into distinct pleomorphic tubular-vesicular carriers targeted to different compartments: the plasma membrane (apical or basolateral in polarized cells), or the endolysosomal compartment. In addition, the TGN receives traffic from the endosomal system (De Matteis *et al.*, 2008). The first step in the formation of pleomorphic carriers is segregation of cargo molecules into distinct tubular TGN export domains, which is followed by their elongation along microtubules with the help of microtubule motors kinesins. The subsequent fission of the tubules is facilitated by the pulling force exerted by kinesins. Other proteins known to be involved in fission are dynamin-2, protein kinase D (PKD), and brefeldin A-ribosylated substrate (BARS) (De Matteis *et al.*, 2008; Anitei *et al.,* 2011). Apical sorting relies on the presence of N- or O-linked glycans, special properties of the transmembrane domain, or on the presence of the glycosyl-phosphatidylinositol (GPI) anchor, together with the ability of the protein to oligomerize (Schuck *et al.*, 2004; Fölsch, 2008). The apical sorting signals act mainly by promoting the incorporation into clustered lipid rafts (Schuck *et al.*, 2004; Schuck *et al.*,

2006; see also sections 1.3.4 and 1.4.1). Until now there has been no evidence for an involvement of coat proteins in apical transport (Anitei *et al.*, 2011). Basolateral and endosomal sorting depends on tyrosine-based or di-leucine-based motifs in the cytoplasmic domains of transmembrane cargo proteins, which are recognized by heterotetrameric adaptor protein complexes (APs) or by monomeric Golgi-localized, γ-ear-containing, Arf-binding proteins (GGAs), which (in most cases) bind clathrin, thus acting as adaptors for clathrin coats (De Matteis *et al.*, 2008; Anitei *et al.,* 2011). Recruitment of both APs and GGAs is promoted by Arf1-GTP (De Matteis *et al.*, 2008; Donaldson *et al.*, 2011). In epithelial cells, transport of basolateral cargo to the plasma membrane is mediated by AP-1B/clathrin (operating only at the recycling endosomes) and AP-4 coats, most probably supporting an indirect (via recycling endosomes) and a direct route to the basolateral plasma membrane, respectively. Sorting to the endosomal system is mediated by AP-1A, AP-3 or GGA, which interact with clathrin (De Matteis *et al.*, 2008; Anitei *et al.,* 2011). It is worth noting that apical and basolateral signals operate also in non-polarized cells, giving rise to different transport routes to the plasma membrane (Müsch *et al.*, 1996).

1.2 Cellular membranes

Eukaryotic cells are separated from the external environment by the plasma membrane and partitioned into membrane-bounded structures (organelles), which compartmentalize metabolic functions. Physical properties of membranes are largely determined by their lipid components, while the proteins are responsible for the unique functions of a particular membrane. All biomembranes have a bilayer structure (Robertson, 1981), with polar head groups facing outward and hydrophobic tails forming a hydrophobic core, which is impermeable to hydrophilic solutes. The Singer-Nicolson fluid-mosaic model of the structure of biological membranes postulated a uniform fluid lipid matrix with randomly distributed proteins (Singer *et al.*, 1972). This model has been revised to consider lateral heterogeneity of lipids and proteins in the membrane resulting from preferential packing of sphingolipids and cholesterol into lipid rafts (Simons *et al.*, 1997; see also section 1.3).

Membrane proteins can be classified as transmembrane, lipid-anchored or peripheral. Transmembrane proteins possess membrane-spanning domains, which consist of one or more α-helices or of multiple β-strands. Lipid-anchored proteins are attached to one leaflet of the bilayer via covalently-bound lipid molecules (Levental *et al.,* 2010a; see also section 1.4). And finally, peripheral proteins associate with membranes by noncovalent interactions with other membrane proteins or with the head groups of membrane lipids.

Biological membranes are composed of three major classes of lipids: glycerophospholipids, sphingolipids and sterols (Holthuis *et al.*, 2005). Glycerophospholipids are based on glycerol 3-phosphate, with two fatty acid chains esterified to its two hydroxyl groups, and a polar head group esterified to the phosphate group. The fatty acid chains commonly contain 16 or 18 carbons, and 0, 1 or 2 c*is*-double bonds. The head group can be either neutral (yielding phosphatidylserine (PS) or phosphatidylinositol (PI), and giving a net negative charge) or basic (forming phosphatidylcholine (PC) or phosphatidylethanolamine (PE), which carry no net charge). Sphingolipids are derivatives of a C18-C20 amino alcohol (C18 sphingosine in animals), containing a C16-C26 saturated fatty acid attached to the amine group through an amide bond (which forms ceramide (Cer)). In animals, the sphingolipid head group attached to the terminal hydroxyl group of sphingosine can be phosphocholine (yielding sphingomyelin (SM)), or in the case of glycosphingolipids, glucose or galactose (yielding glucosylceramide (GlcCer) and galactosylceramide (GalCer), respectively), to which further monosaccharides can be attached. Sterols (cholesterol in animals) contain a planar four-ring carbon structure, with a hydroxyl group on one ring (Holthuis *et al.*, 2005). Synthesis of major glycerophospholipids (PC, PE, PS and PI) takes place on the cytosolic face of the ER membrane (Sprong *et al.*, 2001; Blom *et al.*, 2011). Ceramide, the common precursor of mammalian sphingolipids, is synthesized on the cytosolic face of the ER (Blom *et al.*, 2011), and then converted into SM on the luminal (exoplasmic) face of the *trans*-Golgi, or to GlcCer on the cytosolic face of the *cis*-Golgi. GlcCer is then translocated to the exoplasmic leaflet to be converted into complex glycosphingolipids in the lumen of distal Golgi compartments (De Matteis *et al.*, 2008; Blom *et al.*, 2011). The main site of cholesterol synthesis is the ER (Blom *et al.*, 2011).

The ER membrane is composed mainly of glycerophospholipids. For example, the ER membrane of rat liver contains 50-60 mol% PC, 25 mol% PE, 10 mol% PI, and 5 mol% cholesterol (Holthuis *et al.*, 2005). The transbilayer lipid distribution in the ER membrane is nearly symmetric, as a result of equilibration of newly synthesized glycerophospholipids between leaflets, catalyzed by scramblase, an energy-independent transporter (Daleke, 2003). The lipid composition changes gradually along the secretory pathway to that of the plasma membrane, with cholesterol and sphingolipids being gradually enriched (Holthuis *et al.*, 2005). For example, the plasma membrane of rat liver contains 30-40 mol% cholesterol, 25 mol% PC, 15 mol% PE, 10-15 mol% sphingolipids, 5 mol% PS, and 5 mol% PI (Holthuis *et al.*, 2005). In addition, the distribution of lipids in the plasma membrane is highly asymmetric: PC, SM and glycosphingolipids are enriched primarily in the exoplasmic leaflet, whereas PE, PS and PI are preferentially located in the cytoplasmic leaflet (Sprong *et al.*, 2001; Daleke, 2003). Minor phospholipids, such as phosphatidic acid (PA), phosphatidylinositol-4-monophosphate (PIP) and phosphatidylinositol-4,5-bisphosphate (PIP_2) are enriched also in the cytoplasmic leaflet of the plasma membrane. The transbilayer distribution of cholesterol is not known (Sprong *et al.*, 2001; Daleke, 2003). The asymmetric distribution of PS and PE is maintained by an aminophospholipid flippase, which translocates these lipids from the outer to the inner leaflet of the plasma membrane in an ATP-dependent manner (Daleke, 2003). During platelet activation and apoptosis, the distribution of plasma membrane phospholipids is randomized by a nonspecific Ca^{2+}-activated scramblase, resulting in the exposure of PS at the exoplasmic leaflet, which activates enzymes participating in blood clotting and functions as a signal for phagocytosis of apoptotic cells by macrophages (Daleke, 2003).

1.3 Lipid rafts

1.3.1 The concept of lipid rafts

The lipid raft concept was introduced to explain the preferential apical delivery of newly synthesized glycosphingolipids in epithelial Madin-Darby canine kidney (MDCK) cells (Simons *et al.,* 1988). It was proposed that glycosphingolipids form clusters in the exoplasmic leaflet of the *trans*-Golgi network, which is followed by inclusion of newly

synthesized apical proteins, and transport of both in common carrier vesicles to the apical surface. Over the years, the proposed roles for lipid rafts were expanded to include the involvement in various aspects of intracellular trafficking of lipids and proteins, cell signaling, immune response and the entry of viruses and toxins (Simons *et al.*, 1997; Simons *et al.*, 2010). A recently adopted definition of lipid rafts describes them as: 'small (10-200 nm), heterogeneous, highly dynamic, sterol- and sphingolipid-enriched domains that compartmentalize cellular processes; small rafts can sometimes be stabilized to form larger platforms through protein-protein and protein-lipid interactions' (Pike, 2006).

1.3.2 Detergent insolubility

It has long been known that some membrane components, such as glycosyl-phosphatidylinositol (GPI)-anchored proteins (Vitetta *et al.,* 1973; Hooper *et al.*, 1988), as well as sphingomyelin and glycosphingolipids (Yu *et al.*, 1973; Hagmann *et al.,* 1982), are not solubilized by nonionic detergents, for example Triton X-100. Later, a GPI-anchored protein, placental alkaline phosphatase (PLAP), was found to become insoluble in Triton X-100 in the Golgi complex during its biosynthetic transport to the apical surface of MDCK cells (Brown *et al.*, 1992). The insoluble fraction that contained PLAP floated to low density during centrifugation on sucrose density gradients, and was enriched in cholesterol and sphingolipids, leading to the concept of detergent-insoluble, cholesterol- and sphingolipid-rich membrane domains (rafts).

In model membranes containing high fractions of cholesterol, the cholesterol-poor liquid-disordered (l_d) phase can coexist with the cholesterol-dependent liquid-ordered (l_o) phase (Ipsen *et al.*, 1987; Ahmed *et al.*, 1997). Lipid acyl chains in the former phase are kinked and loosely packed, whereas in the latter, tightly packed and highly extended. In both phases the lipid molecules exhibit high degree of lateral diffusion (Simons *et al.,* 2004). Model membranes in the l_o state were shown to be completely detergent insoluble (Schroeder *et al.*, 1994). Furthermore, the detergent insolubility of cholesterol-containing model membranes correlated well with the amount of the l_o phase, as detected by fluorescence quenching (Ahmed *et al.*, 1997). Consequently, the detergent

insolubility of the cholesterol- and sphingolipid-rich membrane domains was attributed to their existence in the l_o state (London *et al.,* 2000).

Isolation of detergent-resistant membranes (DRMs) became the most widely used method for the identification of lipid raft components, its usefulness being confirmed by the fact that most proteins that have a substantial fraction in DRMs associate with rafts also when analyzed by other methods (Simons *et al.,* 2004). Extraction of cells or isolated membranes with nonionic detergent on ice is followed by equilibrium density gradient centrifugation, usually in sucrose or OptiPrep gradients, during which DRMs, due to high lipid/protein ratio, float to low density (Brown *et al.*, 1992; Schuck *et al.*, 2003). A comprehensive proteomic analysis of DRMs isolated from HeLa cells was performed by Mann and co-workers (Foster *et al.,* 2003). Here, the isolation of Triton X-100 DRMs was combined with treatment with the cholesterol-extracting drug, methyl-β-cyclodextrin (MβCD), and a SILAC (stable isotope labeling with amino acids in cell culture)-based quantitative proteomic approach. As a result, 154 proteins were identified whose presence in DRM fractions was highly sensitive to cholesterol depletion by MβCD, and termed as 'raft proteins'. Moreover, 92 proteins exhibited medium sensitivity to MβCD, and were referred to as 'raft-associated proteins'. There was also a group of proteins whose presence in DRMs was not drastically affected by cholesterol depletion, denoted as nonspecific (i.e. non-raft) proteins.

1.3.3 Phase separation in model and plasma membranes

Model monolayers and bilayers mimicking the composition of the outer leaflet of the plasma membrane can phase separate into microscopically observable l_o and l_d domains (Dietrich *et al.,* 2001a; Dietrich *et al.,* 2001b). Sphingomyelin preferably partitions with cholesterol into l_o phase domains, segregating from phosphatidylcholine, the main component of l_d phase domains (Simons *et al.,* 2004). Recent studies showed that microscopic phase separation into two liquid domains can be induced also in membranes containing native lipids and proteins. Plasma membrane blebs produced by cells upon treatment with N-ethylmaleimide or with formaldehyde and DTT, so-called giant plasma membrane vesicles (GPMVs), were induced to phase separate into l_o-like and l_d-like phases, when cooled below room temperature (Baumgart *et al.*, 2007).

Similarly, plasma membrane spheres (PMS) produced using a cell-swelling procedure, separated into large-scale domains at 37°C, upon crosslinking of the raft ganglioside GM1 with pentavalent cholera toxin B subunit (Lingwood *et al.,* 2008). Those results suggest that plasma membranes exhibit liquid-liquid immiscibility, and thus coexistence of domains in different (l_o and l_d) phase states. The nanoscale l_o domains (rafts) can be induced to coalesce into large-scale domains. Such domains, formed as a result of incubation of live cells with primary antibodies against PLAP (which is embedded via its GPI-anchor in the outer leaflet of the plasma membrane), followed by crosslinking with secondary antibodies, were shown to accumulate the Src family kinase Fyn, which is attached via its acylations to the inner leaflet (Harder *et al.*, 1998). This indicates that rafts exist in both the outer and the inner leaflet of the plasma membrane, with a transbilayer coupling between them. This coupling between the leaflets was proposed to be mediated by transmembrane raft proteins or by the interdigitation of long fatty acid chains of sphingolipids with the cytoplasmic leaflet of the bilayer (Simons *et al.,* 1997; Simons *et al.,* 2004). The preferential packing of sphingomyelin and cholesterol can explain only the formation of l_o phase domains in the outer leaflet of the bilayer, as sphingolipids are almost absent from the inner leaflet of cellular membranes. Studies using asymmetric planar bilayers demonstrate, however, that the formation of l_o phase domains in a phosphatidylethanolamine and phosphatidylserine-containing leaflet can be induced by l_o phase domains in the opposite leaflet (Kiessling *et al.,* 2006), suggesting that lipid rafts in the outer leaflet of the plasma membrane could induce the formation of ordered lipid domains in the inner leaflet.

1.3.4 Role of lipid rafts in post-Golgi trafficking

Post-Golgi transport vesicles carrying a transmembrane raft protein, immunoisolated from the yeast *Saccharomyces cerevisiae*, were found to be enriched in ergosterol (the major yeast sterol) and sphingolipids, and to exhibit a higher membrane order, as compared to the donor organelle (Klemm *et al.*, 2009). Thus, it was directly shown for the first time that the *trans*-Golgi network (TGN) is able to sort membrane lipids, as hypothesized from the study on apical transport in epithelial cells that introduced the concept of lipid rafts (Simons *et al.*, 1988). More recently, a more detailed model of apical trafficking was put forward (Schuck *et al.*, 2004). Sorting of apical from basolateral

cargo was proposed to occur in the TGN and be based on clustering of rafts through the oligomerization of raft components and subsequent recruitment of further proteins to the clustered rafts. Several proteins were proposed to induce raft clustering at the sites where sorting takes place. One such protein might be VIP17/MAL, a raft-associated transmembrane protein with the ability to oligomerize, shown to be involved in apical transport in polarized MDCK cells (Cheong *et al.*, 1999). The clustering may also be induced by annexin-13b and annexin-2, both cytosolic proteins, which preferentially associate with cholesterol-rich membranes, have a tendency to oligomerize, and are involved in apical trafficking in polarized MDCK cells (Lafont *et al.,* 1998; Jacob *et al.*, 2004). The galectin family of lectins might cluster rafts by crosslinking of glycoproteins and glycolipids, due to their ability to engage in multivalent protein-carbohydrate interactions. For example, galectin-4 was shown to associate with DRMs and play a role in apical sorting in enterocyte-like HT-29 cells (Delacour *et al.,* 2005*;* Stechly *et al.,* 2009). Similarly, galectin-9 was shown to be a critical factor in apical membrane biogenesis (Mishra *et al.*, 2010). Raft clustering could also play a role in the generation of transport carriers. Growth of the clustered raft domain beyond a critical size should result in budding driven by the line tension at the phase boundaries, followed by fission and the formation of TGN-derived secretory vesicles strongly enriched in raft components (Schuck *et al.*, 2004; Rajendran *et al.*, 2005). It seems that not only in epithelial cells, but also in fibroblasts (Yoshimori *et al.,* 1996) and neurons (Ledesma *et al.*, 1998), lipid rafts serve as platforms for the delivery of raft-associated cargo to the plasma membrane. As most of the proteins identified in epithelial cells as components of the apical sorting machinery have tissue-specific distributions, other proteins must perform analogous functions in the other cell types (Cheong *et al.*, 1999).

1.4 Lipid modifications of proteins

1.4.1 Glycosyl-phosphatidylinositol (GPI) anchor

Numerous proteins in protozoa, fungi, plants, and animals are attached to the cell surface via the glycolipid structure called glycosyl-phosphatidylinositol (GPI) anchor. GPI-anchored proteins (GPI-APs) mediate diverse cellular functions, such as adhesion, immune signaling, and nutrient uptake (Levental *et al.*, 2010a). All GPI anchors contain

an identical backbone, consisting of phosphoethanolamine linked to a glycan comprising (mannose)$_3$-glucosamine (Manα1-2Manα1-6Manα1-4GlcNH$_2$), which in turn is linked to the position 6 of the *myo*-inositol ring of phosphatidylinositol (PI) (McConville *et al.*, 1993; Fujita *et al.*, 2010). The GPI anchor is attached to the C-terminus of a protein via phosphoethanolamine. GPI anchors are structurally heterogeneous: the tetrasaccharide backbone may be substituted with mannose and/or galactose residues and with an additional phosphoethanolamine, the inositol ring can be acylated, and the nature of aliphatic chains of the PI is variable (McConville *et al.*, 1993; Fujita *et al.*, 2010). Proteins destined to be modified with the GPI anchor contain an N-terminal ER signal sequence, and a C-terminal GPI signal sequence, commonly a stretch of 12-20 hydrophobic residues (McConville *et al.*, 1993). The GPI is assembled by sequential addition of monosaccharides and phosphoethanolamine to PI (McConville *et al.*, 1993; Fujita *et al.*, 2010). The initial steps of GPI biosynthesis occur on the cytosolic face of the ER (Vidugiriene *et al.*, 1993). A biosynthetic intermediate is then flipped into the ER lumen, where a complete GPI precursor is synthesized and transferred on the protein, replacing the GPI signal sequence in a transamidation reaction (Gerber *et al.,* 1992), and attaching the protein to the exoplasmic leaflet through two (sometimes three) acyl or alkyl chains of the PI. GPI anchor undergoes lipid and/or glycan remodeling in the ER and Golgi, and afterwards the protein is transported to the plasma membrane (Fujita *et al.*, 2010).

GPI anchors act as lipid raft-targeting signals (Levental *et al.*, 2010a). GPI-APs were the first proteins found to associate with DRMs (Brown *et al.*, 1992). More recently, they were shown to preferentially partition into the l_o-like phase in both plasma membrane spheres (PMS; Lingwood *et al.*, 2008) and giant plasma membrane vesicles (GPMVs; Baumgart *et al.,* 2007; Johnson *et al.,* 2010) with liquid/liquid phase coexistence. Moreover, fluorescence resonance energy transfer (FRET)-based experiments revealed that GPI-APs are present in nanoscale cholesterol-dependent clusters on the surface of living cells (Sharma *et al.,* 2004). GPI anchor was shown to serve as a signal for transport to the apical membrane of polarized epithelial cells (Brown *et al.,* 1989; Lisanti *et al.,* 1989). Later, a GPI-AP was found to become associated with sphingolipid-rich detergent-resistant membranes during its transport through the Golgi (Brown *et al.*, 1992), supporting the model that sphingolipids form transport platforms (rafts) in the

Golgi, the association with which is responsible for apical targeting (Simons *et al.*, 1988). Subsequently it became clear, however, that raft association is insufficient to direct apical targeting. The original model was refined to take into account the requirement for oligomerization or lectin-mediated crosslinking of GPI-APs in their association with, and possibly also in the formation of, clustered rafts, which then facilitate direct apical delivery of their components (Schuck *et al.*, 2004; Schuck *et al.*, 2006; see also section 1.3.4).

1.4.2 Prenylation

Prenylation is a posttranslational modification that involves the attachment of a 15-carbon farnesyl or a 20-carbon geranylgeranyl isoprenoid to a cysteine residue of the target protein via a covalent thioether bond. Modified in this way are, for example, many members of the Ras superfamily of small GTPases (Wennerberg *et al.,* 2005). Prenylation is catalyzed by a cytosolic prenyltransferase (Casey *et al.*, 1996), and occurs at a cysteine located within the C-terminal CaaX box, where 'a' is an aliphatic amino acid, and 'X' is an amino acid that determines whether the prenyl group that is added is a farnesyl or a geranylgeranyl isoprenoid. Upon prenylation, the three C-terminal amino acids (-aaX) are removed by prenylcysteine endoprotease, and the resulting C-terminal prenylated cysteine is carboxyl methylated by a prenylcysteine carboxyl methyltransferase. The last two modifications take place at the cytosolic surface of the ER (Romano *et al.,* 1998; Schmidt *et al.,* 1998). Cysteine residues immediately upstream of the prenylated cysteine can be then palmitoylated, as in the case of H-Ras and N-Ras (Hancock *et al.,* 1989). Prenylation provides only weak membrane association, and thus a second signal (palmitate or a cluster of basic amino acids) is required for stable membrane attachment (Resh, 2006; see also section 1.4.4). It is expected that the bulky branched structure of prenyl groups should not fit well into the l_o phase of lipid rafts. In agreement, peptides dually modified with a palmitoyl and a prenyl group show very low affinities for l_o domains in model bilayers with coexisting l_d and l_o phases (Wang *et al.*, 2001), and DRMs isolated from cells contain few prenylated proteins (Melkonian *et al.,* 1999). However, it seems that this raft-disfavoring tendency of prenyl groups can be overcome, as in the case of doubly palmitoylated H-Ras, which is excluded from rafts in

its GTP-bound active state, but raft-associated when in the GDP-bound inactive state (Prior *et al.*, 2001).

1.4.3 Myristoylation

Protein N-myristoylation refers to the attachment of a 14-carbon saturated fatty acid myristate to eukaryotic and viral proteins. Proteins that are destined to become myristoylated begin with the sequence: methionine-glycine (Met-Gly). The initiating methionine residue is removed cotranslationally by methionine aminopeptidase. Myristate is linked to the resulting N-terminal glycine via an irreversible amide bond, which also occurs cotranslationally in the cytosol (Wilcox *et al.*, 1987), and is catalyzed by N-myristoyltransferase, NMT (Johnson *et al.,* 1994; Farazi *et al.,* 2001). In addition to the key glycine, the ability of a protein to be recognized by NMT depends also on other N-terminal residues: serine or threonine is preferred at position 6, and lysine or arginine at positions 7 and/or 8 (Resh, 1999).

Myristoylation can play a role in stabilizing three-dimensional protein conformation, as in the case of the VP4 capsid protein of picornaviruses (Chow *et al.,* 1987), or the catalytic subunit of cAMP-dependent protein kinase (Zheng *et al.*, 1993). In the case of many cytoplasmic proteins myristoylation provides weak and reversible membrane attachment, with a second signal being required for stable anchoring to the lipid bilayer (the 'two-signal hypothesis'; Resh, 1994; Resh, 1999; Resh, 2006). For some proteins, stable membrane binding is mediated by myristoylation in combination with an N-terminal cluster of basic amino acids that form electrostatic interactions with negatively charged phospholipids, primarily PS and PI, enriched in the cytoplasmic leaflet of cellular membranes (Resh, 1993; Resh, 1994; Resh, 2006). Examples of such proteins include Src kinase (Sigal *et al.*, 1994), HIV-1 Gag and HIV-1 Nef proteins (Zhou *et al.*, 1994; Welker *et al.*, 1998), and the myristoylated alanine-rich C kinase substrate (MARCKS; Taniguchi *et al.*, 1993). For endothelial nitric-oxide synthase (eNOS), *Leishmania* hydrophilic acylated surface protein B (HASPB), many α subunits of heterotrimeric G proteins, as well as most members of the Src family of protein tyrosine kinases, stable membrane attachment is mediated by modification with both myristate and palmitate at the N-terminus (Resh, 1994; Resh, 1999; Resh, 2006; see also section

1.4.4). Membrane binding of myristoylated proteins can be subject to regulation. Some myristoylated proteins exist in two conformations in which the myristoyl chain is either sequestered in a hydrophobic pocket within the protein, or exposed and available for membrane binding. The trigger for the conformational change can be ligand binding or proteolytic cleavage. In the case of GDP-bound Arf1, its myristoylated N-teminal α-helix is buried in a hydrophobic pocket, from which it is displaced by GTP binding, which results in membrane association of Arf1 (Goldberg, 1998). Proteolytic cleavage of HIV-1 Gag precursor, Pr55(gag), causes a conformational change that sequesters myristate within the proteolytic product, p17MA, resulting in its release from the membrane (Hermida-Matsumoto *et al.*, 1999).

1.4.4 Palmitoylation

Protein S-palmitoylation involves the attachment of a 16-carbon saturated palmitic acid to the sulfhydryl group of cysteine residues of eukaryotic and viral proteins via a reversible thioester bond, and takes place posttranslationally in the membrane fraction (Paige *et al.*, 1993). There is no clear sequence requirement for palmitoylation other than the presence of a cysteine residue (Smotrys *et al.*, 2004). Palmitoylated proteins can be categorized into four types (Resh, 1999). Type I consists of membrane proteins that are palmitoylated on one or several cysteine residues located close to or within the transmembrane domain. This group is exemplified by transferrin receptor, influenza hemagglutinin (HA), vesicular stomatitis virus glycoprotein (VSVG), and a large number of G protein-coupled receptors (GPCRs). Type II proteins include members of the Ras family (H-Ras and N-Ras) that are farnesylated within their C-terminal CaaX box. Farnesylation is a prerequisite for subsequent palmitoylation of cysteines in the C-terminal region (Hancock *et al.,* 1989). The third group includes proteins palmitoylated at cysteine residues near the N- or C-terminus, such as GAP-43 and PSD-95. Type IV proteins are dually fatty acylated with myristate and palmitate, and nearly all (apart from, for example, eNOS and HASPB) contain the consensus sequence Met-Gly-Cys at their N-termini. Myristoylation of glycine 2 is a prerequisite for subsequent palmitoylation (Alland *et al.,* 1994; Galbiati *et al.*, 1994; Koegl *et al.,* 1994; Mumby *et al.*, 1994; Shenoy-Scaria *et al.,* 1994; van't Hof *et al.,* 1997; Wolven *et al.*, 1997).

Palmitoylation is catalyzed by a large family of palmitoyl transferases (PATs) containing a conserved aspartate-histidine-histidine-cysteine (DHHC) cysteine-rich (CR) domain (Putilina *et al.*, 1999). Seven DHHC proteins are expressed in the yeast *S. cerevisiae,* whereas more than 20 DHHCs are encoded by mammalian genomes (Greaves *et al.,* 2011). DHHCs localize to cellular membranes, and are predicted to contain 4-6 transmembrane domains, with the N- and C-terminus and the DHHC-CR domain in the cytosol (Greaves *et al.,* 2011). Subcellular localization of GFP-tagged human DHHCs was analyzed in transfected HEK 293 cells. Most isoforms localized to the ER (DHHC-1, -6, -10, -11, -13, -14, -16 and -19), ER/Golgi (DHHC-2, -9, -12, -22), or the Golgi complex (DHHC-3, -4, -7, -8, -15, -17, -18). A few of them, however (DHHC-5, -20 and -21), exhibited a plasma membrane localization (Ohno *et al.*, 2006). As for the specificity of interaction between DHHC proteins and their substrates, it can be controlled not only by sequences adjacent to the palmitoylated cysteines, but also by more distant regions of the substrate protein. The yeast DHHC protein Pfa3 palmitoylates the vacuolar protein Vac8 within its N-terminal Src homology 4 (SH4) domain, both *in vitro* and *in vivo*. In *in vitro* palmitoylation experiments, the isolated SH4 domain of Vac8, fused to GFP, was still palmitoylated by Pfa3. Unlike the full-length protein, however, it was also palmitoylated by each of the other four yeast DHHCs tested. This suggested that regions C-terminal to the SH4 domain are important for restricting specificity of palmitoylation to a particular enzyme (Nadolski *et al.,* 2009).

Palmitoylation can act as a secondary signal for membrane attachment of proteins synthesized on soluble ribosomes, such as Gα subunits, Src family kinases, and Ras proteins, which were brought to the membrane by primary signals, i.e. myristoyl or prenyl groups (Resh, 1994; Resh, 1999; Resh, 2006). Moreover, in many cases, palmitoylation is necessary for trafficking of these proteins from intracellular membranes of the secretory pathway to the plasma membrane (Apolloni *et al.,* 2000; Sato *et al.*, 2009; Tournaviti *et al.,* 2009; see also section 1.5). According to the 'kinetic bilayer trapping' hypothesis (Shahinian *et al.*, 1995), myristoylated or prenylated proteins transiently interact with ('sample') multiple intracellular membranes until they encounter a membrane with an appropriate PAT, which results in their palmitoylation and stable membrane association. Localization of the partner DHHC protein may thus

determine the sorting of a substrate protein. For example, palmitoylation by a Golgi-localized PAT would lead to enhanced membrane binding, allowing the protein to associate more efficiently with plasma membrane-directed transport vesicles (Greaves *et al.*, 2007). Palmitoylation can play a role in regulating the sorting also of transmembrane proteins. In the case of δ opioid receptor, a GPCR, palmitoylation is required for its efficient biosynthetic delivery to the plasma membrane (Petäjä-Repo *et al.*, 2006). Conversely, palmitoylation of a ligand-gated cation channel, α-amino-3-hydroxy-5-methyl-4-isoxazolepropionic acid (AMPA) receptor, promotes its retention in the Golgi (Hayashi *et al.*, 2005). Moreover, palmitoylation was shown to influence protein stability and aggregation (Linder *et al.*, 2007). Palmitoylation of transmembrane proteins affects their stability by limiting access to E3 ubiquitin ligases, thus preventing their ubiquitylation-dependent targeting to the vacuole or lysosome, and degradation. It occurs either by stabilizing an interaction of the protein with the lipid bilayer, thus evading the quality-control machinery (as for Tlg1, a t-SNARE in *S. cerevisiae*; Valdez-Taubas *et al.*, 2005), or by segregating the palmitoylated protein and the E3 ubiquitin ligase into different membrane subdomains (as for the anthrax toxin receptor; Abrami *et al.*, 2006). Palmitoylation was also shown to inhibit the aggregation of polyglutamine-expanded mutant forms of huntingtin (Yanai *et al.*, 2006). In addition, palmitoylation can serve as a lipid raft-targeting signal (see section 1.3). It has been proposed that the presence of multiple saturated acyl chains targets proteins to lipid rafts due to their high affinity for the ordered lipid environment (Melkonian *et al.*, 1999). Indeed, peptides dually modified with a myristoyl and one or two palmitoyl groups, or with two palmitoyl groups, preferentially partition into l_o domains in model bilayers exhibiting coexisting l_d and l_o phases (Wang *et al.*, 2001). Diverse cytoplasmic proteins modified with multiple saturated acyl chains were found to be enriched in DRMs (Shenoy-Scaria *et al.*, 1994; Wolven *et al.* 1997; Melkonian *et al.*, 1999), and to co-cluster with raft-associated proteins (Harder *et al.*, 1998). Moreover, FRET measurements revealed that variants of GFP, dually modified with myristate and palmitate, exhibit cholesterol-dependent clustering in the plasma membrane of living cells, consistent with their partitioning into lipid rafts (Zacharias *et al.*, 2002). Palmitoylation seems to be necessary also for raft partitioning of the majority of transmembrane raft proteins (Levental *et al.*, 2010b). It is still an open question whether

palmitoylated proteins associate with lipid rafts already on intracellular membranes, which would facilitate their sorting to the plasma membrane (Smotrys *et al.*, 2004; Greaves *et al.*, 2007).

Many proteins undergo cycles of palmitoylation and depalmitoylation throughout their lifetime, which provides a mechanism to regulate their membrane association and/or sorting. This palmitate turnover can occur constitutively or in response to signals. For example, the palmitoylation/depalmitoylation cycle of Gα subunits is accelerated by the activation of GPCRs (Mumby *et al.*, 1994; Wedegaertner *et al.*, 1994; Bhamre *et al.*, 1998). Palmitoylation of farnesylated Ras at the Golgi promotes its transport to the plasma membrane, whereas depalmitoylation releases the protein from the plasma membrane into the cytosol, allowing it to be repalmitoylated at the Golgi membranes. This dynamic acylation cycle not only regulates the trafficking of H-Ras and N-Ras, but also is essential for maintaining their appropriate subcellular distribution (Rocks *et al*., 2005). Depalmitoylation is catalyzed by acyl-protein thioesterases. To date only one enzyme has been shown to remove palmitate from proteins on the cytoplasmic surface of membranes, namely acyl-protein thioesterase 1 (APT1), a cytosolic protein that can depalmitoylate $G\alpha_{i1}$, $G\alpha_s$, eNOS and H-Ras *in vitro*, and $G\alpha_s$ and eNOS *in vivo* (Duncan *et al.*, 1998; Yeh *et al.*, 1999).

1.5 SH4 domain proteins

1.5.1 Src family kinases

Src family kinases (SFKs) are non-receptor protein tyrosine kinases, which play key roles in signal transduction by diverse cell surface receptors, thus regulating many cellular processes including cell proliferation, differentiation, survival, migration, adhesion and cell-shape changes (Thomas *et al.*, 1997). The family is composed of nine highly homologous proteins: c-Src, Fyn, c-Yes, Yrk, Lyn, Hck, c-Fgr, Blk and Lck. C-Src, Fyn, c-Yes and Yrk are expressed in a variety of cell types, whereas Lyn, Hck, c-Fgr, Blk and Lck are found primarily in hematopoietic cells. Both Lyn and Lck are also expressed in neurons (Thomas *et al.*, 1997). All members of the family are composed of six distinct functional regions: (1) the N-terminal Src homology 4 (SH4) domain, (2) poorly conserved unique region, (3) the SH3 domain, (4) the SH2 domain, (5) the SH1 tyrosine kinase catalytic

domain, and (6) a short negative regulatory tail for autoinhibition (Thomas *et al.*, 1997). The SH4 domains of all SFKs are responsible for targeting to cellular membranes and contain a myristoylated N-terminal glycine (glycine 2), as well as either a palmitoylated cysteine(s) or, in the case of Src and Blk, a basic stretch of amino acids (Paige *et al.*, 1993; Resh, 1993; Alland *et al.*, 1994; Koegl *et al*., 1994; Resh*,* 1994; Shenoy-Scaria *et al.,* 1994). The SH3 and SH2 domains are protein-binding domains: SH3 binds to specific proline-rich sequences, and SH2, to sequences containing phosphotyrosine. Intramolecular interactions of the SH3 domain with the SH2-SH1 linker, and the SH2 domain with the tyrosine phosphorylated C-terminal tail, stabilize the inactive conformation of SFKs (Sicheri *et al.*, 1997; Xu *et al.*, 1997).

1.5.1.1 C-Src

C-Src is a non-palmitoylated SFK (Koegl *et al.*, 1994). Its interaction with cellular membranes is mediated by N-terminal myristate, in conjunction with lysines at positions 5, 7, and 9 (Silverman *et al.*, 1993). C-Src was found to localize to the plasma membrane of human platelets (Ferrell *et al.,* 1990), and to endosomal membranes of rat fibroblasts (Kaplan *et al.*, 1992). Src-GFP, transiently expressed in COS-1 cells (simian fibroblasts), was shown to rapidly move between late endosomes or lysosomes and the plasma membrane, possibly through its cytosolic release (Kasahara *et al.*, 2007).

1.5.1.2 Fyn

Apart from N-terminal myristoylation, Fyn undergoes reversible (Wolven *et al.*, 1997) palmitoylation at cysteine 3 and cysteine 6 (Alland *et al*., 1994). Fyn is expressed ubiquitously, and in T lymphocytes it is required for signal transduction via the T cell antigen receptor (TCR), thus regulating the development and activation of T cells (Thomas *et al.,* 1997). Newly synthesized Fyn appears to associate directly with the plasma membrane, rather than to sample intracellular membranes first. Metabolic labeling of transfected NIH-3T3 (mouse embryo fibroblasts) or COS-1 cells with [^{35}S] methionine, followed by subcellular fractionation, showed that the association of Fyn with the plasma membrane is rapid, taking place within 5 minutes after biosynthesis, and is followed by a slower acquisition of detergent resistance, which occurs 10-20 minutes after binding to the plasma membrane (van't Hof *et al.*, 1997). Neither the

kinetics nor the extent of membrane binding of newly synthesized Fyn was affected by brefeldin A (BFA), an inhibitor of protein secretion (van't Hof *et al.*, 1997). Incubation at 19°C to block TGN exit did not cause perinuclear accumulation of Fyn, both in the case of endogenous Fyn in a human megakaryocyte cell line Dami, and full-length Fyn transiently overexpressed in COS-1 cells (Sato *et al.*, 2009). All these results indicate that Fyn is targeted to the plasma membrane directly, with no requirement for the secretory pathway, and suggest that its palmitoylation occurs at the plasma membrane.

1.5.1.3 Lck

Lck is expressed primarily in T lymphocytes, and is required for signal transduction via the TCR, thus playing a role in T cell development and activation (Straus *et al*., 1992). Lck localizes predominantly to the cytosolic side of the plasma membrane, where it associates with cytoplasmic domains of CD4 and CD8 glycoproteins, coreceptors of the TCR on helper and cytotoxic T cells, respectively (Turner *et al.*, 1990), with these interactions being important for T cell activation (Zamoyska *et al.*, 1989; Glaichenhaus *et al.*, 1991). Lck undergoes reversible (Paige *et al.*, 1993) palmitoylation at cysteine 3 and cysteine 5 (Koegl *et al.*, 1994; Shenoy-Scaria *et al.*, 1994). In CD4-positive T cells, shortly after synthesis, palmitoylated Lck associates with CD4 at intracellular membranes, possibly of the ERGIC or *cis*-Golgi. Transport of CD4-bound Lck from intracellular membranes to the plasma membrane, but not its palmitoylation, is inhibited by BFA, indicating that CD4-associated Lck is transported via the secretory pathway (Bijlmakers *et al.*, 1999). Plasma membrane targeting of Lck, however, requires neither CD4, nor other T cell-specific proteins, as shown in T cells and transfected NIH-3T3 fibroblasts (Bijlmakers *et al.*, 1997). Lck was shown to associate with DRMs (Shenoy-Scaria *et al.*, 1993; Shenoy-Scaria *et al.*, 1994). Its engineered form attached to membranes via a transmembrane domain does not associate with DRMs, and is impaired in transducing some of the late events in the T cell receptor signaling (Kabouridis *et al.*, 1997), implying that raft association of Lck is required for it to function properly in signal transduction by the TCR.

1.5.1.4 Lyn

Lyn is myristoylated at glycine 2 and monopalmitoylated at cysteine 3 (Resh, 1994). The kinase plays a role in initiating signal transduction by the B cell antigen receptor (BCR), thus being important for the development, activation and survival of B lymphocytes (Gauld *et al.,* 2004). Lyn-GFP transiently expressed in COS-1 cells, was shown to associate with perinuclear membranes (possibly the Golgi apparatus) soon after biosynthesis. The subsequent trafficking to the plasma membrane was inhibited by N-ethylmaleimide (Kasahara *et al.,* 2004), a reagent which blocks multiple vesicular fusion events. In addition, incubation at 19°C to block TGN exit caused increased levels of perinuclear Lyn, both in the case of transiently expressed Lyn in COS-1 and HeLa cells, and endogenous Lyn in the human megakaryocyte cell line Dami (Sato *et al.*, 2009). These results indicate that Lyn is palmitoylated at the Golgi apparatus, and subsequently traffics to the plasma membrane via the secretory pathway. Overexpression of the dominant-negative Rab11 S25N mutant in COS-1 cells caused increased perinuclear localization of Lyn, suggesting an involvement of Rab11 in the exocytic transport of Lyn (Sato *et al.*, 2009). Moreover, the trafficking of Lyn from the Golgi apparatus to the plasma membrane requires four negatively charged residues in the C-lobe of the kinase domain (Kasahara *et al.,* 2004).

1.5.1.5 C-Yes

C-Yes is myristoylated at glycine 2 and monopalmitoylated at cysteine 3 (Koegl *et al.,* 1994). Yes transiently expressed in COS-1 and HeLa cells, initially associated with membranes in the perinuclear region, partially colocalizing with the Golgi marker GalT, and was found at the plasma membrane in the later phase of expression (Sato *et al.*, 2009). Incubation at 19°C to block TGN exit caused increased levels of perinuclear Yes, both in the case of endogenous Yes in Dami cells, and transiently expressed Yes in COS-1 and HeLa cells (Sato *et al.*, 2009). These results suggest that Yes is palmitoylated at the Golgi apparatus, and subsequently traffics to the plasma membrane via the secretory pathway. Overexpression of the dominant-negative Rab11 S25N mutant caused increased perinuclear localization of Yes in COS-1 cells, suggesting an involvement of Rab11 in the exocytic transport of Yes (Sato *et al.*, 2009).

1.5.2 Heterotrimeric G protein α subunits

Heterotrimeric G proteins, composed of α, β and γ subunits, transduce signals from G protein-coupled receptors (GPCRs). The ligands that bind to and activate these receptors include neurotransmitters, peptide hormones, chemokines, and lipids. Ligand binding to a GPCR induces exchange of bound GDP for GTP on Gα subunits present in Gαβγ heterotrimers, resulting in their dissociation into signaling-competent Gα and Gβγ (Marrari *et al.,* 2007). Gγ subunits are subject to prenylation, whereas Gα subunits undergo myristoylation and/or palmitoylation. Subunits α of the $G\alpha_i$ family (α_i, α_z and α_o subunits) carry both modifications (Linder *et al.*, 1993; Parenti *et al.*, 1993; Galbiati *et al.*, 1994; Resh, 1994). Interaction with Gβγ is necessary for the palmitoylation of Gα, and thus for plasma membrane localization of the heterotrimer (Marrari *et al.,* 2007). Gα, including those of the $G\alpha_i$ family, localize to lipid rafts (Moffett *et al.,* 2000), which can serve as a means of modulating signaling specificity. $G\alpha_z$, following synthesis and myristoylation, first associates with intracellular membranes and subsequently with the plasma membrane, which requires its association with Gβγ. BFA does not prevent α_z from reaching the plasma membrane, suggesting that it does not travel to the plasma membrane through the secretory pathway, and that palmitoylation of $G\alpha_z$ does not occur on intracellular membranes. $G\alpha_z$ seems to sample intracellular membranes, and when it reaches the plasma membrane, association with Gβγ allows for its palmitoylation and stable membrane association (Fishburn *et al.*, 1999).

1.5.3 Hydrophilic acylated surface protein B (HASPB)

Hydrophilic acylated surface proteins (HASPs) are components of the surface coat of protozoan parasites from the *Leishmania* genus, expressed exclusively in the infective stages of their life cycle (Flinn *et al*., 1994; Alce *et al.,* 1999). The N-terminal SH4 domain of hydrophilic acylated surface protein B (HASPB) becomes dually fatty acylated, myristoylated at glycine 2 and palmitoylated at cysteine 5, with both modifications being necessary for the transport of the protein to the surface of *Leishmania* parasites (Denny *et al.*, 2000). 18 N-terminal amino acids of HASPB are sufficient for the targeting of the heterologous *Aequorea victoria* GFP to the inner plasma membrane leaflet of both *Leishmania* and mammalian cells (Denny *et al.*, 2000; Stegmayer *et al.,* 2005), and for its subsequent translocation to the outer leaflet, possibly by a plasma membrane-resident

transporter (Stegmayer *et al.*, 2005). The portion of the fusion protein that could be biochemically detected at the outer surface of *L. major* cells was 20-30% (Denny *et al.*, 2000).

A model of HASPB transport in mammalian cells was proposed, based on the analysis of subcellular localization and DRM association of various mutants of HASPB SH4 domain, fused to GFP, heterologously expressed in either CHO or HeLa cells (Stegmayer *et al.,* 2005; Tournaviti *et al*., 2007; Ritzerfeld, 2009; Tournaviti *et al*., 2009; Ritzerfeld *et al.,* 2011). As in the case of other diacylated SH4 domain proteins, myristoylation of glycine 2 is a prerequisite for subsequent palmitoylation: mutation of this residue results in the lack of both myristoylation and palmitoylation, and as a result, the protein accumulates in the cytosol. Non-palmitoylated mutant (cysteine 5 to alanine or serine) accumulates at intracellular membranes and, unlike the wild-type form, is not recovered in DRMs. All this suggests that myristoylation enables the protein to transiently associate with intracellular membranes, thus bringing it in proximity to a palmitoyl transferase, which was proposed to be Golgi-associated. Only upon palmitoylation can the protein be transported to the plasma membrane, hypothetically - associated with the cytosolic face of secretory vesicles. It was proposed that palmitoylation results in partitioning of HASPB into lipid rafts already at the Golgi, and furthermore, that lipid rafts are necessary for the transport of HASPB to the plasma membrane. In agreement, reduction of cellular cholesterol levels, either by siRNA-mediated down-regulation of the crucial enzyme in early cholesterol biosynthesis, mevalonate-diphospho-dehydrogenase (MVD), or by treatment with the cholesterol-extracting drug, methyl-β-cyclodextrin (MβCD), resulted in increased levels of perinuclear HASPB SH4-GFP, and also Yes SH4-mCherry. The effect of MβCD on the localization of the reporter proteins could be reversed upon replenishment with exogenous cholesterol (Ritzerfeld *et al.,* 2011). Targeted mutagenesis of HASPB SH4 domain led to identification of a mutation (threonine 6 to glutamate) that caused the HASPB SH4-GFP reporter to be retained in intracellular sites, with a strong accumulation at perinuclear membranes. This mutation influenced neither acylation levels of the protein, nor its membrane binding, reduced however its association with DRMs. HASPB SH4 domain was shown to be phosphorylated at threonine 6 *in vivo*. SiRNA-mediated down-regulation of the threonine/serine-specific

phosphatases PP1 and PP2A or their pharmacological inhibition by calyculin A caused reversible accumulation of the wild-type form of HASPB SH4-GFP (but not the non-phosphorylatable threonine 6 to alanine mutant) at intracellular sites. These data led to a hypothesis that a regulatory mechanism exists, in which phosphorylation at threonine 6 induces redistribution of HASPB from the plasma membrane to perinuclear membranes (possibly endosomal recycling compartment), whereas its dephosphorylation by PP1 and PP2A is required for the protein to be recycled back to the plasma membrane (Tournaviti *et al*., 2009).

1.6 Aims of this thesis

The aim of the first part of this study (chapters 2 and 3) was to characterize membrane (both lipid and protein) environment of diacylated SH4 domain proteins residing in lipid rafts. The approach was to analyze lipid and protein components of detergent-resistant membranes (DRMs) immunoaffinity-purified from the total pool with the use of diacylated SH4 domain fusion proteins as bait. In the second part of this study (chapters 4 and 5), we intended to investigate the previously reported (Ritzerfeld, 2009; Ritzerfeld *et al.*, 2011) role of the COPI coatomer complex, as well as of the secretory pathway in general, in the plasma membrane transport of diacylated SH4 domain proteins. To this end we employed: siRNA-mediated knockdown of the β subunit of the COPI complex, expression of constitutively active mutant (Q71L) of the small GTPase Arf1, as well as treatment with brefeldin A.

2 Results I

The aim of this part of the study was to characterize membrane (both lipid and protein) environment of diacylated SH4 domain proteins residing in cholesterol- and sphingolipid-enriched subdomains of cellular membranes, that is lipid rafts. We decided to define lipid raft components based on the detergent-resistant membrane (DRM) approach. We intended to isolate DRMs from a human cell line, and subsequently perform a specific immunoaffinity purification of DRMs that contain either of two diacylated SH4 domain fusion proteins, followed by an analysis of their lipid and protein components.

2.1 Generation of human cell lines stably expressing SH4 domain fusion proteins

Immunoisolation of DRMs that contain diacylated SH4 domain proteins required generating human cell lines stably expressing a SH4 domain fused to an affinity tag. We decided to use for this purpose green fluorescent protein (GFP), the fusion with which also allows selection for transduced cells using fluorescence-activated cell sorting (FACS), visualization of the fusion protein in live cells using fluorescent microscopy, analysis of its expression levels by flow cytometry and finally, detection using Western blotting. A tobacco etch virus (TEV) protease cleavage site was introduced in between the SH4 domain and GFP (Figure 1), to allow for specific elution of the immunoisolated DRMs from the affinity matrix. We designed fusion proteins containing SH4 domains derived either from *Leishmania major* hydrophilic acylated surface protein B (HASPB), or from human Src family kinase Yes. Both SH4 domains become myristoylated at glycine 2 (which is the N-terminal residue after removal of the initiating methionine), and palmitoylated either at cysteine 5 (in the case of HASPB) or at cysteine 3 (in the case of Yes) (Figure 1, A and C, respectively). Apart from the two fusion proteins containing the wild-type SH4 domains, we designed also a palmitoylation-deficient mutant, HASPB SH4 Δpal-TEV-GFP, in which cysteine 5 is replaced with serine (Figure 1 B), to be used as a control.

Figure 1 SH4 domain fusion proteins stably expressed in human cell lines generated in this study. SH4 domains derived either from *Leishmania major* hydrophilic acylated surface protein B (HASPB), or from human Src family kinase Yes, are fused to the N-terminus of green fluorescent protein (GFP), with a tobacco etch virus (TEV) protease cleavage site in between. **(A)** HASPB SH4-TEV-GFP is myristoylated at glycine 2 (N-terminal residue after removal of the initiating methionine) and palmitoylated at cysteine 5. **(B)** HASPB SH4 Δpal-TEV-GFP is a palmitoylation-deficient mutant, in which cysteine 5 was replaced with serine. **(C)** Yes SH4-TEV-GFP is myristoylated at glycine 2 and palmitoylated at cysteine 3. Acylated amino acid residues are shown in bold type, acyl moieties are represented by the squiggly lines, and the mutated residue is highlighted in red.

2.1.1 Construction of plasmids for the generation of human cell lines stably expressing SH4 domain fusion proteins

Inserts encoding each of the SH4 domains and a TEV protease cleavage site, were formed by annealing of oligonucleotides, and contained BamHI and AgeI sticky ends and a Kozak sequence. Moloney murine leukemia virus (MMLV)-based retroviral expression vector pRevTRE2, harboring HASPB SH4-coding sequence flanked by BamHI and AgeI restriction sites, followed by GFP-coding sequence flanked by AgeI and NotI restriction sites (i.e. pRevTRE2/HASPB SH4-GFP; created by Julia Ritzerfeld; Ritzerfeld, 2009), was digested with BamHI and AgeI restriction enzymes to remove the HASPB SH4 insert. Each of the SH4-TEV inserts was ligated into thus obtained pRevTRE2/GFP, upstream of and in frame with the GFP-coding sequence. Sequences encoding HASPB SH4-TEV-GFP, HASPB SH4 Δpal-TEV-GFP and Yes SH4-TEV-GFP were thus located between the MMLV 5' and 3' long terminal repeat sequences (LTRs), downstream of the tetracycline-response element (TRE), which enables their stable insertion into the genome, and inducible expression of the fusion proteins.

2.1.2 Retroviral transduction

The pRevTRE2-based constructs were transiently cotransfected into packaging cells (HEK 293T) together with two vectors encoding viral proteins. As a result, retroviral particles carrying vector RNA encoding the SH4 domain fusion proteins were produced, and subsequently used to infect target cell lines: HeLa (human cervical epitheloid carcinoma) and HeLa S3 (a clonal derivative of HeLa cells, capable of suspension growth). The target cells were MCAT-TAM2 stable cell lines, i.e. stably expressing mouse cationic amino acid transporter 1 (MCAT1), which serves as a receptor for retroviral particles, and rtTA-M2, a Tet-On transactivator, which binds to the tetracycline-response element.

2.1.3 Fluorescence-activated cell sorting

Following retroviral transduction, cells expressing each of the SH4 domain fusion proteins in a doxycycline-inducible manner were selected by several rounds of fluorescence-activated cell sorting (FACS). During the first round of sorting, transduced cells were selected. The second round excluded cells that expressed the fusion protein in a constitutive manner. The final, third sort isolated pools and single cells, in which the transduced fragment was stably integrated into the genome.

2.2 Characterization of human cell lines stably expressing SH4 domain fusion proteins

2.2.1 Analysis of expression levels of SH4 domain fusion proteins by flow cytometry

To characterize the inducibility and expression levels of HASPB SH4-TEV-GFP, HASPB SH4 Δpal-TEV-GFP, and Yes SH4-TEV-GFP fusion proteins stably expressed in the generated HeLa (Figure 2) and HeLa S3 (Figure 3) cell lines, pools and clones were cultivated in the absence or presence of 4 µg/ml doxycycline for 16 hours and analyzed using flow cytometry, by detecting the fluorescence of GFP. Autofluorescence of the respective MCAT-TAM2 cell lines was adjusted to 10^1.

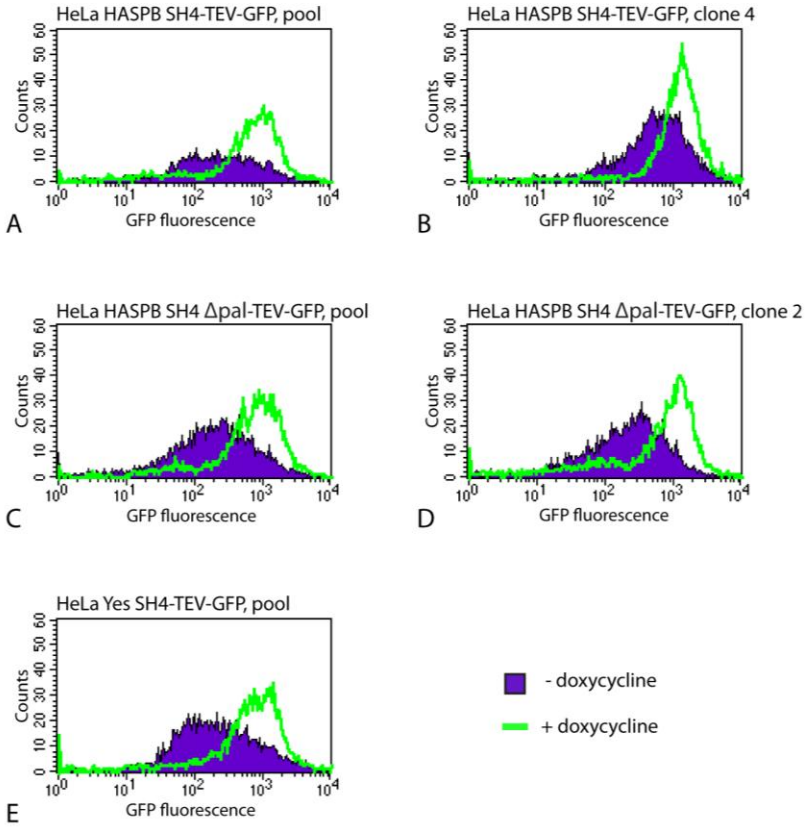

Figure 2 Analysis of expression levels of SH4-TEV-GFP fusion proteins stably expressed in HeLa cells. HeLa cell lines stably expressing HASPB SH4-TEV-GFP **(A, B)**, HASPB SH4 Δpal-TEV-GFP **(C, D)**, or Yes SH4-TEV-GFP **(E)** in a doxycycline-inducible manner, were grown in the absence (blue profile) or in the presence (green profile) of 4 µg/ml doxycycline for 16 hours, detached, and analyzed by flow cytometry. Autofluorescence of HeLa MCAT-TAM2 cells was adjusted to 10^1.

All generated cell lines exhibited some level of constitutive SH4 domain fusion protein synthesis. Expression levels in the absence of doxycycline were lower for HeLa S3 cell lines than for HeLa cell lines. In all cases, upon induction with doxycycline, expression levels were significantly increased. For the immunoisolation procedure we decided to use clonal (i.e. obtained by sorting single cells) HeLa S3 cell lines. Clones were chosen in which the expression levels of HASPB SH4 and Yes SH4 fusion proteins were low without doxycycline, and were high and similar upon cultivation in its presence, that is: clone 7 for HeLa S3 HASPB SH4-TEV-GFP (Figure 3 B), and clone 1 for HeLa S3 Yes SH4-TEV-GFP (Figure 3 F).

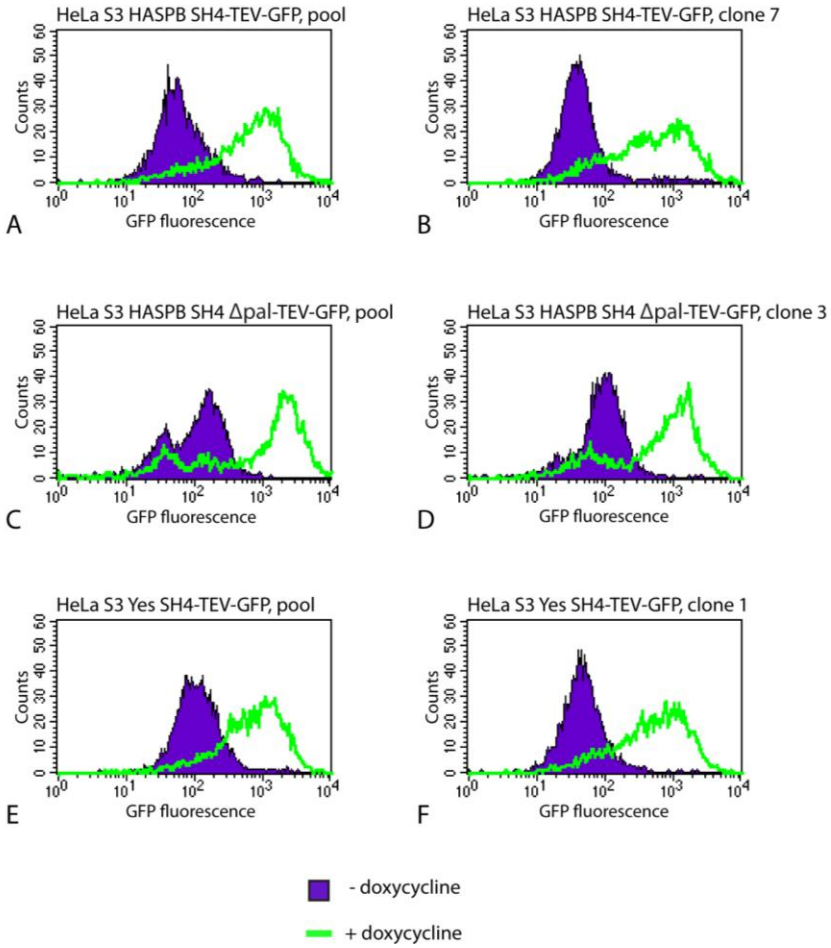

Figure 3 Analysis of expression levels of SH4-TEV-GFP fusion proteins stably expressed in HeLa S3 cells. HeLa S3 cell lines stably expressing HASPB SH4-TEV-GFP **(A, B)**, HASPB SH4 Δpal-TEV-GFP **(C, D)**, or Yes SH4-TEV-GFP **(E, F)** in a doxycycline-inducible manner, were grown in the absence (blue profile) or in the presence (green profile) of 4 µg/ml doxycycline for 16 hours, detached, and analyzed by flow cytometry. Autofluorescence of HeLa S3 MCAT-TAM2 cells was adjusted to 10^1.

2.2.2 Analysis of subcellular localization of SH4 domain fusion proteins by confocal microscopy

Subcellular localization of HASPB SH4-TEV-GFP, HASPB SH4 Δpal-TEV-GFP, and Yes SH4-TEV-GFP fusion proteins stably expressed in HeLa (Figure 4) and HeLa S3 (Figure 5) cells was examined by live-cell confocal microscopy, after cultivation of the stable cell lines in the presence of 1 µg/ml doxycycline for 24 hours in 8-well Lab-Tek Chambered Coverglass plates.

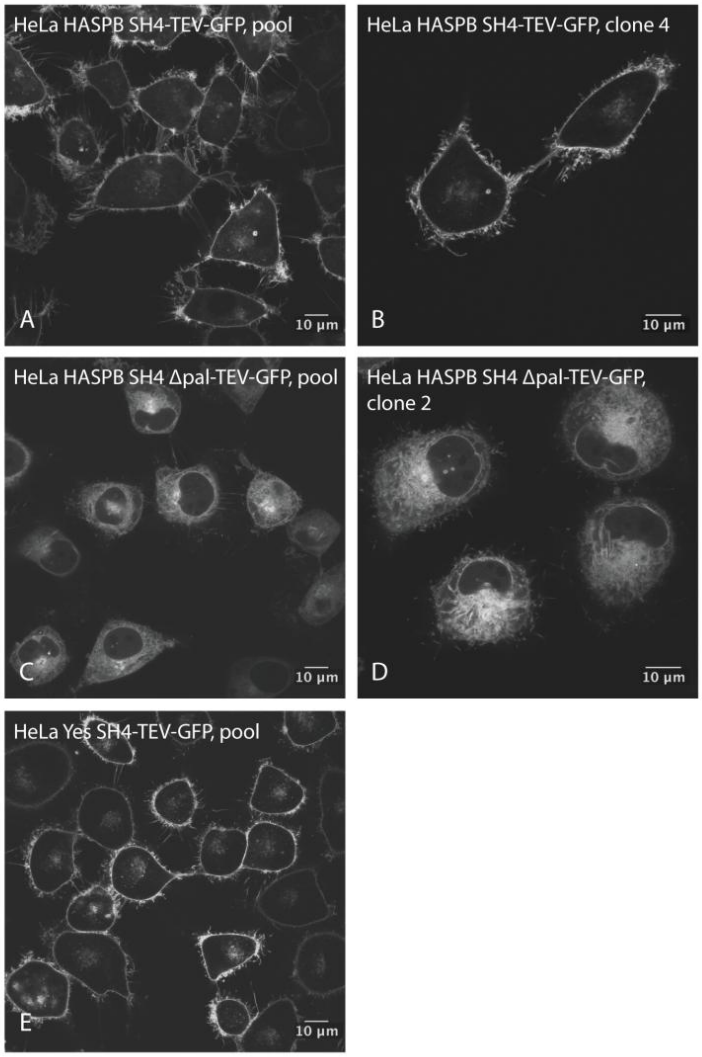

Figure 4 Analysis of subcellular localization of SH4-TEV-GFP fusion proteins stably expressed in HeLa cells. HeLa cell lines stably expressing HASPB SH4-TEV-GFP **(A, B)**, HASPB SH4 Δpal-TEV-GFP **(C, D)**, or Yes SH4-TEV-GFP **(E)** in a doxycycline-inducible manner, were grown in 8-well Lab-Tek Chambered Coverglass plates in the presence of 1 µg/ml doxycycline for 24 hours and imaged by live-cell confocal microscopy (objective 63x). Scale bar, 10 µm.

At steady state, both wild-type fusion proteins, HASPB SH4-TEV-GFP (Figure 4, A, B; Figure 5, A, B), and Yes SH4-TEV-GFP (Figure 4 E; Figure 5, E, F), localized mainly to the plasma membrane of both HeLa and HeLa S3 cells, with a small amount in the perinuclear region. This is in agreement with what was previously reported for GFP-tagged HASPB and Yes SH4 domains stably expressed in CHO (Stegmayer *et al.*, 2005; Tournaviti *et al.*, 2007) and in HeLa cells (Ritzerfeld, 2009; Ritzerfeld *et al.*, 2011), as well as for HASPB and Yes SH4 domains fused to GFP-protein A, stably expressed in CHO and HeLa cells (Tournaviti *et al.*, 2009).

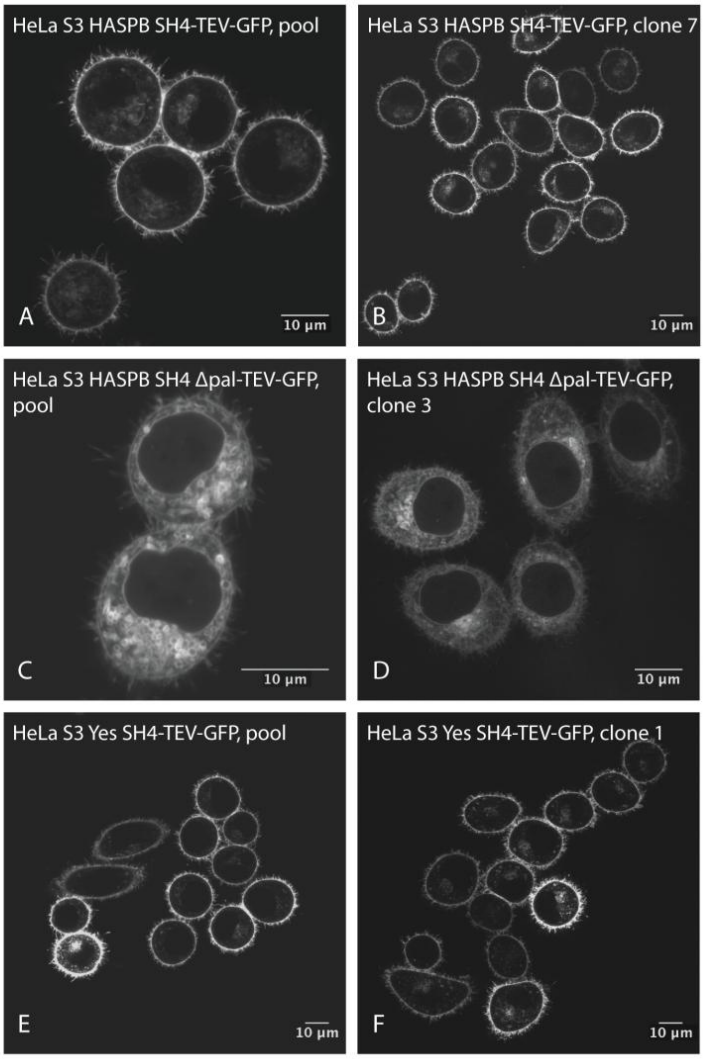

Figure 5 Analysis of subcellular localization of SH4-TEV-GFP fusion proteins stably expressed in HeLa S3 cells. HeLa S3 cell lines stably expressing HASPB SH4-TEV-GFP **(A, B)**, HASPB SH4 Δpal-TEV-GFP **(C, D)**, or Yes SH4-TEV-GFP **(E, F)** in a doxycycline-inducible manner, were grown in 8-well Lab-Tek Chambered Coverglass plates in the presence of 1 µg/ml doxycycline for 24 hours and imaged by live-cell confocal microscopy (objective 63x). Scale bar, 10 µm.

The palmitoylation-deficient cysteine 5 to serine (C5S) mutant, HASPB SH4 Δpal-TEV-GFP, was retained at intracellular membranes in both HeLa (Figure 4, C, D), and HeLa S3 cells (Figure 5, C, D), in agreement with what was previously reported for GFP-tagged C5S mutant of HASPB SH4 domain stably expressed in CHO cells (Stegmayer *et al.*, 2005; Tournaviti *et al.*, 2007), as well as for C5A and C3A mutants of HASPB and Yes SH4 domains, respectively, fused to GFP, stably expressed in HeLa cells (Ritzerfeld, 2009; Ritzerfeld *et al.*, 2011), and for C5A mutant of HASPB SH4 fused to GFP-protein A, stably expressed in CHO and HeLa cells (Tournaviti *et al.*, 2009).

2.2.3 Analysis of detergent-resistant membrane association of SH4 domain fusion proteins

We examined the degree of detergent-resistant membrane (DRM) association of HASPB SH4-TEV-GFP, HASPB SH4 Δpal-TEV-GFP, and Yes SH4-TEV-GFP stably expressed in HeLa (Figure 6) and HeLa S3 (Figure 7) cells. The cells, grown in 10 cm plates in the presence of 1 µg/ml doxycycline for 24-48 hours, were extracted on ice with 1% Triton X-100 in MBS buffer. The lysate was centrifuged, and the resulting post-nuclear supernatant (PNS) adjusted with OptiPrep (i.e. 60% iodixanol) to 40% iodixanol, overlayered with 28% iodixanol in MBS buffer, and finally with MBS (0% iodixanol). After equilibrium density gradient centrifugation, eight fractions were collected from the top of the gradient, and analyzed by Western blotting.

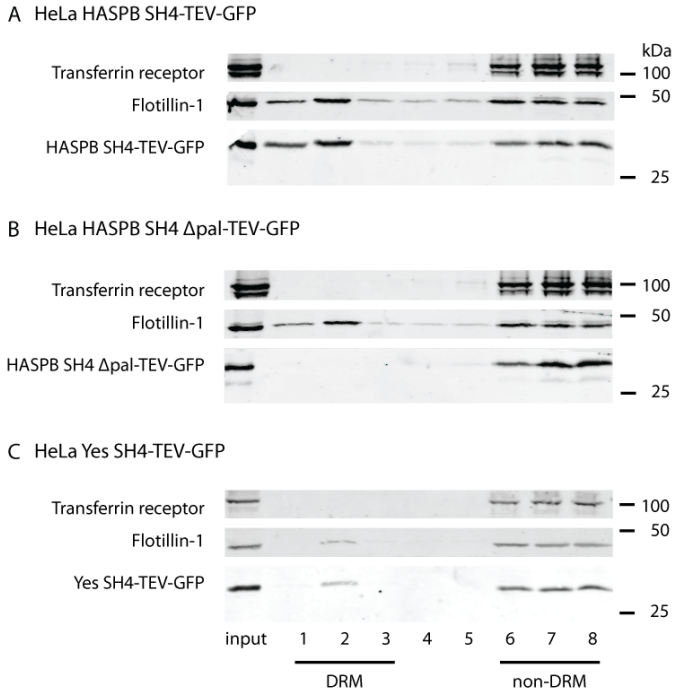

Figure 6 Analysis of detergent-resistant membrane (DRM) association of SH4-TEV-GFP fusion proteins stably expressed in HeLa cells. HeLa cell lines stably expressing **(A)** HASPB SH4-TEV-GFP, **(B)** HASPB SH4 Δpal-TEV-GFP, or **(C)** Yes SH4-TEV-GFP in a doxycycline-inducible manner, were grown in 10 cm plates in the presence of 1 µg/ml doxycycline for 24-48 hours. The cells were extracted on ice with 1% Triton X-100 in MBS buffer. Post-nuclear supernatant (PNS) was floated on an OptiPrep step density gradient (40/28/0% iodixanol). Eight fractions were collected from the top of the gradient, and an aliquot of each was analyzed by Western blotting, together with an aliquot of PNS (denoted as input). As DRM and non-DRM markers, flotillin-1 and transferrin receptor were used, respectively.

Both wild-type SH4-TEV-GFP fusion proteins were found in low-density, that is DRM fractions (fractions 1-3; Figure 6, A, C and Figure 7, A, C), which is in agreement with what was previously reported for HASPB SH4 domain fused to GFP-protein A, stably expressed in CHO cells (Tournaviti *et al.*, 2009). Flotillin-1, which was used here as a DRM marker, exhibited a very similar distribution across the eight fractions of the density gradient as the wild-type SH4-TEV-GFP fusion proteins, whereas transferrin receptor, a non-DRM marker, was found exclusively in the bottom fractions of the gradient, which contain fully solubilized proteins (fractions 6-8; Figure 6 and Figure 7). In contrast to the wild-type fusion proteins, HASPB SH4 Δpal-TEV-GFP was not detected in DRM fractions (Figure 6 B; Figure 7 B), which is consistent with what was previously shown for GFP-protein A-tagged C5A mutant of HASPB SH4 domain, stably expressed in CHO cells, of which less than 1% was recovered in DRMs (Tournaviti *et al.*, 2009).

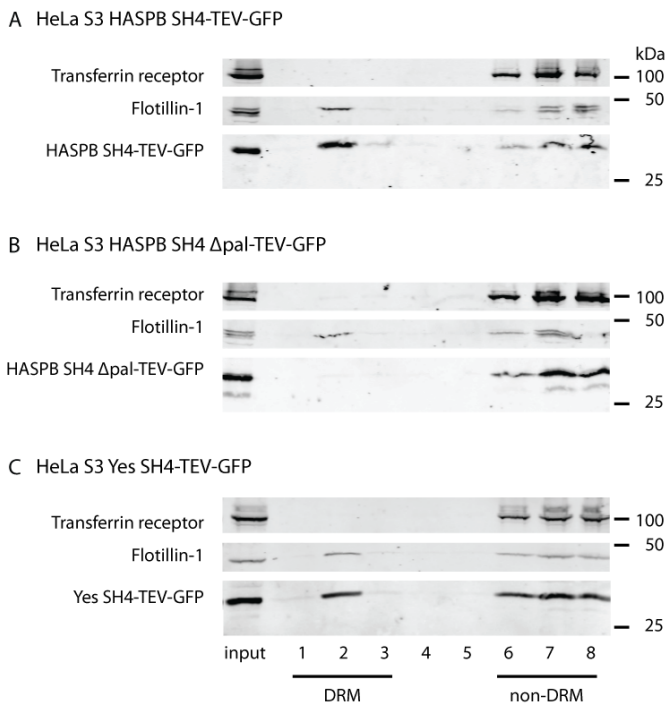

Figure 7 Analysis of detergent-resistant membrane (DRM) association of SH4-TEV-GFP fusion proteins stably expressed in HeLa S3 cells. HeLa S3 cell lines stably expressing **(A)** HASPB SH4-TEV-GFP, **(B)** HASPB SH4 Δpal-TEV-GFP, or **(C)** Yes SH4-TEV-GFP in a doxycycline-inducible manner, were grown in 10 cm plates in the presence of 1 µg/ml doxycycline for 24-48 hours. The cells were extracted on ice with 1% Triton X-100 in MBS buffer. Post-nuclear supernatant (PNS) was floated on an OptiPrep step density gradient (40/28/0% iodixanol). Eight fractions were collected from the top of the gradient, and an aliquot of each was analyzed by Western blotting, together with an aliquot of PNS (denoted as input). As DRM and non-DRM markers, flotillin-1 and transferrin receptor were used, respectively.

2.3 Immunoaffinity purification of detergent-resistant membranes containing SH4 domain fusion proteins

2.3.1 Experimental workflow

After having obtained human cell lines stably expressing either HASPB SH4-TEV-GFP or Yes SH4-TEV-GFP in a doxycycline-inducible manner (section 2.1), which was followed by the characterization of fusion protein expression levels and inducibility, as well as subcellular localization and DRM association (section 2.2), we could proceed to perform immunoaffinity purification of detergent-resistant membranes containing the SH4 domain fusion proteins. To be able to obtain large amounts of cells easily, we decided to use HeLa S3 cells, a clonal derivative of adherent HeLa cells, capable of growing in suspension. Two clonal stable cell lines were used, HeLa S3 HASPB SH4-TEV-GFP clone 7, and HeLa S3 Yes SH4-TEV-GFP clone 1, which exhibited very similar expression levels and inducibility of the SH4 domain fusion proteins (Figure 3 B and Figure 3 F, respectively). As a control for nonspecific binding to the affinity matrix and nonspecific release of the bound material, the below-described immunoaffinity isolation procedure was performed using also HeLa S3 cells that do not express any SH4-TEV-GFP fusion protein (i.e. HeLa S3 MCAT-TAM2 cells).

The subsequent steps of the immunoisolation procedure are presented in Figure 8. The three HeLa S3 cell lines were first grown adherently, followed by the establishment of suspension cultures. Expression of SH4 domain fusion proteins was induced by incubation in the presence of 1 µg/ml doxycycline for 48 hours. Afterwards, the cells were harvested by centrifugation, disrupted with the use of nitrogen cavitation, and the lysates were subjected to differential centrifugation to remove first the nuclei (centrifugation at 3000 g for 10 minutes), and then mitochondria (15000 g, 10 minutes). The final centrifugation (60 minutes at more than 100000 g) was performed to pellet microsomal membranes (membrane fragments derived from the plasma membrane, Golgi apparatus and endoplasmic reticulum). Microsomal pellets were then extracted on ice with 1% Triton X-100 in MBS buffer and floated on OptiPrep step density gradients (40/28/0%).

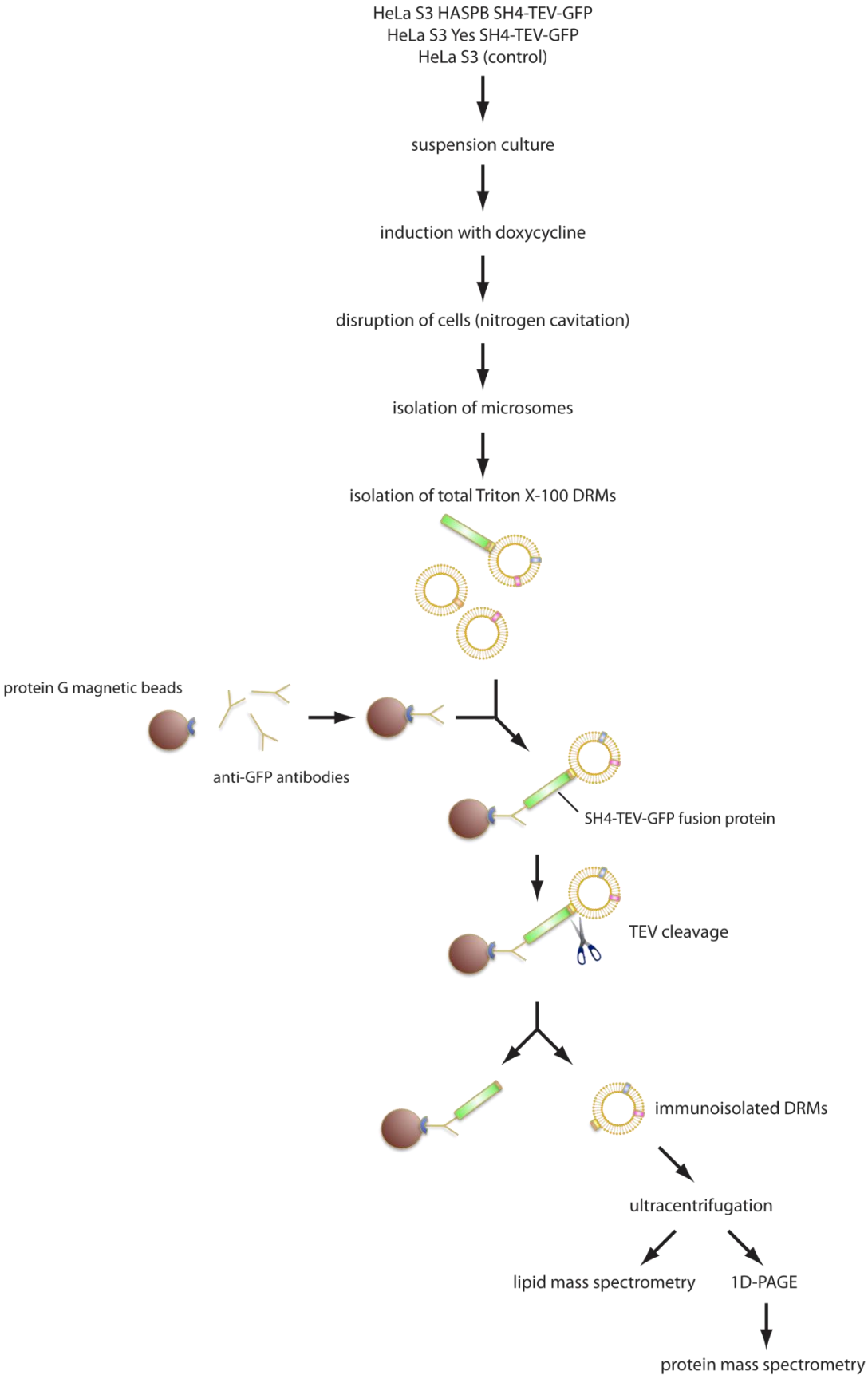

Figure 8 Caption on page 39.

Caption for figure on page 38. Figure 8 Workflow of immunoaffinity purification of detergent-resistant membranes (DRMs) containing SH4 domain fusion proteins. Clonal HeLa S3 cell lines stably expressing HASPB SH4-TEV-GFP or Yes SH4-TEV-GFP in a doxycycline-inducible manner, and HeLa S3 cells that do not express any SH4-TEV-GFP fusion protein (control), were grown in suspension. Expression of the SH4 domain fusion proteins was induced with 1 µg/ml doxycycline for 48 hours. Cells were harvested, disrupted with the use of nitrogen cavitation, and the lysates were subjected to differential centrifugation to remove nuclei and mitochondria, and to obtain pelleted microsomes, which were then extracted on ice with 1% Triton X-100 in MBS buffer and floated on OptiPrep step density gradients (40/28/0%). Eight fractions were collected from the top of each gradient. The second fraction of each gradient (denoted as total DRMs, represented in the figure by protein-containing lipid vesicles) was then incubated with anti-GFP antibodies coupled to protein G magnetic beads, to immunoisolate SH4-TEV-GFP fusion proteins, together with their associated DRMs, which were then eluted from the beads by tobacco etch virus (TEV) protease cleavage, and pelleted by ultracentrifugation. Lipids present in those pelleted immunoisolated DRMs were subjected to lipid extraction and analysis by mass spectrometry, and proteins were partially resolved by 1-dimensional polyacrylamide gel electrophoresis (1D-PAGE) and analyzed by mass spectrometry.

After overnight centrifugation at more than 100000 g, eight fractions were collected from the top of each gradient. The low-density fraction from each gradient with the highest content of the SH4 domain fusion proteins, or the corresponding fraction from the control cells (fraction number 2, denoted from now on as total DRMs), was then incubated with protein G magnetic beads to which anti-GFP antibodies had been coupled, with the aim of immunoisolating SH4-TEV-GFP fusion proteins, together with their associated DRMs, which were then eluted from the beads by TEV protease cleavage, and pelleted by ultracentrifugation. The pellets were subjected to lipid extraction and analysis by mass spectrometry (see section 2.3.2), or dissolved in 1x gel loading buffer, and the proteins partially resolved by 1-dimensional polyacrylamide gel electrophoresis (1D-PAGE) and analyzed by mass spectrometry (see section 2.3.3).

Figure 9 presents Western blot analysis of several steps of the immunoaffinity purification procedure. GM130 and ribophorin-1, non-raft membrane proteins localized in the Golgi and endoplasmic reticulum, respectively, as well as the non-raft plasma membrane marker transferrin receptor, were present in lysates, post-mitochondrial supernatants (PMS) and solubilized microsomal pellets, but not (or barely) detectable in

total DRMs, in contrast to lipid raft markers, Yes and flotillin-1, and the two SH4-TEV-GFP fusion proteins. Substantial amounts of both fusion proteins were bound to magnetic beads, and afterwards, the SH4 domains were efficiently cleaved off by TEV protease, as seen from the 2-kDa shift to higher electrophoretic mobility of the fusion proteins that remained bound to magnetic beads after incubation with the protease (Figure 9).

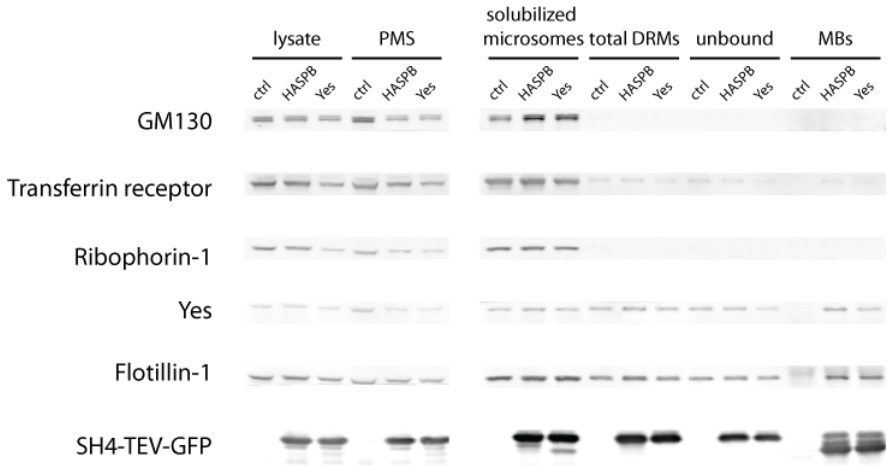

Figure 9 Steps of immunoaffinity purification of detergent-resistant membranes (DRMs) containing SH4 domain fusion proteins. The immunoisolation was performed from HeLa S3 cell lines stably expressing HASPB SH4-TEV-GFP (denoted as HASPB) or Yes SH4-TEV-GFP (denoted as Yes), as well as from control cells (HeLa S3 cells that do not express any SH4-TEV-GFP fusion protein, denoted as ctrl). PMS, post-mitochondrial supernatant; solubilized microsomes, microsomal pellet after solubilization with detergent (Triton X-100); total DRMs, fraction 2 from OptiPrep step density gradient; unbound, material unbound to magnetic beads after their incubation with total DRMs; MBs, material associated with magnetic beads after their incubation with tobacco etch virus (TEV) protease. GM130 was used as a Golgi marker, transferrin receptor as a non-DRM plasma membrane marker, ribophorin-1 was used for the endoplasmic reticulum, Yes and flotillin-1 were used as DRM markers.

Samples from the different stages of immunoisolation performed from HASPB SH4-TEV-GFP-expressing cells and from control cells were reanalyzed (Figure 10), this time including also the respective TEV eluates (i.e. material eluted from magnetic beads by TEV protease cleavage). We could detect the presence of lipid raft markers, Yes and flotillin-1, in TEV eluate obtained from HASPB SH4-TEV-GFP-expressing cells (while analyzing 5% and 50% of the sample), which were not detectable in 2% of TEV eluate from control cells. Upon cleaving off the SH4 domain from the HASPB SH4-TEV-GFP

fusion protein, GFP and any uncleaved HASPB SH4-TEV-GFP should remain bound to magnetic beads via anti-GFP antibodies. We could detect, however, the presence of the full-length fusion protein in HASPB TEV eluates, indicating that uncleaved protein detached from the beads, which suggests that some amount of HASPB DRMs was eluted from the affinity matrix not due to specific cleavage with the protease. This amount was, however, small, as can be seen by comparing the amount of cleaved protein remaining on magnetic beads to the amount of uncleaved protein in TEV eluate (compare Western blot band intensity for 0.6% of the material remaining on magnetic beads after TEV cleavage to the intensities for 5% and 50% of HASPB TEV eluate; Figure 10).

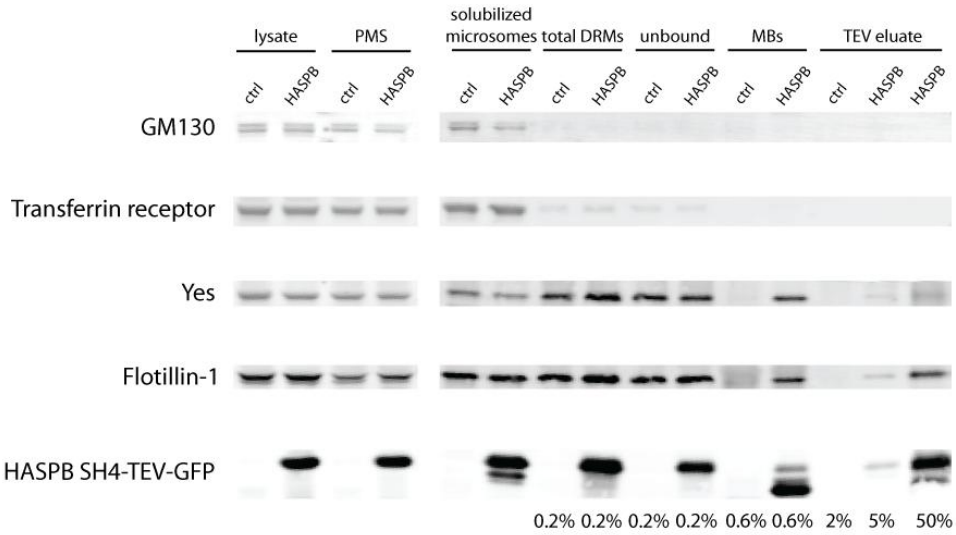

Figure 10 Steps of immunoaffinity purification of detergent-resistant membranes (DRMs) containing SH4 domain fusion proteins. Analyzed were samples from the different stages of immunoisolation performed from HeLa S3 HASPB SH4-TEV-GFP (denoted as HASPB), and from control cells (denoted as ctrl). PMS, post-mitochondrial supernatant; solubilized microsomes, microsomal pellet after solubilization with detergent (Triton X-100); total DRMs, fraction 2 from OptiPrep step density gradient; unbound, material unbound to magnetic beads after their incubation with total DRMs; MBs, material associated with magnetic beads after their incubation with tobacco etch virus (TEV) protease; TEV eluate, material eluted from magnetic beads by TEV protease cleavage. GM130 was used as a Golgi marker, transferrin receptor as a non-DRM plasma membrane marker, Yes and flotillin-1 were used as DRM markers. The percentage of sample analyzed is indicated for total DRMs, unbound, MBs and TEV eluate.

2.3.2 Lipid components of immunoaffinity-purified detergent-resistant membranes containing SH4 domain fusion proteins

Lipids present in solubilized microsomal pellets (i.e. the input for DRM gradients), total Triton X-100 DRMs, as well as in DRMs immunoprecipitated from the total pool using SH4-TEV-GFP as bait and subsequently eluted from the affinity matrix by TEV protease cleavage and pelleted (denoted further as TEV eluates), were subjected to lipid extraction in the presence of internal standards, and analyzed by nano-ESI-MS/MS using a triple quadrupole mass spectrometer (Dr. Britta Brügger, Research Group Prof. Dr. Felix Wieland/Dr. Britta Brügger, Heidelberg University Biochemistry Center). TEV eluates obtained from HeLa S3 cells expressing a SH4-TEV-GFP fusion protein contained on average 0.21% and 0.08% (in the case of HASPB SH4-TEV-GFP and Yes SH4-TEV-GFP-expressing cells, respectively) of the lipids present in the total DRMs from which they were immunoprecipitated, as compared to 0.03% of the input in the case of control cells, i.e. HeLa S3 cells that do not express any SH4-TEV-GFP fusion protein (averaged data from three independent experiments). Moreover, TEV eluates obtained from cells expressing a SH4-TEV-GFP fusion protein contained on average 8.0 times (in the case of HASPB SH4-TEV-GFP) or 2.7 times (Yes SH4-TEV-GFP) more total lipid than the respective TEV eluates from control cells (data from three independent experiments), suggesting that DRMs that contain SH4 domains were successfully immunoisolated. However, the relatively low total lipid yields for Yes SH4 DRMs, on average only 2.7 times higher than the nonspecific lipid background present in control TEV eluates, and thus the possibility of substantial contribution of nonspecifically copurified lipids to the observed lipid composition of Yes SH4 DRMs, make the results less certain.

The charts in Figure 11 A, as well as the table in Figure 11 B, depict lipid class composition of solubilized microsomes, total DRMs and immunoisolated SH4 DRMs (TEV eluates) from HeLa S3 cells expressing HASPB SH4-TEV-GFP (denoted as HASPB) or Yes SH4-TEV-GFP (denoted as Yes). The content of each lipid class is presented as a molar percentage of the total lipid (mean ± standard deviation from three independent experiments). The table in Figure 11 B presents also statistical significance of the differences in lipid composition between solubilized microsomes from HeLa S3 HASPB

SH4-TEV-GFP or HeLa S3 Yes-TEV-GFP cells and the respective total DRMs, and between total DRMs and the respective TEV eluates.

A

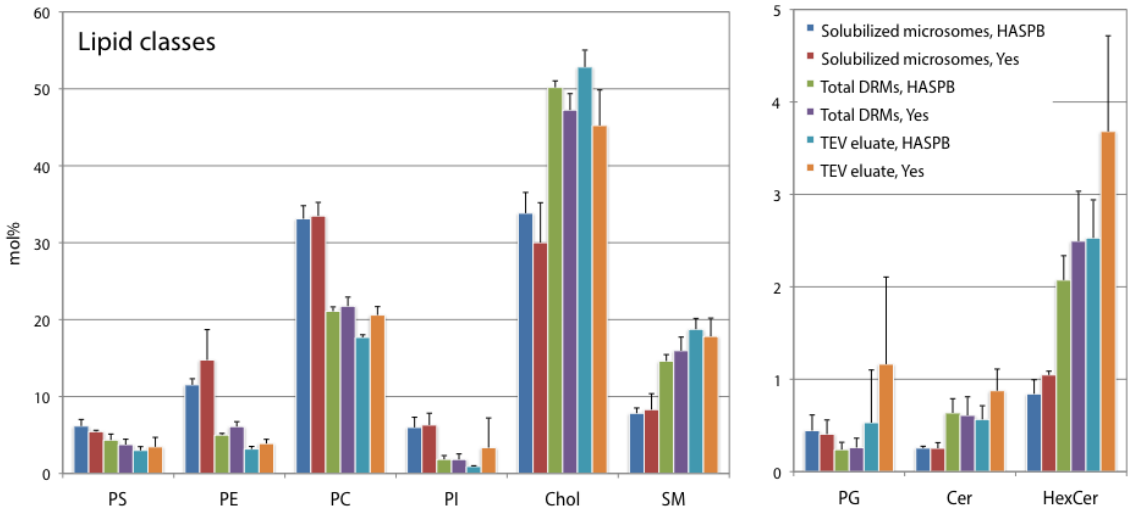

B

	mol% ± SD solubilized microsomes		*p* value solubilized microsomes vs. total DRMs		mol% ± SD total DRMs		*p* value total DRMs vs. TEV eluate		mol% ± SD TEV eluate	
	HASPB	**Yes**	**HASPB**	**Yes**	**HASPB**	**Yes**	**HASPB**	**Yes**	**HASPB**	**Yes**
PS	6.2 ± 0.9	5.4 ± 0.2	**	ns	4.3 ± 0.8	3.8 ± 0.7	ns	ns	3.0 ± 0.5	3.5 ± 1.2
PE	11.5 ± 0.8	14.8 ± 3.9	**	*	5.0 ± 0.2	6.1 ± 0.6	**	*	3.2 ± 0.3	3.9 ± 0.5
PC	33.1 ± 1.7	33.5 ± 1.8	**	*	21.1 ± 0.6	21.7 ± 1.2	*	ns	17.7 ± 0.3	20.6 ± 1.1
PI	6.0 ± 1.3	6.3 ± 1.5	*	*	1.8 ± 0.5	1.8 ± 0.7	ns	ns	0.9 ± 0.1	3.4 ± 3.9
Chol	33.8 ± 2.7	30.0 ± 5.2	**	*	50.2 ± 0.9	47.2 ± 2.1	ns	ns	52.8 ± 2.2	45.2 ± 4.6
SM	7.8 ± 0.7	8.3 ± 2.1	**	*	14.6 ± 0.8	16.0 ± 1.8	*	ns	18.7 ± 1.4	17.8 ± 2.4
PG	0.4 ± 0.2	0.4 ± 0.2	ns	ns	0.2 ± 0.1	0.3 ± 0.1	ns	ns	0.5 ± 0.6	1.2 ± 0.9
Cer	0.3 ± 0.02	0.3 ± 0.1	*	ns	0.6 ± 0.2	0.6 ± 0.2	ns	ns	0.6 ± 0.1	0.9 ± 0.2
HexCer	0.8 ± 0.2	1.0 ± 0.04	*	*	2.1 ± 0.3	2.5 ± 0.5	ns	ns	2.5 ± 0.4	3.7 ± 1.0

Figure 11 Lipid class composition of solubilized microsomes, total Triton X-100 detergent-resistant membranes (DRMs), and immunoisolated SH4 DRMs (TEV eluates) from HeLa S3 cells expressing HASPB SH4-TEV-GFP (denoted as HASPB) or Yes SH4-TEV-GFP (denoted as Yes). (A) The charts show mean molar percentages (mol%) of the total lipid ± standard deviation from three independent experiments. The right chart has an expanded scale to show minor lipid classes. **(B)** The table shows mean mol% of the total lipid ± standard deviation (SD) from three independent experiments, and statistical significance of the differences in lipid composition of solubilized microsomes versus total DRMs, and total DRMs versus TEV eluates (*, $p \leq 0.05$; **, $p \leq 0.01$; ns, $p > 0.05$, paired Student's t-test). PS, phosphatidylserine; PE, phosphatidylethanolamine; PC, phosphatidylcholine; PI, phosphatidylinositol; Chol, cholesterol; SM, sphingomyelin; PG, phosphatidylglycerol; Cer, ceramide; HexCer, hexosylceramide.

The proportion of most lipid classes differed significantly between solubilized microsomal pellets and the respective total DRMs. Total DRMs, compared with solubilized microsomes, had significantly higher levels of cholesterol (1.5 and 1.6 fold higher for HASPB and Yes, respectively), sphingomyelin (SM; 1.9 fold higher for both HASPB and Yes), and hexosylceramide (HexCer; 2.5 and 2.4 fold higher for HASPB and Yes, respectively). Moreover, total DRMs, compared with the respective solubilized microsomes, were found to be significantly depleted in phosphatidylethanolamine (PE; 2.3 and 2.4 fold for HASPB and Yes, respectively), phosphatidylcholine (PC; 1.6 and 1.5 fold, respectively) and phosphatidylinositol (PI; 3.3 and 3.5 fold). Immunoprecipitated DRMs (TEV eluates) from both SH4-TEV-GFP-expressing cell lines had significantly lower levels of PE (1.6 fold for both HASPB and Yes) than the respective total DRMs. What is more, TEV eluates prepared from cells expressing HASPB SH4-TEV-GFP, as compared with total DRMs, were significantly enriched in SM (1.3 fold), and depleted in PC (1.2 fold), whereas the differences between mean molar percentages of PS, PI, cholesterol, phosphatidylglycerol (PG), Cer or HexCer, were not statistically significant (p>0.05). The differences in mean molar percentages of the various lipid classes (except for PE) between total DRMs and immunoisolated SH4 DRMs prepared from Yes SH4-TEV-GFP-expressing cells, were all not statistically significant (Figure 11 B).

Figure 12 depicts relative proportions of saturated, monounsaturated, diunsaturated, as well as tri- and more unsaturated PC species in solubilized microsomes, total DRMs, and immunoisolated DRMs from HeLa S3 cells expressing HASPB SH4-TEV-GFP, presented as mean molar percentages of the total PC ± standard deviation from three independent experiments. Total DRMs, compared with the membranes from which they were isolated, had a significantly higher proportion of saturated PC species (3.2 fold), and moreover, were significantly depleted in diunsaturated, as well as in tri- and more unsaturated PC species (3.3 and 3.2 fold, respectively). In each of the three independent experiments, HASPB SH4 DRMs had a higher percentage of saturated, and a lower percentage of mono- and diunsaturated PC species than the total DRMs from which they were immunoprecipitated. However, these observed differences in the degree of PC saturation between HASPB SH4-containing DRMs and total DRMs were not statistically

significant (Figure 12 B). It seems likely, though, that this lack of significance could be overcome by performing more independent experiments.

A

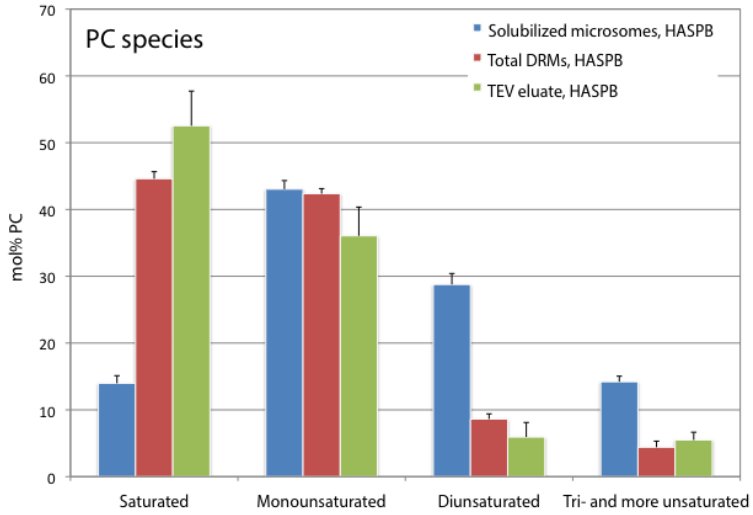

B

	HASPB				
	mol% PC ± SD solubilized microsomes	*p* value solubilized microsomes vs. total DRMs	mol% PC ± SD total DRMs	*p* value total DRMs vs. TEV eluate	mol% PC ± SD TEV eluate
Saturated	14.0 ± 1.1	***	44.6 ± 1.0	ns	52.5 ± 5.2
Monounsaturated	43.0 ± 1.3	ns	42.4 ± 0.8	ns	36.1 ± 4.3
Diunsaturated	28.8 ± 1.6	***	8.6 ± 0.8	ns	5.9 ± 2.2
Tri- and more unsaturated	14.2 ± 0.8	***	4.4 ± 0.9	ns	5.5 ± 1.2

Figure 12 Extent of phosphatidylcholine (PC) saturation in solubilized microsomes, total Triton X-100 detergent-resistant membranes (DRMs), and immunoisolated DRMs (TEV eluates) from HeLa S3 cells expressing HASPB SH4-TEV-GFP (denoted as HASPB). (A) Values presented in the chart are mean molar percentages (mol%) of the total PC ± standard deviation from three independent experiments. **(B)** The table shows mean mol% of the total PC ± standard deviation (SD) from three independent experiments, and significance of the differences between solubilized microsomes versus total DRMs, and total DRMs versus TEV eluate (***, $p \leq 0.001$; ns, $p > 0.05$, paired Student's t-test).

2.3.3 Protein components of immunoaffinity-purified detergent-resistant membranes containing SH4 domain fusion proteins

Proteins present in total Triton X-100 DRMs and in pelleted immunoprecipitated DRMs (i.e. TEV eluates), were partially resolved by 1D-PAGE in precast 10% Bis-Tris gels, stained with Colloidal Coomassie, and then each lane was cut into three pieces, which were individually processed: subjected to reduction, alkylation and digestion with

trypsin, and analyzed by a nano-HPLC system coupled to a nano-ESI-LTQ-Orbitrap mass spectrometer (Dr. Thomas Ruppert, Core Facility for Mass Spectrometry and Proteomics, Heidelberg University Center for Molecular Biology). MS/MS spectra were analyzed using Mascot (Matrix Science; Perkins *et al.*, 1999). Peptide and protein identifications were validated using Scaffold 3 (Proteome Software; Searle, 2010).

Table S1 (Appendix) depicts a list of 177 proteins identified in at least three out of six preparations of total DRMs (i.e. fractions number 2 from OptiPrep DRM gradients), isolated from the three different HeLa S3 cell lines used in this study (two independent preparations for each cell line, all considered together). The table lists also primary subcellular localizations of the identified proteins, and their classification into raft, raft-associated and nonspecific, according to the sensitivity of their presence in Triton X-100 DRMs to cholesterol depletion, as determined for HeLa cells with the use of a SILAC (stable isotope labeling with amino acids in cell culture)-based quantitative proteomic approach, combined with methyl-β-cyclodextrin (MβCD) treatment (Foster *et al.,* 2003; see also section 1.3.2). Out of these 177 proteins, 68% were identified also in Triton X-100 DRMs isolated from HeLa cells in the study by Foster *et al.,* and 51% were among proteins whose degree of sensitivity to MβCD was established in the same study, resulting in their classification into the three above-mentioned groups. In turn, in the study by Foster *et al.,* out of all non-contaminating proteins identified, 53% were classifiable. Out of these, 43% were classified as raft proteins (as compared to 46% in our study), 26% as raft-associated (25% in our study), and finally 31% as nonspecific (i.e. non-raft) proteins (29% in our study). Of the proteins identified by us in at least three out of six preparations of total Triton X-100 DRMs from HeLa S3 cells, 34% are reported to localize primarily to the plasma membrane (Figure 13 A; Table S1, Appendix). A substantial amount of the identified proteins localizes to the nucleus (24%) and to the cytosol (23%). Among the identified DRM proteins were also cytoskeletal (6.8%), mitochondrial (6.2%) and endoplasmic reticulum (4.5%) proteins. The remaining 1.7% localize to lysosomes and peroxisomes (Table S1, Appendix). In the pie chart in Figure 13 B, all identified plasma membrane proteins are classified according to the type of membrane association. As much as almost 30% of them associate with the membrane via lipid anchors, which is a common property among lipid raft proteins (see section 1.4).

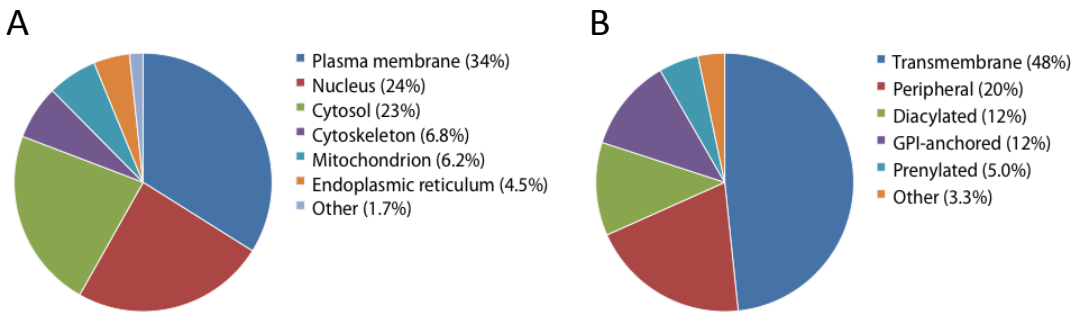

Figure 13 Classification of proteins identified in total Triton X-100 detergent-resistant membranes (DRMs) isolated from HeLa S3 cells (in at least three out of six preparations). Pie charts of the identified proteins classified according to: **(A)** their primary subcellular localization, and **(B)** subclasses of plasma membrane proteins.

Table S2 (Appendix) lists 52 proteins that were identified (i.e. that met criteria for positive protein identification specified in Scaffold 3) in at least one TEV eluate sample out of six (two independent experiments, each performed using the three HeLa S3 cell lines: the control cells and the two SH4-TEV-GFP stable cell lines). The number of proteins identified in the immunoisolates from DRMs prepared from the control cells was 1 and 0 in two different experiments, suggesting that almost no protein was nonspecifically immunoprecipitated in the absence of a SH4-TEV-GFP bait, or that the amounts of the nonspecific proteins were below the sensitivity limit of the mass spectrometer used. In immunoisolates from HeLa S3 HASPB SH4-TEV-GFP DRMs, 12 and 37 proteins were identified, with 9 proteins common for the two experiments. Immunoisolates from HeLa S3 Yes SH4-TEV-GFP DRMs contained 20 and 31 proteins, with 14 overlapping proteins between the two experiments. All of the 9 proteins present in immunoisolated HASPB SH4 DRMs in both experiments were also identified in both immunoisolates from HeLa S3 Yes SH4-TEV-GFP DRMs. Of the proteins identified in at least two out of four preparations of DRMs immunoprecipitated from the total pool using a SH4-TEV-GFP fusion protein as bait (two independent preparations for each HeLa S3 SH4-TEV-GFP cell line, all considered together), 39% are known to localize primarily to the plasma membrane (Figure 14 A; Table S2, Appendix). Out of these, as much as 40% associate with the membrane via lipid anchors (Figure 14 B). Among the proteins identified in at least two out of four preparations of immunoprecipitated SH4 DRMs, there were also cytoskeletal (23%), nuclear (19%), and cytosolic (19%) proteins. Furthermore, 88% of the identified proteins were detected also in Triton X-100 DRMs

isolated from HeLa cells (Foster *et al.*, 2003), and 69% had their degree of sensitivity to MβCD determined. Among those, 67% were classified as raft proteins, 17% as raft-associated, and finally 17% as nonspecific (i.e. non-raft) proteins (Table S2, Appendix).

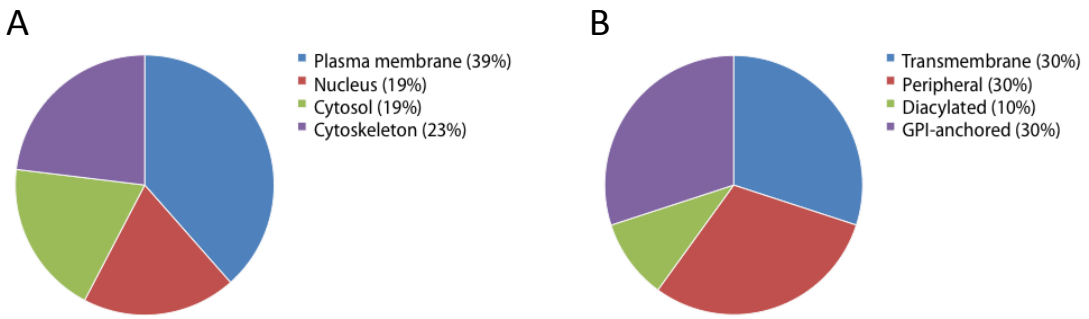

Figure 14 Classification of proteins identified in at least two out of four preparations of detergent-resistant membranes (DRMs) immunoprecipitated from the total DRM pool using a SH4-TEV-GFP fusion protein as bait. Pie charts of the identified proteins classified according to: **(A)** their primary subcellular localization, and **(B)** subclasses of plasma membrane proteins.

We decided to compare the relative abundances of proteins in immunoprecipitated and total DRMs. We expected that proteins which preferentially associate with membrane environments of diacylated SH4 domain proteins would be enriched over total DRMs. Conversely, we would expect non-raft proteins nonspecifically copurifying with DRMs, to be depleted as compared to the total DRM pool. Finally, raft proteins which do not preferentially associate with membrane environments surrounding SH4 domain fusion proteins, should be either unchanged or depleted relative to total DRMs. To estimate relative amounts of the proteins identified in immunoprecipitated DRMs as compared to total DRMs, we employed two different methods of label-free mass spectrometry-based protein quantification. The first method entails calculating the exponentially modified protein abundance index (emPAI), equal to 10^{PAI}–1, where PAI is defined as the number of peptides detected for a given protein, divided by the theoretical number of tryptic peptides for this protein (Ishihama *et al.,* 2005). EmPAI was shown to be directly proportional to protein content, allowing for estimating both the absolute and relative protein abundance. The number of identified peptides for each protein in each sample was exported from Scaffold 3, and the number of theoretically observable tryptic peptides for each protein was calculated using Protein Digestion Simulator. The

calculated emPAI values were normalized for different protein amounts in each of the samples using data from mass spectrometry lipid analysis, assuming that the amounts of total lipid correspond to total protein amounts. Relative abundance of each protein in immunoisolated DRMs and the respective total DRMs was then calculated by comparing its normalized emPAI values in the two samples. In the other method used here, relative protein quantification is based on the integration of liquid chromatography-mass spectrometry (LC-MS) ion chromatograms. In each MS scan, peptide ions with a particular m/z (mass-to-charge ratio) values are detected with a particular signal intensity. Coupling MS with LC introduces a retention time dimension. Thus, during LC-MS experiments, peptide peaks are detected as three-dimensional objects in m/z, signal intensity and retention time space (Zhang *et al.,* 2010). The intensities of these three-dimensional peptide peak hills in LC-MS ion chromatograms are integrated, and used as a measure of quantity, as the signal intensity from electrospray ionization corresponds to ion concentration (Voyksner *et al.*, 1999), and therefore relative amounts of a peptide can be determined by comparing its integrated peak areas in different samples. Integrated areas of LC-MS peptide peaks were calculated with the use of MaxQuant software (Cox *et al.*, 2008). For each protein, 2 or 3 most intense peptides were chosen, and their ratios between peak areas in TEV eluates and in the respective total DRMs were calculated and then averaged, to obtain protein ratios. To correct for unequal protein amounts between samples, based on the assumption that the lipid/protein ratio is constant across all of them, the calculated protein ratios were normalized using data on amounts of total lipid, acquired using lipid mass spectrometry. For each protein identified in at least one TEV eluate sample, enrichment factors relative to the respective total DRMs, calculated using the two above-mentioned label-free quantitative proteomic methods, are listed in Table S2 (Appendix). The direction of change (assuming: depleted, values ≤0.5; unchanged, between 0.5 and 2; enriched, ≥2) was consistent between the two methods of calculation for almost 60% of value pairs. For none of the pairs did one value indicate depletion, and the other, enrichment (Table S2, Appendix). As expected, proteins which were the most abundant in immunoisolated DRMs, were not necessary also the most enriched, as exemplified by actin, cytoplasmic 2, the most abundant protein (i.e. with the highest emPAI value) in each preparation of immunoprecipitated SH4 DRMs, which, however, was not among the most enriched

proteins (as indicated by emPAI enrichment factors). Similarly, tubulin beta chain was more abundant than many other proteins, but was among proteins with the lowest enrichment factors (Table S2, Appendix).

We decided to select a subset of proteins identified in immunoisolated SH4 DRMs, and validate their enrichment factors over total DRMs calculated by label-free quantitative proteomic methods, with the use of quantitative Western blotting. We chose proteins that were consistently present in total DRMs (i.e. that were identified in at least three out of six preparations of total DRMs; see Table S1 in Appendix). Three of the selected proteins: moesin, non-POU domain-containing octamer-binding protein (NONO), and splicing factor, proline- and glutamine-rich (SFPQ), were among the proteins identified in immunoisolated HASPB SH4-containing DRMs and Yes SH4-containing DRMs in both experiments (Table S2, Appendix). NONO and SFPQ were consistently enriched in the immunoisolated SH4 DRMs, having one of the highest enrichment factors (according to both methods of quantification; Table S2, Appendix). Most of the selected proteins are known to localize primarily to the plasma membrane, namely: brain acid soluble protein 1 (BASP1), flotillin-1, moesin, Ras GTPase-activating-like protein (IQGAP1), and Yes (Table S1 and Table S2, Appendix). The remaining two proteins (NONO and SFPQ) localize primarily to the nucleus. Among the chosen proteins were those whose presence in DRMs was previously shown (Foster *et al.,* 2003; see also section 1.3.2) to be highly sensitive to cholesterol depletion, termed as raft proteins (moesin, SFPQ, and the well-established lipid raft markers, flotillin-1 and Yes), or moderately sensitive, termed as raft-associated (IQGAP1) (Table S1 and Table S2, Appendix). Sensitivity of BASP1 and NONO was not determined in the study by Foster *et al*. There are, however, other studies which support lipid raft association of BASP1 (Khan *et al.*, 2003). With the aim of performing quantitative Western blot analysis, two further immunoisolation experiments were carried out, each using the control HeLa S3 cells, and the two SH4-TEV-GFP cell lines. Figure 15 depicts the distribution of the selected proteins across DRM gradients, whose fractions number 2 were used for subsequent immunoprecipitation in one of the two experiments. The proportion of protein present in floating (i.e. DRM) fractions, in the case of SFPQ, moesin, NONO and BASP1, was

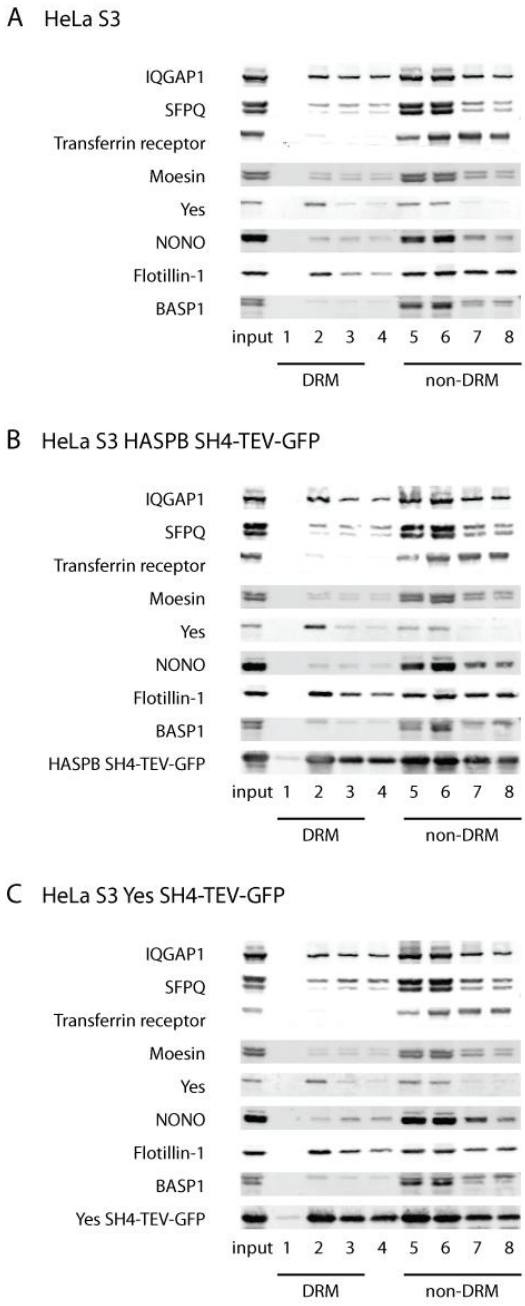

Figure 15 Distribution of selected proteins across DRM gradients. HeLa S3 cells **(A)** that do not express any SH4-TEV-GFP fusion protein, and stable cell lines expressing **(B)** HASPB SH4-TEV-GFP or **(C)** Yes SH4-TEV-GFP in a doxycycline-inducible manner, were grown in suspension. Expression of the fusion proteins was induced with 1 µg/ml doxycycline for 48 hours. Upon cell disruption with the use of nitrogen cavitation, and several rounds of differential centrifugation, microsomal membranes were obtained, which was followed by their extraction with 1% Triton X-100 in MBS buffer and flotation on OptiPrep step density gradients (40/28/0%). Eight fractions were collected from the top, and an aliquot of each was analyzed by Western blotting, together with an aliquot of solubilized microsomes (denoted as input). Yes and flotillin-1 were used as DRM markers, transferrin receptor was used as a non-DRM marker. IQGAP1, Ras GTPase-activating-like protein; SFPQ, splicing factor, proline- and glutamine-rich; NONO, non-POU domain-containing octamer-binding protein; BASP1, brain acid soluble protein 1.

much smaller than for the well-established lipid raft markers, flotillin-1 and Yes, and than for both SH4-TEV-GFP fusion proteins, with the proportion for IQGAP1 being intermediate (Figure 15).

Figure 16 depicts one out of two Western blots used for calculating the abundance of the selected proteins in immunoisolated DRMs (TEV eluates) relative to total DRMs. Assuming a constant lipid/protein ratio across all samples, we used mass spectrometry data on amounts of total lipid in each sample to analyze equal amounts of lipid (and thus protein) from each sample (and also five times the amount for total DRMs).

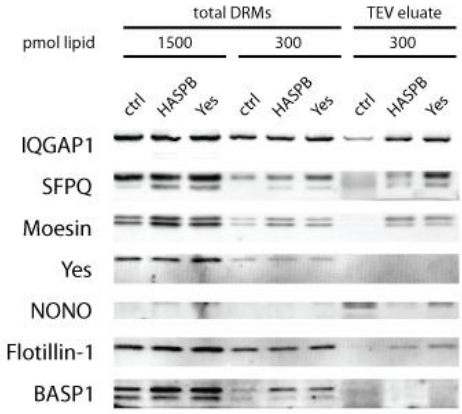

Figure 16 Western blot analysis of total Triton X-100 detergent-resistant membranes (DRMs) and immunoisolated DRMs (TEV eluates). DRMs were prepared from HeLa S3 cell lines stably expressing HASPB SH4-TEV-GFP (denoted as HASPB), Yes SH4-TEV-GFP (denoted as Yes), or from control cells (HeLa S3 cells that do not express any SH4-TEV-GFP fusion protein, denoted as ctrl), and served as input for immunoprecipitation with the use of anti-GFP antibodies coupled to magnetic beads, which was followed by tobacco etch virus (TEV) protease cleavage to elute bound SH4 DRMs (yielding TEV eluates). Assuming a constant lipid/protein ratio across all samples, we used mass spectrometry data on amounts of total lipid to analyze equal amounts of lipid (and thus protein) from each sample (and also five times the amount for total DRMs). Western blot band intensities were used for calculating enrichment factors of the indicated proteins in TEV eluates as compared to the respective total DRMs. IQGAP1, Ras GTPase-activating-like protein; SFPQ, splicing factor, proline- and glutamine-rich; NONO, non-POU domain-containing octamer-binding protein; BASP1, brain acid soluble protein 1.

Enrichment factors were calculated as the ratio between Western blot band intensities (adjusted to equal lipid amounts) in TEV eluate and in the respective total DRMs, and are listed in Table 1, together with the enrichment factors calculated for the two

preceding experiments using the above-mentioned label-free quantitative proteomic methods. Moreover, the detected Western blot band intensities in TEV eluates were adjusted to the yield of total lipid in the whole sample amount, thus obtaining values that reflect the total amounts of each protein in each TEV eluate. For each protein, the values for SH4 TEV eluates were compared to the value for the control TEV eluate, obtaining ratios, which are listed in Table 1. Consistent with quantitative proteomic results, Western blot-based quantification showed depletion of BASP1, and lack of enrichment of flotillin-1 and Yes in the immunoisolated SH4 domain-containing DRMs, as well as enrichment of NONO and SFPQ in most samples of SH4 DRMs (Table 1). Enrichment factor values for moesin were not consistent either between experiments, or between HASPB and Yes SH4 DRMs, as already observed for mass spectrometry-based quantification. IQGAP1 seemed to be neither depleted nor enriched, unlike what we previously observed. Again, unlike for mass spectrometry results, most of the proteins probed for were detected also in TEV eluates from control cells, and were thus nonspecifically isolated in the absence of any SH4-TEV-GFP bait. As already mentioned, the results for NONO and SFPQ seem in agreement with their enrichment in the immunoprecipitated SH4 DRMs, as compared to total DRMs. However, their enrichment in the control immunoprecipitates is, in most cases, even higher than in the immunoisolated SH4 DRMs, which suggests that at least some amounts of both proteins bind to the affinity matrix nonspecifically, possibly as soluble contaminants of DRM preparations, and nonspecifically detach during TEV cleavage. Similar or even higher total amounts of NONO and SFPQ were recovered in the control TEV eluates, compared to SH4 TEV eluates (Table 1), which suggests that the apparent high enrichment of both proteins in SH4 TEV eluates may in fact be due to nonspecific isolation of the two proteins, and not due to their preferential association with membrane environments surrounding SH4 domain fusion proteins.

Protein name	Enrichment factor TEV eluate/ total DRMs (emPAI)						Enrichment factor TEV eluate/ total DRMs (peak area)						Enrichment factor TEV eluate/ total DRMs (Western blot)						Total amount TEV eluate SH4/ total amount TEV eluate ctrl (Western blot)			
	ctrl		HASPB		Yes		ctrl		HASPB		Yes		ctrl		HASPB		Yes		HASPB		Yes	
	Experiment No.						Experiment No.						Experiment No.						Experiment No.			
	1	2	1	2	1	2	1	2	1	2	1	2	1	2	1	2	1	2	1	2	1	2
Brain acid soluble protein 1				0.2						0.7			<1.0	<1.0	<0.4	<0.2	<0.4	<0.4				
Flotillin-1				0.4						0.7			<0.3	0.7	0.3	0.4	0.5	0.8	>5.8	10.9	>3.4	4.0
Moesin			1.0	0.8	0.9	7.0				2.0	1.4	10.2	0.1	1.0	1.0	0.4	1.3	11.7	196.5	2.1	57.2	3.8
Non-POU domain-containing octamer-binding protein			17.5	18.7	46.5	56.3				15.0	6.2	26.9	32.5	9.5	3.1	1.3	14.4	7.6	0.7	0.5	1.5	1.0
Ras GTPase-activating-like protein IQGAP1				12.6	0.4	8.2			0.9	13.3	1.7	5.7	0.3	1.5	0.8	1.0	0.8	1.4	14.0	6.9	6.1	1.7
Splicing factor, proline- and glutamine-rich			1.8	2.1	6.8	29.3				1.7	5.2	24.7	1.9	16.5	1.5	2.0	2.4	8.4	7.3	0.6	7.9	0.7
Tyrosine-protein kinase Yes *										0.6			<1.0	<1.0	<0.8	0.4	<1.0	0.7		>8.1		>2.5

* in TEV eluates, Yes did not fulfill the criteria for positive protein identification specified in Scaffold 3, but was nevertheless included in quantitative Western blot analysis

Table 1 Selected proteins identified in TEV eluates (i.e. immunoisolated detergent-resistant membranes, DRMs), together with their enrichment factors over total Triton X-100 DRMs. Total DRMs prepared from HeLa S3 cell lines stably expressing HASPB SH4-TEV-GFP (denoted as HASPB), Yes SH4-TEV-GFP (denoted as Yes), or from control cells (HeLa S3 cells that do not express any SH4-TEV-GFP fusion protein, denoted as ctrl), were incubated with anti-GFP antibodies coupled to magnetic beads, which was followed by tobacco etch virus (TEV) protease cleavage to elute bound SH4 DRMs (yielding TEV eluates). Listed are enrichment factors of the selected proteins in TEV eluates relative to the respective total DRMs, calculated using two label-free quantitative proteomic methods (based on the comparison of exponentially modified protein abundance index (emPAI) values, and on the comparison of integrated areas of liquid chromatography-mass spectrometry (LC-MS) peptide peaks between samples), and using quantitative Western blotting. To correct for unequal protein amounts between samples, based on the assumption that the lipid/protein ratio is constant across all of them, we used mass spectrometry data on amounts of total lipid in each sample either to normalize protein ratios calculated using label-free quantitative proteomic methods, or to analyze equal amounts of protein by Western blotting. Label-free quantification with both methods was performed using the same dataset (two experiments, each for the three cell lines), whereas for quantitative Western blotting two further experiments were used. For those proteins that were only detected in a TEV eluate (and not in the respective total DRMs), the missing emPAI values were replaced by minimal emPAI values (calculated for 1 observed unique spectrum), allowing us to calculate minimal enrichment factors (underlined). Listed are also ratios between total amounts of each protein in SH4 TEV eluates and in the control TEV eluate, calculated based on Western blot band intensities and data on the yield of total lipid in the whole sample amount. Blank cells indicate that values could not be calculated.

3 Discussion I

3.1 Generation and characterization of human cell lines stably expressing SH4 domain fusion proteins

With the aim of characterizing lipid and protein environment of diacylated SH4 domain proteins associated with lipid rafts, we decided to specifically immunoisolate from human cells detergent-resistant membranes (DRMs) that contain SH4 domain fusion proteins, and analyze their components. SH4 domains, derived either from *Leishmania major* hydrophilic acylated surface protein B (HASPB) or from human Src kinase Yes, were fused to the N-terminus of GFP (to be used as an affinity tag), with a TEV protease cleavage site in between (Figure 1), to allow for specific elution of the immunoisolated DRMs from the affinity matrix. Clonal cell lines of suspension HeLa (HeLa S3) cells were generated, stably and inducibly expressing HASPB SH4-TEV-GFP or Yes SH4-TEV-GFP. The expression level of the fusion proteins was low in the absence of doxycycline, and in its presence, high and very similar for both clonal cell lines (Figure 3, B and F). In agreement with what was previously reported for similar constructs expressed in HeLa or CHO cells (Stegmayer *et al.*, 2005; Tournaviti *et al.*, 2007; Ritzerfeld, 2009; Tournaviti *et al.*, 2009; Ritzerfeld *et al.*, 2011), both fusion proteins localized mainly to the plasma membrane of HeLa S3 cells, with smaller amounts in the perinuclear region (Figure 5, B and F), and were present in DRM fractions (Figure 7, A and C). Thus, the use of the two SH4 domain fusion proteins should allow for immunoisolation of DRMs derived from lipid rafts localized predominantly to the plasma membrane. In contrast, palmitoylation-deficient mutant, HASPB SH4 Δpal-TEV-GFP, was retained at intracellular membranes (Figure 5, C, D), and was absent from DRM fractions (Figure 7 B), indicating that plasma membrane targeting of HASPB SH4-TEV-GFP and its association with DRMs, are dependent on palmitoylation, as reported previously for similar constructs expressed in HeLa or CHO cells (Stegmayer *et al.*, 2005; Tournaviti *et al.*, 2007; Ritzerfeld, 2009; Tournaviti *et al.*, 2009; Ritzerfeld *et al.*, 2011).

3.2 Immunoaffinity purification of detergent-resistant membranes containing SH4 domain fusion proteins

The two clonal HeLa S3 SH4-TEV-GFP cell lines, as well as control HeLa S3 cells (HeLa S3 cells that do not express any SH4-TEV-GFP fusion protein), were grown in suspension. Upon cell disruption and several rounds of differential centrifugation, microsomal membranes were obtained, which was followed by their extraction with 1% Triton X-100 and flotation on OptiPrep step density gradients (Figure 8). The resulting floating (DRM) fractions were relatively enriched in lipid raft markers, and depleted in non-raft plasma membrane, Golgi and ER markers (Figure 9; Figure 10). The low-density fraction with the highest content of the SH4 domain fusion proteins, or the corresponding fraction from the control cells (denoted as total Triton X-100 DRMs), served as input for immunoprecipitation with the use of anti-GFP antibodies coupled to magnetic beads, which was followed by TEV protease cleavage, to elute the immunoisolated DRMs. Both the binding of the SH4-TEV-GFP fusion proteins to the affinity matrix, and their subsequent cleavage, were efficient (Figure 9; Figure 10), and the resulting SH4 TEV eluate contained lipid raft markers (analyzed only for HASPB; Figure 10), suggesting that SH4 DRMs were successfully immunoisolated and eluted from the affinity matrix.

3.2.1 Lipid components of immunoaffinity-purified detergent-resistant membranes containing SH4 domain fusion proteins

Total Triton X-100 DRMs from HeLa S3 cells, as compared to membranes from which they were isolated, were enriched in cholesterol, sphingomyelin (SM) and hexosylceramide (HexCer), and depleted in phosphatidylethanolamine (PE), phosphatidylcholine (PC) and phosphatidylinositol (PI) (Figure 11). Moreover, the former had a significantly higher proportion of saturated PC species, and a significantly lower proportion of diunsaturated, as well as tri- and more unsaturated PC species (Figure 12). This is consistent with previous studies, which reported the lipid composition of DRMs prepared by extraction of whole CHO or MDCK cells with 1% or 0.5% Triton X-100, respectively, and subsequent flotation on linear or step sucrose density gradients (Pike *et al.*, 2005; Delaunay *et al.*, 2008). Even though the protocols used were different than the one employed in our study, the floating fractions were also depleted in PE, PC and

PI, and more importantly, enriched in cholesterol, SM, and saturated phospholipids, relative to the starting material (PNS or lysate). DRMs immunoaffinity-purified using HASPB SH4-TEV-GFP as bait, exhibited statistically significant depletion in PE and PC, and enrichment in SM, with no significant difference in the amounts of phosphatidylserine (PS), PI, cholesterol, phosphatidylglycerol (PG), ceramide (Cer) and HexCer, relative to the input for immunoprecipitation, i.e. total DRMs (Figure 11). Thus, immunoisolated HASPB SH4 DRMs have a lipid composition that is distinct from that of the total population of detergent-resistant membranes, and therefore seem to be a subset of total DRMs. This may suggest that *in vivo*, HASPB SH4-TEV-GFP associates with a specific subset of lipid rafts. It seems likely that our inability to detect statistically significant differences in lipid composition between Yes SH4 DRMs and total DRMs (except for the depletion in PE in the case of the former), may be due to low total lipid yields for Yes SH4 DRMs, and the consequent high contribution of nonspecific lipid background to the observed composition. Nevertheless, our results for HASPB SH4 DRMs indicate that the heterogeneity of lipid rafts can be appreciated also using the DRM approach, which is in agreement with what was reported previously, however for a milder nonionic detergent, namely Brij 96 (Brügger *et al.,* 2004). In the study by Brügger and co-workers, the total pool of DRMs prepared from the rat brain was used to immunoaffinity purify DRMs containing either of the two GPI-anchored proteins: prion protein (PrP) or Thy-1. Not only were the two proteins present in different domains on the neuronal surface, but also the immunopurified PrP and Thy-1 DRMs differed in lipid composition from each other, and from the total DRM pool. This suggested that the immunopurified DRMs contained specific lipid environments surrounding the two proteins, which indicates, in agreement with the results of our study, that the detergent approach does not preclude immunoisolation of specific membrane micro-environments.

3.2.2 Protein components of immunoaffinity-purified detergent-resistant membranes containing SH4 domain fusion proteins

Out of proteins present in at least half of the preparations of total Triton X-100 DRMs isolated from HeLa S3 cells (Table S1, Appendix), almost 70% were identified also in Triton X-100 DRMs from HeLa cells in the study by Mann and co-workers (Foster *et al.*, 2003). This high overlap is remarkable, considering the fact that the exact protocol for

the preparation of DRMs influences the identified proteome, and the two protocols were different, as were the cell lines used (suspension versus adherent HeLa cells). In our study, DRMs were isolated from pelleted microsomal membranes, using flotation on an OptiPrep step density gradient (40/28/0%), as compared to extraction of whole cells and subsequent flotation on a sucrose step density gradient (45/35/5%) in the other study. Out of the DRM proteins in both studies that were classifiable into raft, raft-associated and nonspecific (non-raft), similar proportions belonged to each of the three groups, namely about 45%, 25% and 30%, respectively, which suggests that the purity of DRM preparations was similar between our study and the benchmark study by Mann and co-workers.

Lipid rafts are microdomains of the plasma membrane, believed to be assembled in the Golgi complex (Simons *et al.,* 1997). Therefore, we would expect to identify in DRMs mainly proteins that localize to these two compartments. However, only 34% of the identified proteins localize primarily to the plasma membrane (Figure 13 A; Table S1, Appendix). The primary cellular locations of the remaining proteins (e.g. the nucleus, mitochondrion, ER) are not expected to contain lipid rafts. The presence of these proteins in DRMs may therefore solely reflect the well-known inability to purify membrane microdomains to homogeneity. However, among the identified proteins may also be 'moonlighting' proteins which reside in more than one subcellular location (having different functions at each one of them), the secondary localization being lipid rafts. In agreement with this, the presence in DRMs of some of the proteins whose primary localization is not the plasma membrane, is highly or moderately sensitive to cholesterol depletion (Table S1, Appendix), which suggests that they are *bona fide* raft components. The presence in DRMs of cytoskeletal proteins is in agreement with the previous finding that raft patches formed by the GPI-anchored protein CD59 or the ganglioside GM1 accumulate actin filaments, indicating an interaction of actin cytoskeleton with lipid rafts (Harder *et al.*, 1999). This corresponds to the results by Mann and co-workers which showed moderate sensitivity of major cytoskeletal components to cholesterol depletion (Foster *et al*., 2003).

We analyzed the distribution of several of the identified proteins across DRM gradients. For most of them (SFPQ, moesin, NONO and BASP1), the proportion of protein present in floating (i.e. DRM) fractions was much smaller than for the well-established lipid raft markers, Yes and flotillin-1 (Figure 15). Triton X-100, the most commonly used nonionic detergent for isolating DRMs, is one of the most stringent, and therefore also one of the most reliable detergents (Schuck *et al.*, 2003). It can however solubilize more loosely associated raft proteins. It is therefore possible that a significantly higher proportion of the above-mentioned proteins would be recovered in the floating fractions, if a less stringent detergent was used. Alternatively, the presence of only small amounts of a protein in DRM fractions may reflect its transient association with lipid rafts, or its primary residence in other subcellular locations, with rafts being the secondary localization.

Among the proteins identified in at least half of the preparations of immunoprecipitated SH4 DRMs, 39% are known to localize primarily to the plasma membrane, as compared to 34% in the case of total DRMs (Figure 13 A; Figure 14 A; Table S1 and Table S2, Appendix). Moreover, out of the plasma membrane proteins in total DRMs and immunopurified SH4 DRMs, 28% and 40%, respectively, associate with the membrane via lipid anchors (Figure 13 B; Figure 14 B). Finally, out of the proteins in immunoprecipitated SH4 DRMs whose sensitivity to cholesterol depletion is known (Foster *et al.,* 2003), 83% were highly or moderately sensitive, as compared to 71% in the case of total DRMs (Table S1 and Table S2, Appendix). These results suggest that our immunoaffinity purification approach enriches for *bona fide* raft proteins.

To estimate relative amounts of the identified proteins in immunoprecipitated SH4 DRMs, as compared to total DRMs, we employed two different methods of label-free mass spectrometry (MS)-based protein quantification: based on the comparison of exponentially modified protein abundance index (emPAI) values, and based on the comparison of integrated areas of liquid chromatography-mass spectrometry (LC-MS) peptide peaks between samples (Table S2, Appendix). We selected several proteins to validate their enrichment using quantitative Western blotting. The obtained values corresponded fairly well with the MS-based enrichment factors (Table 1). However,

whereas almost no proteins were identified by MS in the immunoisolates from control cells (Table S2, Appendix), we were able to detect the majority of proteins probed for by Western blotting (Figure 16; Table 1), which indicates their nonspecific isolation in the absence of a SH4-TEV-GFP bait. Total amounts of flotillin-1, IQGAP1 and Yes, recovered in the control immunoprecipitates, were much lower than in the immunoisolated SH4 DRMs (Table 1), which may indicate their specific copurification with SH4 DRMs, and thus association with membrane environments of SH4 domain fusion proteins, however, not preferential, as indicated by their lack of enrichment in SH4 DRMs over the total DRM pool. For NONO and SFPQ, the total amounts of protein immunoisolated in the presence and absence of a SH4-TEV-GFP bait seemed similar, suggesting that their apparent enrichment in SH4 DRMs may be due to nonspecific isolation, which could explain their high enrichment factors observed also for the control. We thus did not confirm any of the selected proteins to be specifically enriched, and thus to preferentially associate with membrane environments of SH4 domain fusion proteins, which, however, does not preclude the presence of such proteins among all identified in SH4 DRMs. The absence of enrichment of endogenous Yes kinase in Yes SH4 DRMs may point out to the difference in raft partitioning of full-length Yes and Yes SH4-TEV-GFP. It seems conceivable that the identity of lipid rafts in which a protein resides could be controlled also by interactions conferred by domains distal from the SH4 domain. In our model system however, membrane micro-localization is determined only by dual fatty acylation with myristate and palmitate.

4 Results II

In a whole-genome primary RNAi screen aimed at identifying factors involved in the transport of diacylated SH4 domain proteins to the plasma membrane, and subsequently in a validation screen, which used independent siRNAs (both performed by Julia Ritzerfeld; Ritzerfeld, 2009; Ritzerfeld *et al.*, 2011), the most clear-cut hit phenotypes (increased perinuclear localization of HASPB SH4-GFP) were exhibited after knockdowns of α- and β-COP, two subunits of the heptameric coatomer (COPI) protein complex, which coats vesicles that mediate retrograde transport from the *cis*-Golgi to the ER, as well as retrograde and possibly anterograde transport across the Golgi stack (Beck *et al.,* 2009; Popoff *et al.,* 2011; see also section 1.1). The effect of down-regulation of the two coatomer subunits on the localization of Yes SH4-mCherry was less pronounced. Further analyses showed that knockdowns of other coatomer subunits, β' and δ, also result in a pronounced increase in perinuclear accumulation of HASPB SH4-GFP, with a milder effect on the localization of Yes SH4-mCherry (Ritzerfeld, 2009; Ritzerfeld *et al.*, 2011). Moreover, microinjection of recombinant coatomer complex prevented the increased perinuclear accumulation of HASPB SH4-mCherry in β-COP knockdown cells (Ritzerfeld *et al.*, 2011). We intended to investigate the apparent role of coatomer, as well as of the secretory pathway in general, in the plasma membrane transport of diacylated SH4 domain proteins.

4.1 Analysis of subcellular localization of a HASPB SH4 domain fusion protein and a VSVG fusion protein upon β-COP knockdown

We analyzed the subcellular localization of a HASPB SH4 domain fusion protein upon siRNA-mediated knockdown of the β subunit of the COPI coatomer complex, as compared to scrambled siRNA-transfected cells. HeLa cell line stably expressing HASPB SH4-mCherry in a doxycycline-inducible manner (Ritzerfeld, 2009; Ritzerfeld *et al.*, 2011) was transfected with a scrambled siRNA or an siRNA targeting β-COP, using Oligofectamine. 48 hours upon transfection (20 hours upon the induction with 1 μg/ml doxycycline) the cells were imaged using live-cell confocal microscopy, by collecting Z stacks. Magnitude of perinuclear accumulation of HASPB SH4-mCherry upon the siRNA

transfections was determined by intensity quantification of sum intensity projections of Z stack images (Figure 17, A, B; each image represents a sum intensity projection of one Z stack). In agreement with what was previously reported for HASPB SH4-GFP (Ritzerfeld, 2009; Ritzerfeld *et al.*, 2011), there was an increase in perinuclear localization of HASPB SH4-mCherry upon β-COP knockdown, which was highly statistically significant ($p \leq 0.0001$, unpaired Student's t-test; Figure 17 C).

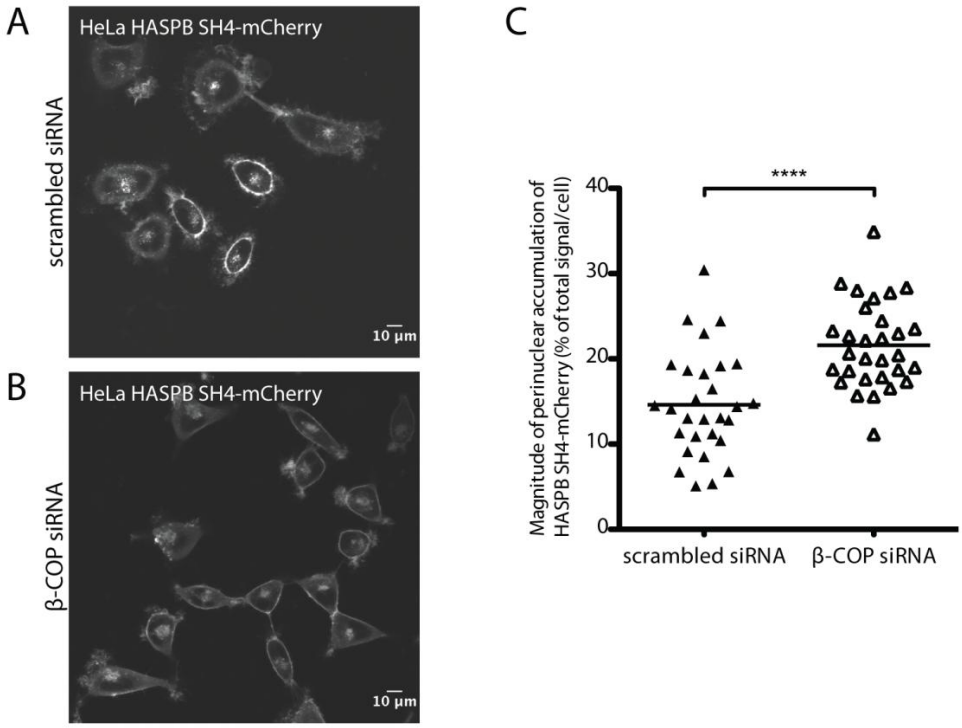

Figure 17 Quantitative analysis of subcellular localization of a HASPB SH4 domain fusion protein (HASPB SH4-mCherry) upon siRNA knockdown of the β subunit of the COPI coatomer complex (β-COP). HeLa cell line stably expressing HASPB SH4-mCherry in a doxycycline-inducible manner was transfected with a scrambled siRNA or an siRNA targeting β-COP, using Oligofectamine. 48 hours upon transfection (20 hours upon the induction with 1 µg/ml doxycycline) the cells were imaged using live-cell confocal microscopy, by collecting Z stacks (objective 40x). **(A, B)** Each image represents a sum intensity projection of Z stack images. Scale bar, 10 µm. **(C)** Magnitude of perinuclear accumulation of HASPB SH4-mCherry upon transfection with a scrambled or β-COP siRNA, determined by intensity quantification of sum intensity projections of Z stacks. Perinuclear accumulation per cell is expressed as the percentage of perinuclear signal respective to the total signal per cell. Values for individual cells are depicted as triangles, horizontal bars represent arithmetic means for each condition; ****, $p \leq 0.0001$, unpaired Student's t-test.

Next, we analyzed the subcellular localization under control and β-COP knockdown conditions of a model transmembrane glycoprotein commonly used to study the transport through the secretory pathway, vesicular stomatitis virus glycoprotein (VSVG;

Tisdale *et al.*, 1992), and compared it to the localization of a HASPB SH4 domain fusion protein. HeLa MCAT-TAM2 cells were transfected with a scrambled siRNA or an siRNA targeting β-COP, using Oligofectamine. 24 hours later the cells were cotransfected with pEGFP-N1/VSVG-SP (Keller *et al.*, 2001; courtesy of Prof. Dr. Kai Simons, Max Planck Institute of Molecular Cell Biology and Genetics, Dresden; SP, long spacer arm between VSVG and GFP) and pRevTRE2/HASPB SH4-mCherry (Ritzerfeld, 2009), using FuGENE HD transfection reagent. 45 hours upon siRNA transfection (18 hours upon the induction with 1 µg/ml doxycycline) the cells were imaged using live-cell confocal microscopy.

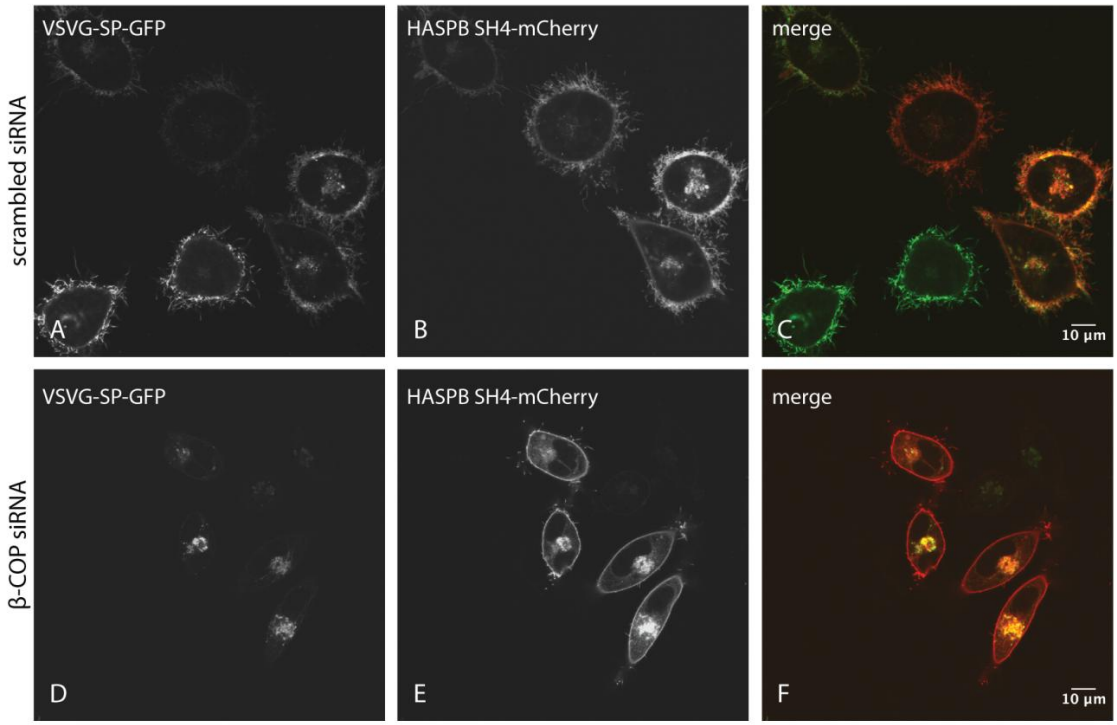

Figure 18 Analysis of subcellular localization of a vesicular stomatitis virus G protein fusion protein (VSVG-SP-GFP) upon siRNA knockdown of the β subunit of the COPI coatomer complex (β-COP), as compared to the localization of a HASPB SH4 domain fusion protein (HASPB SH4-mCherry). HeLa MCAT-TAM2 cells were transfected with a scrambled siRNA or an siRNA targeting β-COP, using Oligofectamine. 24 hours later the cells were cotransfected with pEGFP-N1/VSVG-SP and pRevTRE2/HASPB SH4-mCherry, using FuGENE HD transfection reagent. 45 hours upon siRNA transfection (18 hours upon the induction with 1 µg/ml doxycycline) the cells were imaged using live-cell confocal microscopy (objective 63x). Scale bar, 10 µm.

In scrambled siRNA-transfected cells, both VSVG-SP-GFP and HASPB SH4-mCherry localized to the plasma membrane and perinuclear membranes (Figure 18, A-C). In β-COP-depleted cells, however, we could observe complete intracellular retention of

VSVG-SP-GFP (Figure 18 D), in contrast to HASPB SH4-mCherry, which as previously observed (Figure 17 B; Ritzerfeld, 2009; Ritzerfeld *et al.*, 2011), except for exhibiting increased perinuclear localization, was also found at the plasma membrane (Figure 18 E).

4.2 Analysis of subcellular localization of a HASPB SH4 domain fusion protein and a VSVG fusion protein upon coexpression with Arf1 Q71L

We decided to examine whether the subcellular localization of a HASPB SH4 domain fusion protein is dependent not only on β-COP, but also on ADP-ribosylation factor 1 (Arf1), a small GTPase that controls the biogenesis of COPI vesicles by playing a role in recruitment of coatomer, uptake of cargo proteins, and finally, in scission and uncoating of the vesicles (Beck *et al.,* 2009; Popoff *et al.,* 2011). We analyzed the subcellular localization of HASPB SH4-mCherry upon its coexpression with the wild-type (WT) Arf1, or its trans-dominant constitutively active (i.e. GTP-bound) mutant (Q71L), known to cause stable association of coatomer with the Golgi complex (Dascher *et al*., 1994; Teal *et al.*, 1994), and to inhibit transport through the secretory pathway, both ER to *medial*-Golgi and intra-Golgi (Dascher *et al.,* 1994; Zhang *et al.,* 1994). HeLa MCAT-TAM2 cells were cotransfected in the presence of 4 μg/ml doxycycline, using FuGENE HD transfection reagent, with pRevTRE2/HASPB SH4-mCherry and pIRES2-EGFP/Arf1 (WT or Q71L; courtesy of Prof. Dr. Felix Wieland, Heidelberg University Biochemistry Center), a bicistronic vector coexpressing Arf1 and GFP. The cells were imaged 18 hours after transfection using live-cell confocal microscopy (Figure 19 A). We analyzed also the subcellular localization of a VSVG fusion protein (VSVG-SP-mRFP) upon its coexpression with the wild-type Arf1, or its Q71L mutant. HeLa MCAT-TAM2 cells were cotransfected with pIRES2-EGFP/Arf1 (WT or Q71L) and pmRFP-N1/VSVG-SP (courtesy of Prof. Dr. Kai Simons) using FuGENE HD transfection reagent, and imaged 20 hours after transfection with the use of live-cell confocal microscopy (Figure 19 B). Both HASPB SH4-mCherry and VSVG-SP-mRFP when coexpressed with Arf1 WT localized to the plasma membrane and perinuclear membranes (Figure 19 A, b; Figure 19 B, b). Upon coexpression with Arf1 Q71L, VSVG-SP-mRFP exhibited complete intracellular retention (Figure 19 B, e), which is in striking contrast to what we observed for HASPB SH4-mCherry, which under these conditions was able to reach the plasma membrane (Figure 19 A, e).

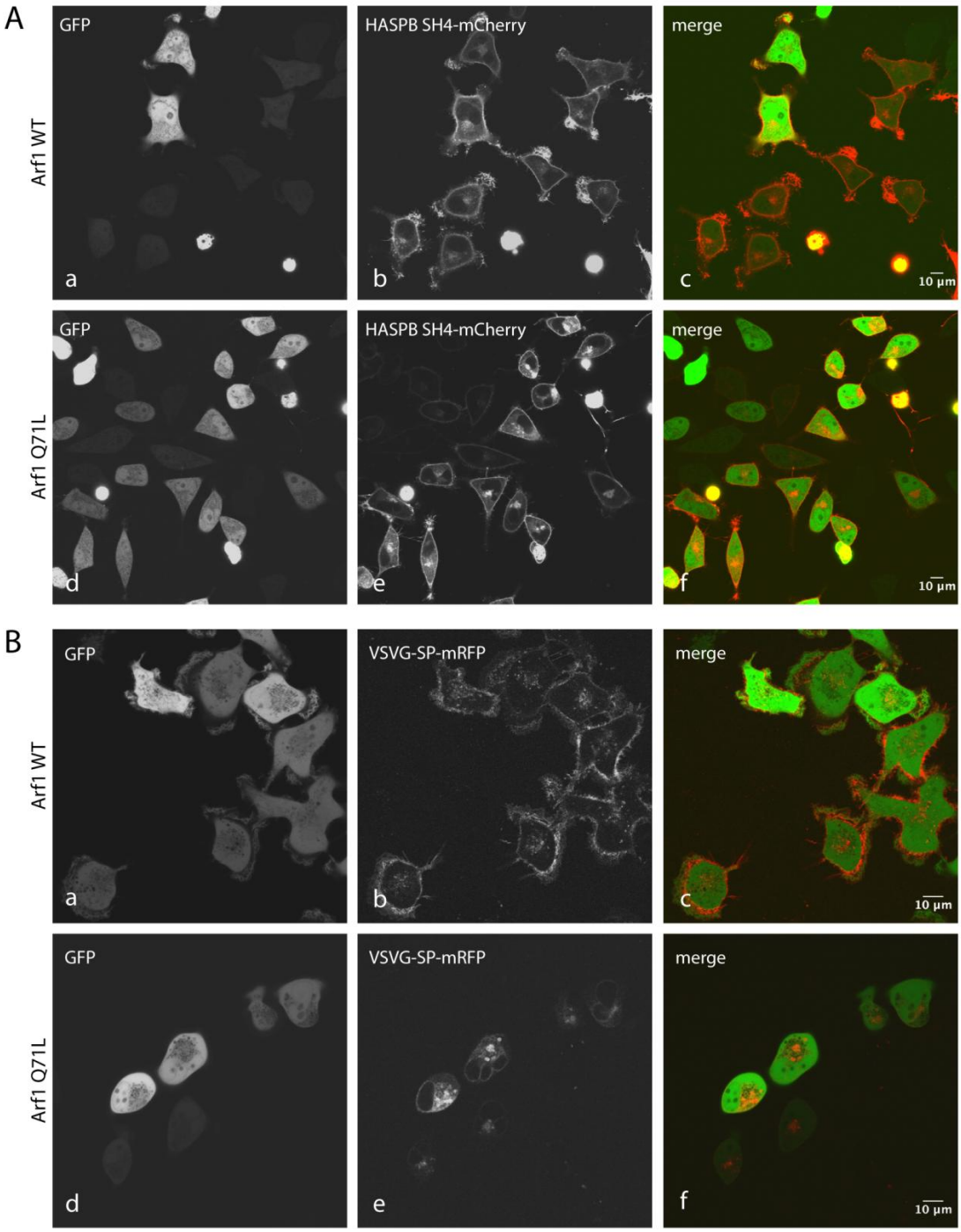

Figure 19 Analysis of subcellular localization of a HASPB SH4 domain fusion protein (HASPB SH4-mCherry) and a vesicular stomatitis virus G protein fusion protein (VSVG-SP-mRFP) upon their coexpression with the wild-type (WT) Arf1, or its constitutively active mutant (Q71L). (A) HeLa MCAT-TAM2 cells were cotransfected with pIRES2-EGFP/Arf1 (WT or Q71L) and pRevTRE2/HASPB SH4-mCherry using FuGENE HD transfection reagent, in the presence of 4 µg/ml doxycycline. The cells were imaged 18 hours after transfection using live-cell confocal microscopy (objective 40x). **(B)** HeLa MCAT-TAM2 cells were cotransfected with pIRES2-EGFP/Arf1 (WT or Q71L) and pmRFP-N1/VSVG-SP using FuGENE HD transfection reagent, and imaged 20 hours after transfection with the use of live-cell confocal microscopy (objective 63x). Scale bar, 10 µm.

Upon coexpression with Arf1 Q71L, apart from plasma membrane localization, HASPB SH4-mCherry exhibited also perinuclear localization, the magnitude of which was significantly increased as compared to cells expressing Arf1 WT ($p \leq 0.001$, unpaired Student's t-test; Figure 20 C), which was determined by intensity quantification of sum intensity projections of Z stack images (Figure 20, A, B; each image represents a sum intensity projection of one Z stack).

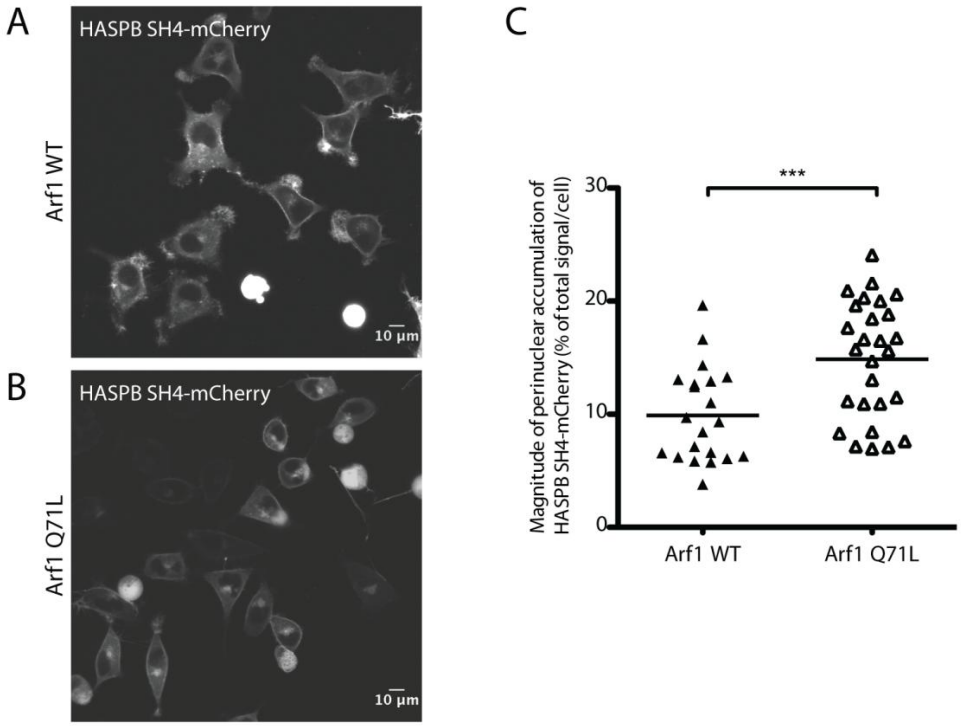

Figure 20 Quantitative analysis of subcellular localization of a HASPB SH4 domain fusion protein (HASPB SH4-mCherry) upon its coexpression with the wild-type (WT) Arf1, or its constitutively active mutant (Q71L). HeLa MCAT-TAM2 cells were cotransfected with pIRES2-EGFP/Arf1 (WT or Q71L) and pRevTRE2/HASPB SH4-mCherry using FuGENE HD transfection reagent, in the presence of 4 µg/ml doxycycline. The cells were imaged 18 hours after transfection using live-cell confocal microscopy, by collecting Z stacks (objective 40x). **(A, B)** Each image represents a sum intensity projection of Z stack images. Scale bar, 10 µm. **(C)** Magnitude of perinuclear accumulation of HASPB SH4-mCherry upon its coexpression with Arf1 WT or Arf1 Q71L, determined by intensity quantification of sum intensity projections of Z stacks. Perinuclear accumulation per cell is expressed as the percentage of perinuclear signal respective to the total signal per cell. Values for individual cells are depicted as triangles, horizontal bars represent arithmetic means for each condition; ***, $p \leq 0.001$, unpaired Student's t-test.

4.3 Analysis of subcellular localization of a HASPB SH4 domain fusion protein and a VSVG fusion protein upon their expression in the presence of brefeldin A

We analyzed the subcellular localization of HASPB SH4-mCherry and VSVG-SP-GFP, transiently coexpressed in the presence of brefeldin A (BFA), a drug known to inhibit protein trafficking in the secretory system of mammalian cells (Misumi *et al.*, 1986; Lippincott-Schwartz *et al.,* 1989; Miller *et al.*, 1992), by preventing Arf1 activation and thus also the Arf1-dependent recruitment of coatomer to membranes (Donaldson *et al.*, 1990; Donaldson *et al.*, 1991). HeLa MCAT-TAM2 cells were cotransfected with pEGFP-N1/VSVG-SP and pRevTRE2/HASPB SH4-mCherry using FuGENE HD transfection reagent, in the presence of 1 µg/ml doxycycline and 100 µg/ml cycloheximide. 4 hours later, cycloheximide was washed out, followed by incubation in the presence of 1 µg/ml doxycycline and BFA (0.1 µg/ml) or methanol as a mock control, for 16 hours. The cells were imaged using live-cell confocal microscopy. In mock-treated cells, both VSVG-SP-GFP (Figure 21 A) and HASPB SH4-mCherry (Figure 21 B) localized to the plasma membrane and perinuclear membranes. Upon expression in the presence of BFA, VSVG-SP-GFP exhibited complete intracellular retention (Figure 21 D), whereas HASPB SH4-mCherry under these conditions reached the plasma membrane (Figure 21 E).

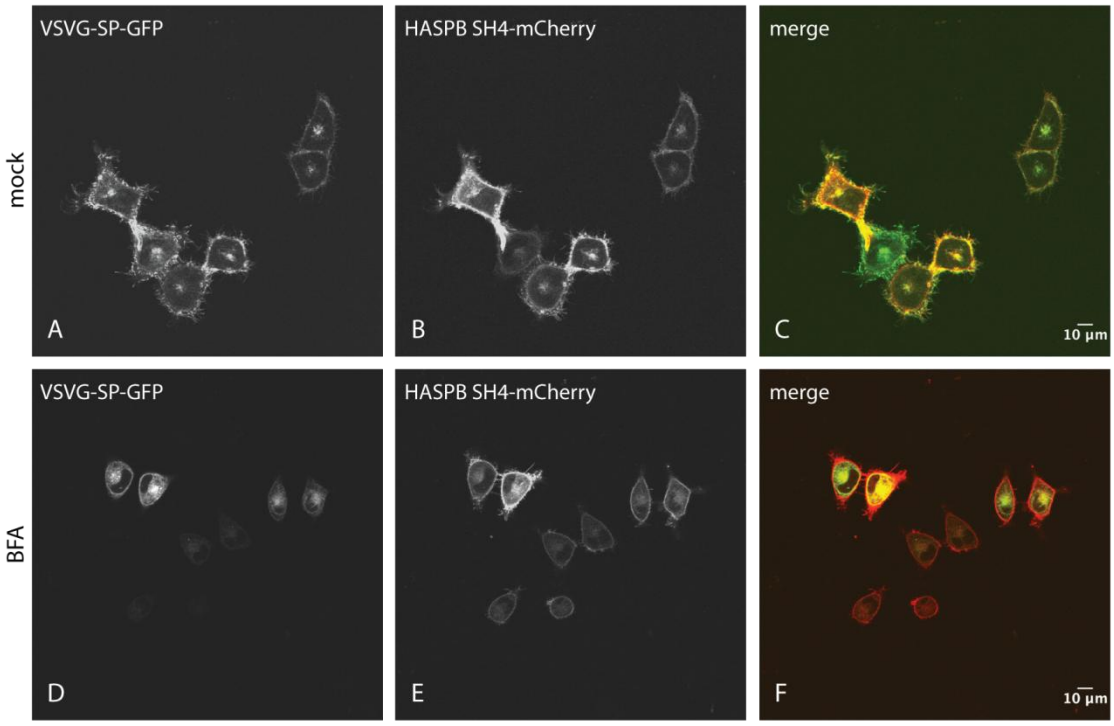

Figure 21 Analysis of subcellular localization of a HASPB SH4 domain fusion protein (HASPB SH4-mCherry) and a vesicular stomatitis virus G protein fusion protein (VSVG-SP-GFP), coexpressed in the presence of brefeldin A (BFA). HeLa MCAT-TAM2 cells were cotransfected with pEGFP-N1/VSVG-SP and pRevTRE2/HASPB SH4-mCherry using FuGENE HD transfection reagent, in the presence of 1 µg/ml doxycycline and 100 µg/ml cycloheximide. 4 hours later, cycloheximide was washed out, followed by incubation in the presence of 1 µg/ml doxycycline and BFA (0.1 µg/ml) or methanol as a solvent control (mock), for 16 hours. The cells were imaged using live-cell confocal microscopy (objective 40x).

Magnitude of perinuclear and intracellular accumulation of HASPB SH4-mCherry upon expression in the presence of BFA or methanol was determined by intensity quantification of sum intensity projections of Z stack images (Figure 22, A, B; each image represents a sum intensity projection of one Z stack). Expression in the presence of BFA resulted in increased perinuclear localization of HASPB SH4-mCherry as compared to mock-treated cells ($p \leq 0.05$, unpaired Student's t-test; Figure 22 C), as well as in increased intracellular localization ($p \leq 0.001$, unpaired Student's t-test; Figure 22 D). The increase in intracellular localization was more pronounced (1.50x versus 1.27x when comparing arithmetic means of percentages of accumulated protein in relation to total protein per cell), and more homogeneous across the cell population than the increase in perinuclear localization.

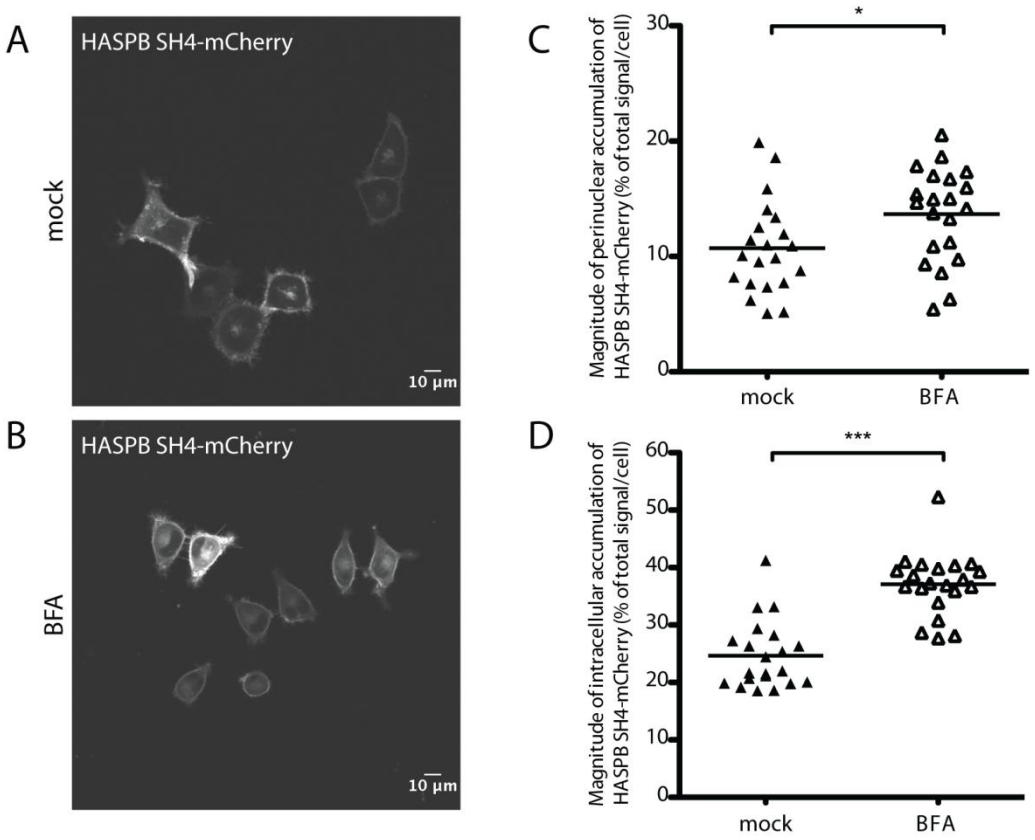

Figure 22 Quantitative analysis of subcellular localization of a HASPB SH4 domain fusion protein (HASPB SH4-mCherry) expressed in the presence of brefeldin A (BFA). HeLa MCAT-TAM2 cells were transfected with pRevTRE2/HASPB SH4-mCherry using FuGENE HD transfection reagent, in the presence of 1 µg/ml doxycycline and 100 µg/ml cycloheximide. 4 hours later, cycloheximide was washed out, followed by incubation in the presence of 1 µg/ml doxycycline and BFA (0.1 µg/ml) or methanol as a solvent control (mock), for 16 hours. The cells were imaged using live-cell confocal microscopy, by collecting Z stacks (objective 40x). **(A, B)** Each image represents a sum intensity projection of Z stack images. Scale bar, 10 µm. Magnitude of perinuclear **(C)** and intracellular **(D)** accumulation of HASPB SH4-mCherry upon expression in the presence of BFA or methanol (mock), determined by intensity quantification of sum intensity projections of Z stacks. Perinuclear/intracellular accumulation per cell is expressed as the percentage of perinuclear/intracellular signal respective to the total signal per cell. Values for individual cells are depicted as triangles, horizontal bars represent arithmetic means for each condition; * $p \leq 0.05$; ***, $p \leq 0.001$, unpaired Student's t-test.

4.4 Immunogold electron microscopy analysis of subcellular localization of a HASPB SH4 domain fusion protein upon transfection with a scrambled or β-COP siRNA

We analyzed the subcellular localization of a HASPB SH4 domain fusion protein (HASPB SH4-TEV-GFP) upon transfection with a scrambled or β-COP siRNA with the use of immunogold electron microscopy, conducted in collaboration with Dr. Jacomine Krijnse-Locker from the Electron Microscopy Core Facility (EMCF), BioQuant, University of Heidelberg. The aim was to establish the identity of the perinuclear membranes on which HASPB SH4 fusion protein accumulates upon β-COP knockdown (see Figure 17 B and Figure 18 E), and thus determine at which step its transport is blocked under these conditions. HeLa cell line stably expressing HASPB SH4-TEV-GFP in a doxycycline-inducible manner (HeLa HASPB SH4-TEV-GFP clone 4; Figure 2 B; Figure 4 B) was transfected with a scrambled siRNA (Figure 23, A, B) or a β-COP siRNA (Figure 23, C-F), using Oligofectamine. 48 hours upon transfection (24 hours upon the induction with 2 µg/ml doxycycline) the cells were fixed, embedded in gelatin, which was followed by sucrose infiltration and cryosectioning. Cryosections were double labeled using anti-GFP and anti-GM130 antibodies (Figure 23, A, C, E), or anti-GFP and anti-TGN46 antibodies (Figure 23, B, D, F), and protein A-gold conjugates of different sizes. Subsequently, cryosections were imaged using a transmission electron microscope.

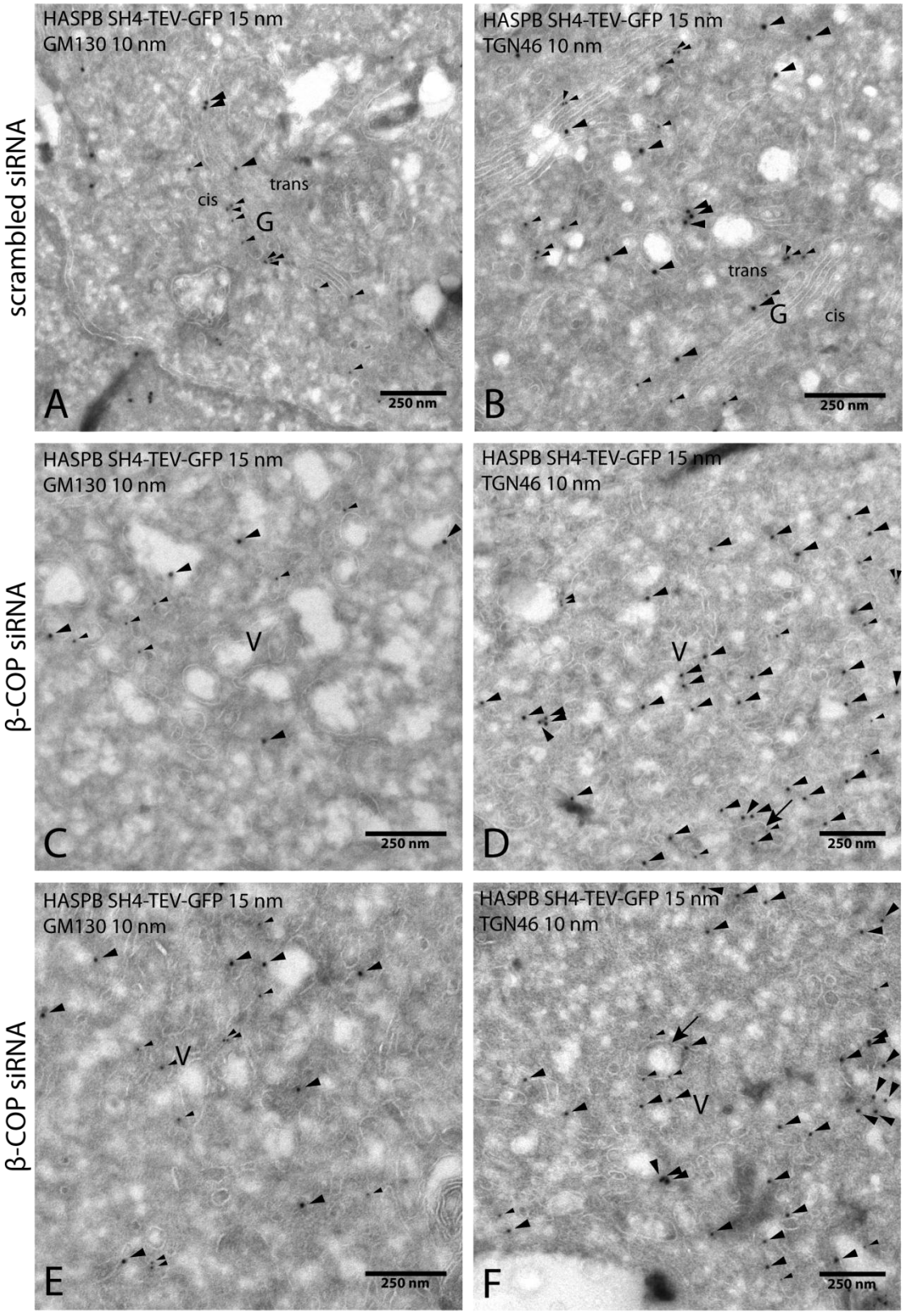

Figure 23 Caption on page 72.

Caption for figure on page 71. Figure 23 Immunoelectron microscopy analysis of subcellular localization of a HASPB SH4 domain fusion protein (HASPB SH4-TEV-GFP), upon transfection with a scrambled siRNA or an siRNA targeting the β subunit of the COPI coatomer complex (β-COP). HeLa cell line stably expressing HASPB SH4-TEV-GFP in a doxycycline-inducible manner (HeLa HASPB SH4-TEV-GFP, clone 4) was transfected with a scrambled siRNA **(A, B)** or a β-COP siRNA **(C-F)**, using Oligofectamine. 48 hours upon transfection (24 hours upon the induction with 2 μg/ml doxycycline) the cells were fixed, followed by embedding in gelatin, sucrose infiltration and cryosectioning. **(A, C, E)** Cryosections were double labeled using anti-GFP antibodies and 15 nm protein A-gold, followed by anti-GM130 antibodies and 10 nm protein A-gold. **(B, D, F)** Cryosections were double labeled using anti-GFP antibodies and 15 nm protein A-gold, followed by anti-TGN46 antibodies and 10 nm protein A-gold. Cryosections were imaged using a transmission electron microscope. Pictures were taken at magnifications of 20000-25000x. Scale bar, 250 nm. G, Golgi stack; V, vesiculated Golgi. Small and large arrowheads point to 10 nm and 15 nm gold particles, respectively. Arrows point to Golgi-derived vesicles labeled with both 10 nm and 15 nm gold particles.

In the control cells (transfected with a scrambled siRNA), gold labeling for HASPB SH4-TEV-GFP in the perinuclear region was localized mainly to the opposite side of the Golgi apparatus, as compared to the labeling for GM130 (a marker for *cis*-Golgi; Figure 23 A). Consistently, HASPB SH4-TEV-GFP was localized on the side of the Golgi labeled for TGN46 (a *trans*-Golgi network marker), mainly outside of the Golgi stack (Figure 23 B), and less commonly, within the stack (not shown). SiRNA-mediated knockdown of β-COP caused striking changes in the morphology of the Golgi apparatus, namely complete loss of Golgi cisternae and vesiculation of the Golgi apparatus, with HASPB SH4-TEV-GFP localizing to some of those vesicles (Figure 23, C-F). Labeling for HASPB SH4-TEV-GFP and GM130 in the β-COP knockdown cells was localized to distinct regions of the vesiculated Golgi, with GM130 being localized more centrally (Figure 23, C, E). On the other hand, HASPB SH4-TEV-GFP and TGN46 in the knockdown cells seemed to be less separated than HASPB SH4-TEV-GFP and GM130, and localized more to the perimeter of the vesiculated Golgi area (Figure 23, D, F). We could also observe the occurrence of labeling for both HASPB SH4-TEV-GFP and TGN46 on the same vesicles (Figure 23, D, F; arrows).

4.5 Immunogold electron microscopy analysis of subcellular localization of a HASPB SH4 domain fusion protein upon its coexpression with Arf1 WT or Arf1 Q71L

We then analyzed the subcellular localization of HASPB SH4-mCherry upon its coexpression with the wild-type (WT) Arf1, or its constitutively active mutant (Q71L), with the use of immunogold electron microscopy, to establish the identity of the perinuclear membranes on which the fusion protein accumulates upon coexpression with Arf1 Q71L (Figure 19 A, e; Figure 20 B). HeLa cell line stably expressing HASPB SH4-mCherry in a doxycycline-inducible manner was transfected with pIRES2-EGFP/Arf1 WT (Figure 24, A, B) or pIRES2-EGFP/Arf1 Q71L (Figure 24, C-F) using jetPRIME transfection reagent, in the presence of 2 µg/ml doxycycline. 15 hours later, the cells were fixed, which was followed by embedding in gelatin, sucrose infiltration and cryosectioning. Cryosections were double labeled using anti-mRFP and anti-GM130 antibodies (Figure 24, A, C, E), or anti-mRFP and anti-TGN46 antibodies (Figure 24, B, D, F), and protein A-gold conjugates of different sizes. Subsequently, cryosections were imaged using a transmission electron microscope.

Caption for figure on page 74. Figure 24 Immunoelectron microscopy analysis of subcellular localization of a HASPB SH4 domain fusion protein (HASPB SH4-mCherry) upon its coexpression with the wild-type (WT) Arf1, or its constitutively active mutant (Q71L). HeLa cell line stably expressing HASPB SH4-mCherry in a doxycycline-inducible manner was transfected with pIRES2-EGFP/Arf1 WT **(A, B)** or pIRES2-EGFP/Arf1 Q71L **(C-F)** using jetPRIME transfection reagent, in the presence of 2 µg/ml doxycycline. 15 hours later, the cells were fixed, followed by embedding in gelatin, sucrose infiltration and cryosectioning. **(A, C, E)** Cryosections were double labeled using anti-GM130 antibodies and 10 nm protein A-gold, followed by anti-mRFP antibodies (diluted 1:50) and 15 nm protein A-gold. **(B, D, F)** Cryosections were double labeled using anti-mRFP antibodies (diluted 1:30) and 15 nm protein A-gold, followed by anti-TGN46 antibodies and 10 nm protein A-gold. Cryosections were imaged using a transmission electron microscope. Pictures were taken at magnifications of 20000-50000x. Scale bar, 250 nm. G, Golgi stack; V, vesiculated Golgi. Small and large arrowheads point to 10 nm and 15 nm gold particles, respectively. Arrow points to a Golgi-derived vesicle labeled with both 10 nm and 15 nm gold particles.

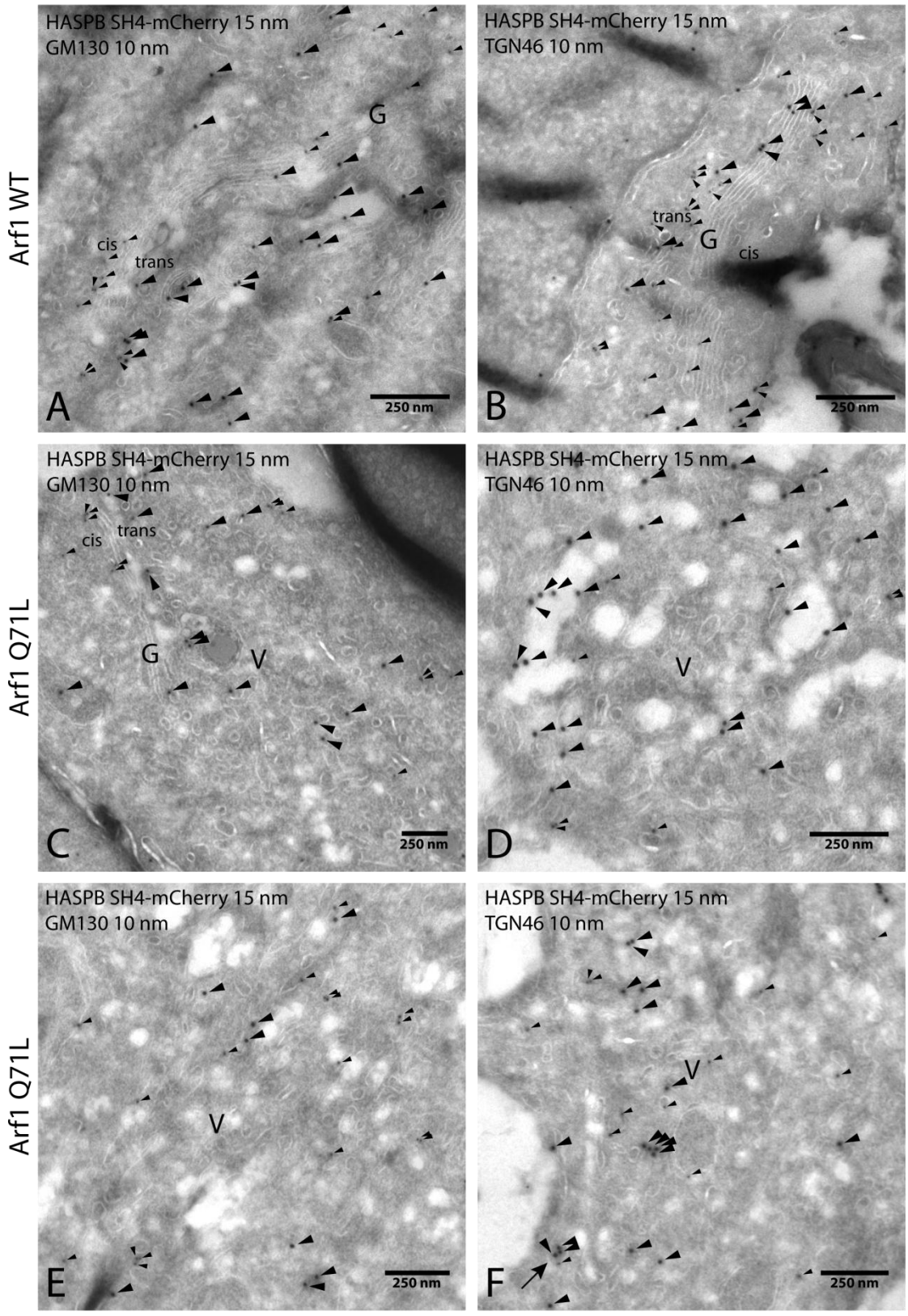

Figure 24 Caption on page 73.

In the control cells (i.e. expressing Arf1 WT), gold labeling for HASPB SH4-mCherry was localized mainly to the opposite side of the Golgi apparatus, as compared to the labeling for GM130 (Figure 24 A). Consistently, HASPB SH4-mCherry was localized on the side of the Golgi labeled for TGN46, mainly outside of the Golgi stack, but also within the stack (Figure 24 B). Expression of Arf1 Q71L resulted in almost complete (Figure 24 C), or complete (Figure 24, D-F) loss of Golgi cisternae, which were replaced by a great quantity of vesicular structures. HASPB SH4-mCherry and GM130 in Arf1 Q71L-expressing cells were localized to distinct regions of the vesiculated Golgi, GM130 being localized more centrally (Figure 24, C, E). HASPB SH4-mCherry and TGN46 in Arf1 Q71L-expressing cells seemed to be less separated than HASPB SH4-mCherry and GM130, and localized more to the perimeter of the vesiculated Golgi area (Figure 24, D, F). We could also observe the occurrence of labeling for both HASPB SH4-mCherry and TGN46 on the same vesicles (Figure 24 F; arrow).

5 Discussion II

Previous result from our laboratory (Ritzerfeld, 2009; Ritzerfeld *et al.,* 2011) suggested an involvement of the β subunit of the COPI coatomer complex in the subcellular trafficking of diacylated SH4 domain proteins. Namely, siRNA-mediated knockdown of β-COP resulted in an increased perinuclear localization of a SH4 domain reporter fusion protein (HASPB SH4-GFP) in HeLa cells. It was also shown that down-regulation of β-COP results in decreased levels of δ-COP, and vice versa (Ritzerfeld *et al.,* 2011), indicating that depletion of one coatomer subunit inhibits the assembly of the whole complex. Moreover, also knockdowns of other coatomer subunits, α, β' and δ, were shown to result in a pronounced increase in perinuclear accumulation of HASPB SH4-GFP (Ritzerfeld, 2009; Ritzerfeld *et al.,* 2011). Furthermore, the targeting of HASPB SH4-mCherry was unaffected in cells that were microinjected with recombinant coatomer complex prior to transfection with β-COP siRNA (Ritzerfeld *et al.,* 2011). Thus, phenotypic changes induced by the β-COP knockdown result from depletion of the coatomer complex. We decided to examine in more detail the involvement of coatomer in the transport of diacylated SH4 domain proteins to the plasma membrane.

5.1 Analysis of subcellular localization of a HASPB SH4 domain fusion protein and a VSVG fusion protein upon β-COP knockdown

SiRNA-mediated knockdown of the β subunit of the COPI coatomer complex in a stable HeLa cell line expressing HASPB SH4-mCherry in a doxycycline-inducible manner, resulted in a statistically significant increase in perinuclear localization of the fusion protein. The protein, however, was also found at the plasma membrane (Figure 17, B, C). The seeming failure of β-COP knockdown to completely inhibit the transport of HASPB SH4-mCherry to the plasma membrane may reflect insufficient knockdown efficiency, but it is also possible that the stable cell line exhibits some level of constitutive expression of HASPB SH4-mCherry, and thus the fusion protein was localized to the plasma membrane already before siRNA transfection and subsequent induction with doxycycline, and a low turnover rate of the protein let it remain at the plasma membrane.

In a different experiment, HeLa cells that do not stably express any reporter fusion protein (HeLa MCAT-TAM2) were first transfected with an siRNA targeting β-COP, and 24 hours later cotransfected with constructs encoding VSVG-SP-GFP, a GFP-tagged version of a model transmembrane glycoprotein, vesicular stomatitis virus glycoprotein (VSVG; Keller *et al.*, 2001), and HASPB SH4-mCherry (Figure 18, D-F). In contrast to the above experiment, in this experiment there was no fusion protein at the plasma membrane before the siRNA transfection. Similarly to the previous experiment, despite exhibiting increased perinuclear localization, HASPB SH4-mCherry was again found at the plasma membrane (Figure 18 E). On the other hand, the transport of VSVG-SP-GFP to the plasma membrane was totally abolished under β-COP knockdown conditions (Figure 18 D), and the protein accumulated, similarly as the intracellular pool of HASPB SH4-mCherry, within a perinuclear globular compartment. In agreement with our results, anterograde transport of VSVG-GFP in β-COP-depleted HeLa cells was previously shown to be arrested at the level of large globular structures, with no VSVG-GFP detectable at the plasma membrane (Styers *et al.*, 2008). The complete block in the transport of VSVG-SP-GFP under β-COP knockdown conditions suggests that the knockdown was efficient and abolished transport via the secretory pathway. It implies that the presence of HASPB SH4-mCherry at the plasma membrane does not result from insufficient knockdown efficiency, but rather suggests that the transport of HASPB SH4-mCherry to the plasma membrane is operational under β-COP knockdown conditions. The perinuclear accumulation of HASPB SH4-mCherry may reflect a transport block occurring at perinuclear membranes, pointing to their involvement in the transport of HASPB SH4-mCherry. The protein, however, seems to be able to reach the plasma membrane via an alternative pathway which bypasses the transport block.

5.2 Analysis of subcellular localization of a HASPB SH4 domain fusion protein and a VSVG fusion protein upon coexpression with Arf1 Q71L

Association of the COPI coatomer complex with membranes (and thus the formation of COPI vesicles) depends on its recruitment by the small GTPase Arf1, which in turn requires GTP binding by Arf1 and the resulting exposure of its myristoylated N-terminal amphipathic α-helix that provides stable membrane anchorage (Antonny *et al.*, 1997; see sections 1.1 and 1.4.3). Hydrolysis of GTP by Arf1 was shown to be involved in the

uptake of cargo proteins into COPI vesicles (Malsam *et al.,* 1999; Pepperkok *et al.,* 2000), and in uncoating of the vesicles (Tanigawa *et al.,* 1993). Replacement of glutamine 71 in Arf1 with leucine in the guanine nucleotide binding pocket results in a mutant (Q71L) which is unable to hydrolyze GTP and is thus constitutively active (Dascher *et al.,* 1994; Teal *et al*., 1994; Zhang *et al*., 1994). Its trans-dominant effect is thought to result from the sequestration of Arf GTPase-activating proteins (Arf GAPs), thus preventing inactivation of endogenous Arf1 (Zhang *et al.*, 1994).

Either HASPB SH4-mCherry or VSVG-SP-mRFP was transiently coexpressed with Arf1 Q71L in HeLa MCAT-TAM2 cells. Under these conditions, VSVG-SP-mRFP exhibited a complete intracellular retention, and accumulated at perinuclear structures (Figure 19 B, e), indicating a complete block in the transport of the protein to the plasma membrane, and suggesting that transport via the secretory pathway was abolished. Similarly, Arf1 Q71L expressed in normal rat kidney (NRK) cells was shown to inhibit secretion of [^{35}S] methionine-labeled proteins (Zhang *et al.*, 1994), and its overexpression in HeLa cells resulted in the inhibition of ER to *medial*-Golgi and intra-Golgi transport of VSVG (Dascher *et al.*, 1994). HASPB SH4-mCherry expressed in the presence of Arf1 Q71L exhibited an increased perinuclear accumulation (Figure 19 A, e; Figure 20, B, C), but nevertheless localized also to the plasma membrane, indicating that the transport of HASPB SH4-mCherry is operational under these conditions. The perinuclear accumulation of HASPB SH4-mCherry may reflect a transport block occurring at perinuclear membranes, pointing to their involvement in the transport of HASPB SH4-mCherry. The protein, however, seems to be able to bypass the transport block and reach the plasma membrane via an alternative pathway.

5.3 Analysis of subcellular localization of a HASPB SH4 domain fusion protein and a VSVG fusion protein upon their expression in the presence of brefeldin A

Brefeldin A (BFA) is a fungal macrocyclic lactone (Härri *et al*., 1963), which stabilizes a non-productive complex between Arf1-GDP and Sec7 domain of BFA-sensitive Arf GEFs (Peyroche *et al.,* 1999), thus sequestering Arf GEFs and acting as a noncompetitive inhibitor of Arf1 activation. BFA induces dissociation of Arf1 and β-COP from the Golgi

apparatus into the cytoplasm, thus inhibiting the formation of COPI vesicles (Donaldson *et al.*, 1990; Donaldson *et al.*, 1991), which is followed by the breakdown of the Golgi stacks into tubules that extend along microtubules and fuse with the endoplasmic reticulum, resulting in redistribution of *cis-, medial-* and *trans*-Golgi enzymes back to the ER (Lippincott-Schwartz *et al.,* 1989; Chege *et al.*, 1990; Sciaky *et al.,* 1997). Transport out of the mixed Golgi-ER system is blocked (Misumi *et al.*, 1986; Lippincott-Schwartz *et al.,* 1989). The dissociation of β-COP, disruption of the Golgi apparatus, and inhibition of protein secretion, take place already at relatively low concentrations of BFA (0.05 µg/ml) (Klausner *et al.*, 1992). It was proposed that upon inhibition of the formation of COPI vesicles by BFA, retrograde vesicle-associated SNARE proteins (v-SNARES) remain exposed on the Golgi, which underlies the direct and uncontrolled fusion of Golgi cisternae with the ER (Elazar *et al.,* 1994). BFA was also shown to induce tubulation of endosomes, lysosomes and the *trans*-Golgi network (TGN), at the same concentrations that affect the Golgi apparatus (Lippincott-Schwartz *et al.,* 1991). TGN-resident proteins, such as sialyltransferase and TGN38, were shown not to redistribute to the ER upon BFA treatment (Chege *et al.*, 1990; Lippincott-Schwartz *et al.,* 1991; Ladinsky *et al.*, 1992), but rather mix with the early endosomal system (Lippincott-Schwartz *et al.,* 1991). Moreover, BFA was shown to inhibit transport from distal Golgi compartments to the plasma membrane, via both constitutive and regulated pathways, for example, it blocked plasma membrane transport of VSVG accumulated at 20°C in the TGN of BHK-21 cells (Miller *et al.*, 1992).

To test whether HASPB SH4-mCherry travels to the plasma membrane via the secretory pathway, we expressed the fusion protein in the presence of BFA. As a control for the effect of BFA, HASPB SH4-mCherry was coexpressed with VSVG-SP-GFP, a transmembrane protein, the transport of which should be inhibited by BFA at the level of the fused ER-Golgi compartment. Both proteins were expressed transiently to ascertain that none of the proteins was localized to the plasma membrane before the addition of BFA, and that the whole expression took place in the presence of the drug. Upon expression in the presence of BFA, VSVG-SP-GFP exhibited complete intracellular retention (Figure 21 D), accumulating most possibly in the fused ER-Golgi compartment. HASPB SH4-mCherry however, under these conditions reached the plasma membrane

(Figure 21 E), despite disruption of the structure and compromising the function of secretory organelles by BFA, as demonstrated by the inhibition of VSVG-SP-GFP transport. Thus, functional secretory pathway, and even properly organized secretory organelles, are dispensable for the transport of HASPB SH4-mCherry to the plasma membrane. When expressed in the presence of BFA, apart from plasma membrane localization, HASPB SH4-mCherry exhibited also highly significant increase in intracellular localization (Figure 22 D), possibly reflecting its accumulation in the ER-Golgi hybrid compartment. The quantified increase in perinuclear localization, which was much less significant (Figure 22 C), could be due to accumulation of HASPB SH4-mCherry in the perinuclear portion of the hybrid compartment. Accumulation of HASPB SH4-mCherry in the fused ER-Golgi compartment upon BFA treatment suggests that under control conditions the protein at one point associates with the ER, or more probably, with *cis-, medial-* or *trans*-Golgi, as these Golgi subcompartments, as already mentioned, are known to fuse back to the ER in the presence of BFA (Lippincott-Schwartz *et al.,* 1989; Chege *et al.*, 1990; Sciaky *et al.,* 1997). What is more, the observed accumulation points out to the involvement of the secretory pathway in the plasma membrane transport of HASPB SH4-mCherry. However, there seems to exist an alternative pathway, which is independent from the secretory pathway, as suggested by the appearance of the HASPB SH4 domain fusion protein at the plasma membrane in the presence of BFA.

5.4 Immunogold electron microscopy analysis of subcellular localization of a HASPB SH4 domain fusion protein upon transfection with a scrambled or β-COP siRNA

Immunogold electron microscopy analysis of the perinuclear Golgi region of scrambled siRNA-transfected HeLa cells stably expressing HASPB SH4-TEV-GFP (Figure 23, A, B), indicates that the protein localizes mainly to the *trans*-Golgi network, an array of tubules and vesicles found on one side of the Golgi stack. In contrast, in β-COP-depleted cells there were no stacks, and the Golgi complex was fragmented into vesicular structures, which accumulated in the perinuclear region, with HASPB SH4-TEV-GFP localizing to some of those vesicles (Figure 23, C-F). This fragmented Golgi phenotype of β-COP knockdown cells is in agreement with what was previously observed (Guo *et al.*, 2008; Saitoh *et al.*, 2009), and indicates that depletion of COPI affects not only the function (as

indicated by complete intracellular retention of VSVG-SP-GFP and increased perinuclear accumulation of HASPB SH4-mCherry; Figure 17, B, C and Figure 18, D-F), but also the structure of the secretory pathway. Our results suggest that even though under β-COP knockdown conditions the Golgi is fragmented, its polarity is to some extent maintained, as HASPB SH4-TEV-GFP did not seem to localize to vesicular structures labeled for the *cis*-Golgi marker GM130, which were localized to the center of the vesiculated Golgi area (Figure 23, C, E), but was rather observed in the region containing vesicles labeled for the TGN marker TGN46, with the occurrence of labeling for HASPB SH4-TEV-GFP and TGN46 on the same vesicles (Figure 23, D, F). Similarly, it was previously shown using immunofluorescence that whereas ERGIC and *cis*-Golgi markers exhibit significant colocalization in β-COP knockdown cells, ERGIC and *trans*-Golgi markers do not significantly overlap under these conditions (Saitoh *et al.*, 2009).

It seems likely that the effect of COPI depletion on anterograde transport of both VSVG-SP-GFP and HASPB SH4-mCherry is not a direct consequence of the lack of formation of COPI vesicles (which are known to mediate primarily retrograde transport), but a result of changes in Golgi morphology due to the inhibition of retrograde transport or the lack of COPI coats on Golgi membranes. It seems reasonable to expect that upon the disruption of the Golgi stack and vesiculation of Golgi cisternae, the cisternal maturation and progression responsible for anterograde intra-Golgi transport cannot occur anymore, hence the observed transport block. It has been proposed that palmitoylation, and therefore also the initial stable membrane association of diacylated SH4 domain proteins occurs at the Golgi (Kasahara *et al.*, 2004; Sato *et al.*, 2009). If HASPB SH4-TEV-GFP was palmitoylated at the *cis*-Golgi, under β-COP knockdown conditions (i.e. in the absence of anterograde intra-Golgi transport) the protein would accumulate at *cis*-Golgi-derived fragments. The lack of HASPB SH4-TEV-GFP localization to vesicular structures labeled for GM130 (Figure 23, C, E) suggests that its initial stable membrane association (and thus also palmitoylation) does not take place at the *cis*-Golgi, but rather at more distal Golgi compartments.

5.5 Immunogold electron microscopy analysis of subcellular localization of a HASPB SH4 domain fusion protein upon its coexpression with Arf1 WT or Arf1 Q71L

Immunogold electron microscopy analysis of the perinuclear Golgi region of HeLa cells stably expressing HASPB SH4-mCherry, transiently transfected with a plasmid encoding the wild-type (WT) Arf1 (Figure 24, A, B), indicates that HASPB SH4-mCherry localizes primarily to the *trans*-Golgi network, but also to the distal portions of the Golgi stack, which is in agreement with the localization of HASPB SH4-TEV-GFP, stably expressed in scrambled siRNA-transfected HeLa cells (Figure 23, A, B). In cells expressing Arf1 Q71L, the Golgi apparatus disassembled into vesicular structures accumulating in the perinuclear region (Figure 24, C-F), which is in agreement with what was previously reported for Arf1 Q71L overexpressed in NRK cells (Zhang *et al.*, 1994).

Apart from the coatomer complex, Arf1 has many other effectors at the Golgi (such as various coat proteins, lipid-modifying enzymes, lipid-transfer proteins and tethers; Donaldson *et al.,* 2011). However, the similarity of the phenotypes (both with regard to protein localization and Golgi morphology) caused by Arf1 Q71L expression, to those upon β-COP knockdown, suggests that the effect of Arf1 Q71L on Golgi structure and function results primarily (if not completely) from interfering with COPI functions, and is not caused by the inhibition of other Arf1 effectors. It was previously shown that Arf1 Q71L leads to stable association of COPI with the Golgi membranes (Dascher *et al*., 1994; Teal *et al.*, 1994), which may be what causes the Golgi to vesiculate. Thus, maintenance of the Golgi structure would require Arf1 to undergo cycles of membrane association and dissociation. Alternatively, the fragmentation of the Golgi could be caused by inhibition of COPI-dependent transport as a result of impaired cargo uptake into COPI vesicles, in agreement with the reported role of Arf1-mediated GTP hydrolysis in this process (Malsam *et al.*, 1999; Pepperkok *et al.,* 2000). In turn, the vesiculation of the Golgi complex may underlie the observed inhibition of transport through the secretory pathway (indicated by complete intracellular retention of VSVG-SP-mRFP, and increased perinuclear accumulation of HASPB SH4-mCherry; Figure 19 A, e and B, e; Figure 20, B, C).

In some cells, the disassembly of the Golgi apparatus was not complete, with only the *trans*-face transformed into vesicles, and the *cis*-face intact (Figure 24 C), which indicates that the vesiculation starts from the *trans*-side of the Golgi. Similarly as in the control cells (Figure 24 A), also upon partial or complete fragmentation of the Golgi in Arf1 Q71L-expressing cells, HASPB SH4-mCherry remained segregated from the *cis*-Golgi marker GM130 (Figure 24, C, E), indicating that the polarity of the Golgi was to some extent retained, which is similar to what we observed for β-COP knockdown conditions (Figure 23, C, E). The lack of accumulation of HASPB SH4-mCherry on *cis*-Golgi-derived fragments upon Arf1 Q71L expression, once again suggests that under control conditions HASPB SH4-mCherry does not pass through the *cis*-Golgi, but rather associates with more distal Golgi compartments, which is followed by Golgi-dependent transport of the protein to the plasma membrane.

5.6 Concluding remarks

The localization phenotypes of the HASPB SH4 fusion protein under conditions that disrupt the structure and function of the Golgi apparatus, i.e. β-COP knockdown, expression of Arf1 Q71L and BFA treatment, indicate that the initial stable membrane association of the fusion protein (most probably as a result of palmitoylation) could occur at *medial/trans*-Golgi (possibly also at the TGN), and what is more, point out to the role of the Golgi in the plasma membrane transport of SH4 reporter proteins. This apparent involvement of the secretory pathway is in agreement with what was observed by others for full-length diacylated Src family kinases Lyn and Yes, which associate with the Golgi complex in the initial phase of their expression, exhibit increased perinuclear localization upon incubation at 19°C, and whose Golgi to plasma membrane transport is inhibited by N-ethylmaleimide (Kasahara *et al.*, 2004; Sato *et al.*, 2009; see also sections 1.5.1.4 and 1.5.1.5).

We could observe that none of the treatments that disrupt the Golgi block the appearance of the SH4 reporter protein at the plasma membrane, suggesting the existence of an alternative trafficking pathway that does not require the Golgi complex. Palmitoyl transferases (PATs) are mostly known to localize to the ER/Golgi membranes,

and the Golgi apparatus was proposed to function as a hub for palmitoylation (Rocks *et al.,* 2010). However, there exist PATs which exhibit plasma membrane localization (Ohno *et al.*, 2006; see section 1.4.4), indicating that some of the palmitoylation events may occur at the plasma membrane, a possibility which was not excluded by Rocks *et al.* Proteins palmitoylated at the plasma membrane would not depend on a functional secretory pathway for their plasma membrane localization, unlike proteins palmitoylated at the ER/Golgi membranes. The SH4 domain reporter protein seems to reach the plasma membrane also via a secretory pathway-independent route, which could involve its palmitoylation directly at the plasma membrane, as proposed for the Src kinase Fyn (van't Hof *et al.*, 1997; Sato *et al.*, 2009; see section 1.5.1.2). Although the SH4 domain alone was shown to be sufficient for palmitoylation to occur (McCabe *et al.,* 1999; Tournaviti *et al*., 2009), the specificity of interaction with the appropriate PAT may be controlled also by distal parts of the protein to be palmitoylated (Nadolski *et al*., 2009; see section 1.4.4). Thus, our model system, consisting of a SH4 domain fused to a fluorescent protein, may in fact be an oversimplified one, allowing palmitoylation, but making it promiscuous, i.e. occurring at multiple subcellular locations, including the plasma membrane. For the palmitoylation to occur only at locations within the cell typical for endogenous diacylated SH4 domain proteins, interactions mediated by domains downstream of the SH4 domain would be required. As a heterologous protein, however, full-length HASPB may lack domains conferring specificity of interaction with human DHHCs, and thus its palmitoylation could still occur promiscuously. The presence of two alternative pathways in the plasma membrane transport of SH4 domain reporter fusion proteins may explain why during the whole-genome RNAi screen aimed at identifying factors involved in this process, down-regulation of none of the gene products caused complete intracellular retention of the reporter proteins (Ritzerfeld, 2009; Ritzerfeld *et al.,* 2011).

6 Materials and methods

6.1 Materials

6.1.1 Chemicals and consumables

1 kb DNA Ladder	New England Biolabs, Frankfurt, Germany
2-(N-morpholino)ethanesulfonic acid (MES)	Carl Roth GmbH, Karlsruhe, Germany
4-(2-hydroxyethyl)piperazine-1-ethanesulfonic acid (HEPES)	Sigma-Aldrich Chemie GmbH, Steinheim, Germany
5ml Polystyrene Round-Bottom Tubes with Cell-Strainer Cap	BD Biosciences, Erembodegem, Belgium
Acetic acid (CH_3COOH)	Sigma-Aldrich Chemie GmbH, Steinheim, Germany
Agar	Becton Dickinson, Le Pont de Claix, France
Agarose	Invitrogen Ltd., Paisley, UK
Ammonium acetate (CH_3COONH_4)	Sigma-Aldrich Chemie GmbH, Taufkirchen, Germany
Ammonium persulfate (APS)	Carl Roth GmbH, Karlsruhe, Germany
Ampicillin sodium salt	Gerbu Biotechnik GmbH, Gaiberg, Germany
Aqua ad iniectabilia	Braun AG, Melsungen, Germany
BD Microlance 3 27G x 3/4", 0,4 mm x 19 mm needles	Becton Dickinson, Drogheda, Ireland
BD Plastipak 1 ml syringe	Becton Dickinson S.A., Madrid, Spain
BD Plastipak 50 ml syringe	Becton Dickinson, Drogheda, Ireland
Bovine serum albumin (BSA)	Carl Roth GmbH, Karlsruhe, Germany
Brefeldin A (BFA)	Sigma-Aldrich Chemie GmbH, Steinheim, Germany
Bromophenol blue Na-salt	Serva Electrophoresis GmbH, Mannheim, Germany
BSA (100X)	New England Biolabs, Frankfurt, Germany
Cell culture dishes	Corning Inc., Corning, USA
Cell Dissociation Buffer	Invitrogen Ltd., Paisley, UK
Cell scraper 23 cm	Orange Scientific, Braine-l'Alleud, Belgium
Cell scraper 25 cm	Sarstedt AG & Co., Nümbrecht, Germany
Chloroform	Sigma-Aldrich Chemie GmbH, Taufkirchen, Germany
Chloroquine diphosphate salt	Sigma F and D, St. Louis, USA
Collagen R	Serva Electrophoresis GmbH, Heidelberg, Germany
Complete Protease Inhibitor Cocktail Tablets, EDTA-free	Roche Diagnostics, Mannheim, Germany
COPB1 Silencer Pre-designed siRNA, ID: 24546	Ambion, Applied Biosystems, Darmstadt, Germany

CryoTubes Cryo.s	Greiner Bio-One GmbH, Frickenhausen, Germany
Cycloheximide	Sigma-Aldrich Chemie GmbH, Steinheim, Germany
D(+)-saccharose	Applichem GmbH, Darmstadt, Germany
Diethylaminoethyl-dextran (DEAE-dextran)	Sigma-Aldrich Chemie GmbH, Steinheim, Germany
Dimethyl sulfoxide (DMSO)	Sigma-Aldrich Chemie GmbH, Steinheim, Germany
Doxycycline	Clontech Laboratories Inc., Mountain View, USA
Dulbecco's modified Eagle's medium (DMEM)	Biochrom AG, Berlin, Germany
Dynabeads Protein G for Immunoprecipitation	Invitrogen Dynal AS, Oslo, Norway
EM copper grids, hexagonal 100 meshes, G2410C	Plano GmbH, Wetzlar, Germany
Eppendorf tubes 1.5 ml, 2 ml	Sarstedt AG & Co., Nümbrecht, Germany
Erlenmeyer (Fernbach design) cell culture flasks, 3 l	Corning Inc., Corning, USA
Ethanol absolute	Sigma-Aldrich Chemie GmbH, Steinheim, Germany
Ethidium bromide	Carl Roth GmbH, Karlsruhe, Germany
Ethylene glycol-bis(2-aminoethylether)-N,N,N',N'-tetraacetic acid (EGTA)	Sigma-Aldrich Chemie GmbH, Steinheim, Germany
Ethylenediaminetetraacetic acid (EDTA) disodium salt dihydrate	Applichem GmbH, Darmstadt, Germany
Fetal Calf Serum (FCS) gold	PAA Laboratories GmbH, Cölbe, Germany
Formaldehyde 16%	Electron Microscopy Sciences, Science Services GmbH, Munich , Germany
FuGENE HD Transfection Reagent	Promega Corporation, Madison, USA
Gelatin	Merck KGaA, Darmstadt, Germany
Gelatin from cold water fish skin	Sigma-Aldrich Chemie GmbH, Steinheim, Germany
Glass vials, 4 ml + Teflon lined screw caps	Neolab, Heidelberg, Germany
Glutaraldehyde 25%	Electron Microscopy Sciences, Science Services GmbH, Munich , Germany
Glycerol	Carl Roth GmbH, Karlsruhe, Germany
Glycine	Sigma-Aldrich Chemie GmbH, Steinheim, Germany
Hydrochloric acid (HCl) 37%	Merck KGaA, Darmstadt, Germany
Immobilon-FL Transfer Membrane	Millipore Corporation, Bedford, USA
Isopropanol	Merck KGaA, Darmstadt, Germany
JetPRIME transfection reagent	Polyplus-transfection SA, Illkirch, France
Kanamycin sulfate	Gerbu Biotechnik GmbH, Gaiberg, Germany
L-glutamine	Biochrom AG, Berlin, Germany
Lab-Tek Chambered Coverglass, 8-well	Thermo Fisher Scientific, Rochester, USA
Lab-Tek II Coverglass, 2-well	Thermo Fisher Scientific, Rochester, USA
Lipid standards, PC and PI	Avanti Polar Lipids Inc., Alabaster, USA

Magnesium acetate tetrahydrate ($(CH_3COO)_2Mgx4H_2O$)	Sigma-Aldrich Chemie GmbH, Steinheim, Germany
Magnesium chloride, anhydrous ($MgCl_2$)	Sigma-Aldrich Chemie GmbH, Steinheim, Germany
Methanol	Applichem GmbH, Darmstadt, Germany
Methyl cellulose	Sigma-Aldrich Chemie GmbH, Steinheim, Germany
Methylene blue	Carl Roth GmbH, Karlsruhe, Germany
Microfuge Tube Polyallomer, 1.5 ml	Beckman Instruments Inc., Palo Alto, USA
Milk powder	Carl Roth GmbH, Karlsruhe, Germany
Mycoplasma Removal Agent	MP Biomedicals Inc., Solon, USA
N,N,N',N'-tetramethylethylenediamine (TEMED)	Carl Roth GmbH, Karlsruhe, Germany
NEBuffer 1 for restriction enzymes	New England Biolabs, Frankfurt, Germany
NuPAGE Antioxidant	Invitrogen Ltd., Paisley, UK
NuPAGE LDS Sample Buffer (4X)	Invitrogen Ltd., Carlsbad, USA
NuPAGE MOPS SDS Running Buffer (20X)	Invitrogen Ltd., Carlsbad, USA
NuPAGE Novex 4-12% and 10% Bis-Tris Gels	Life Technologies, Carlsbad, USA
NuPAGE Sample Reducing Agent (10X)	Invitrogen Ltd., Carlsbad, USA
Oligofectamine Reagent	Invitrogen Ltd., Carlsbad, USA
Oligonucleotides	Thermo Fisher Scientific GmbH, Ulm, Germany
Open-top polyclear centrifuge tubes, 11x60 mm (SW 60)	Seton Scientific, Petaluma, USA
Open-top polyclear centrifuge tubes, 14x89 mm (SW 41)	Seton Scientific, Petaluma, USA
Open-top polyclear centrifuge tubes, 25x89 mm (SW 32)	Science Services GmbH, Munich, Germany
Opti-MEM I + GlutaMAX-I	Invitrogen Ltd., Paisley, UK
OptiPrep Density Gradient Medium	Sigma-Aldrich Chemie GmbH, Steinheim, Germany
PageRuler Prestained Protein Ladder	Fermentas GmbH, St. Leon-Rot, Germany
Parafilm M	BRAND GMBH + CO KG, Wertheim, Germany
PBS-powder without Ca^{2+}, Mg^{2+}	Biochrom AG, Berlin, Germany
Penicillin/Streptomycin	Biochrom AG, Berlin, Germany
Pioloform (polyvinyl butyral)	Plano GmbH, Wetzlar, Germany
Piperazine-N,N'-bis(2-ethanesulfonic acid) (PIPES)	Carl Roth GmbH, Karlsruhe, Germany
Potassium chloride (KCl)	Applichem GmbH, Darmstadt, Germany
Potassium dihydrogen phosphate (KH_2PO_4)	Applichem GmbH, Darmstadt, Germany
Prestained SDS-PAGE Standards, Broad Range	Bio-Rad Laboratories GmbH, Munich, Germany
Roswell Park Memorial Institute medium (RPMI)	Biochrom AG, Berlin, Germany
Roti-Blue 5X	Carl Roth GmbH, Karlsruhe, Germany
Rotilabo syringe filters, 0.22 µm and 0.45 µm	Carl Roth GmbH, Karlsruhe, Germany

Rotiphorese Gel 30 (37.5:1)	Carl Roth GmbH, Karlsruhe, Germany
Serological pipettes	Greiner Bio-One GmbH, Frickenhausen, Germany
Silencer Negative Control siRNA #1	Ambion, Applied Biosystems, Darmstadt, Germany
Sodium acetate (CH_3COONa)	Grüssing GmbH, Filsum, Germany
Sodium azide (NaN_3)	Carl Roth GmbH, Karlsruhe, Germany
Sodium chloride (NaCl)	Applichem GmbH, Darmstadt, Germany
Sodium dodecyl sulfate (SDS)	Sigma-Aldrich Chemie GmbH, Steinheim, Germany
Sodium hydroxide (NaOH)	Sigma-Aldrich Chemie GmbH, Steinheim, Germany
Sodium phosphate dibasic dihydrate ($Na_2HPO_4x2H_2O$)	Riedel de Haën, Seelze, Germany
Sucrose ultrapure MB grade	Affymetrix, Cleveland, USA
Surgical blades	SCHREIBER GmbH, Fridingen, Germany
Tris(hydroxymethyl)aminomethane (Tris)	Carl Roth GmbH, Karlsruhe, Germany
Triton X-100	Merck KGaA, Darmstadt, Germany
Trypan blue 0.5%	Biochrom AG, Berlin, Germany
Trypsin/EDTA	Biochrom AG, Berlin, Germany
Tryptone	Becton Dickinson, Le Pont de Claix, France
Tubes 15 ml, 50 ml	Sarstedt AG & Co., Nümbrecht, Germany
Tween 20	Carl Roth GmbH, Karlsruhe, Germany
Water HiPerSolv Chromanorm for HPLC	VWR International, Leuven, Belgium
Xylene cyanol FF	Serva Electrophoresis GmbH, Heidelberg, Germany
Yeast extract	Carl Roth GmbH, Karlsruhe, Germany
β-mercaptoethanol	Merck Schuchardt OHG, Hohenbrunn, Germany
µ-Dish 35 mm, glass bottom	ibidi GmbH, Martinsried , Germany

6.1.2 Enzymes

AgeI restriction enzyme	New England Biolabs, Frankfurt, Germany
BamHI-HF restriction enzyme	New England Biolabs, Frankfurt, Germany
Tobacco etch virus (TEV) protease	Research Group Prof. Dr. Walter Nickel

6.1.3 Antibodies

6.1.3.1 Primary antibodies

Antigen	Antibody - primary	Manufacturer/source	Application	Dilution
Brain acid soluble protein 1	Nap-22 antibody (H-100): sc-66994, rabbit polyclonal	Santa Cruz Biotechnology Inc., Heidelberg, Germany	Western blotting	1:20, 1:50
Flotillin-1	Flotillin-1 (H-104) antibody: sc-25506, rabbit polyclonal	Santa Cruz Biotechnology Inc., Heidelberg, Germany	Western blotting	1:200
GFP	Rabbit anti-GFP, polyclonal, affinity purified	Research Group Prof. Dr. Walter Nickel	Western blotting Immunoelectron microscopy	1:500 1:20
GFP	Living Colors anti-GFP, mouse monoclonal	Clontech Laboratories Inc., Mountain View, USA	Western blotting	1:5000, 1:10000
GM130	Anti-GOLGA2 antibody, rabbit polyclonal, HPA021799	Sigma-Aldrich Chemie GmbH, Steinheim, Germany	Western blotting Immunoelectron microscopy	1:500 1:5
mCherry, mRFP	Anti-mRFP, rabbit polyclonal	Research Group Dr. Barbara Müller, Department of Infectious Diseases, Virology, University Hospital of Heidelberg	Immunoelectron microscopy	1:30, 1:50
Moesin	Moesin antibody (38/87): sc-58806, mouse monoclonal	Santa Cruz Biotechnology Inc., Heidelberg, Germany	Western blotting	1:50
Non-POU domain-containing octamer-binding protein	P54/nrb antibody (C-16): sc-46220, goat polyclonal	Santa Cruz Biotechnology Inc., Heidelberg, Germany	Western blotting	1:20, 1:50
Ras GTPase-activating-like protein IQGAP1	IQGAP1 antibody (H-109): sc-10792, rabbit polyclonal	Santa Cruz Biotechnology Inc., Heidelberg, Germany	Western blotting	1:500
Ribophorin-1	Ribophorin-1 (C-15) antibody: sc-12164, goat polyclonal	Santa Cruz Biotechnology Inc., Heidelberg, Germany	Western blotting	1:200
Splicing factor, proline- and glutamine-rich	Anti-SFPQ antibody (ab99357), rabbit polyclonal	Abcam, Cambridge, UK	Western blotting	1:5000, 1:10000

Antigen	Antibody - primary	Manufacturer/source	Application	Dilution
TGN46	Anti-TGOLN2 antibody, rabbit polyclonal, HPA012723	Sigma-Aldrich Chemie GmbH, Steinheim, Germany	Immunoelectron microscopy	1:25
Transferrin receptor	Mouse anti-human transferrin receptor, monoclonal, clone H68.4	Zymed Laboratories Inc., San Francisco, USA	Western blotting	1:500
Yes	Purified mouse anti-Yes, monoclonal	BD Transduction Laboratories, San Diego, USA	Western blotting	1:500

6.1.3.2 Secondary antibodies

Antigen	Antibody - secondary	Manufacturer	Application	Dilution
Goat IgG	Alexa Fluor 680 donkey anti-goat IgG (H+L)	Molecular Probes, Leiden, Germany	Western blotting	1:10000
Mouse IgG	Alexa Fluor 680 goat anti-mouse IgG (H+L)	Molecular Probes, Leiden, Germany	Western blotting	1:10000
Mouse IgG	IRDye 800CW goat anti-mouse IgG (H+L)	LI-COR Biosciences, Bad Homburg, Germany	Western blotting	1:10000
Rabbit IgG	Alexa Fluor 680 goat anti-rabbit IgG (H+L)	Molecular Probes, Leiden, Germany	Western blotting	1:10000
Rabbit IgG	Mouse anti-rabbit IgG (conformation specific) (L27A9) mAb	Cell Signaling Technology Inc., Danvers, USA	Western blotting	1:2000

6.1.3.3 Tertiary antibodies

Antigen	Antibody - tertiary	Manufacturer	Application	Dilution
Mouse IgG	Alexa Fluor 680 goat anti-mouse IgG (H+L)	Molecular Probes, Leiden, Germany	Western blotting	1:20000
Mouse IgG	IRDye 800CW goat anti-mouse IgG (H+L)	LI-COR Biosciences, Bad Homburg, Germany	Western blotting	1:20000

6.1.4 Molecular biology and biochemical kits

DNA Ligation Kit Ver.2.1	TaKaRa Biochemical, Berkeley, USA
MBS Mammalian Transfection Kit	Stratagene, La Jolla, USA
NucleoBond PC 100	Macherey-Nagel, Düren, Germany
NucleoSpin Plasmid	Macherey-Nagel, Düren, Germany
QIAGEN Plasmid Midi Kit	QIAGEN GmbH, Hilden, Germany
QIAquick Gel Extraction Kit	QIAGEN GmbH, Hilden, Germany

6.1.5 Technical devices

4639 Cell Disruption Vessel	Parr Instrument Company, Moline, USA
Agarose gel chamber	Bio-Rad Laboratories GmbH, Munich, Germany
BILATEST Separator M12+12	Bilatec AG, Viernheim, Germany
Centrifuge 5415C	Eppendorf AG, Hamburg, Germany
Centrifuge 5417R	Eppendorf AG, Hamburg, Germany
Centrifuge 5804	Eppendorf AG, Hamburg, Germany
Centrifuge 5804R	Eppendorf AG, Hamburg, Germany
CP64 Balance	Sartorius AG, Göttingen, Germany
Cryo-ultramicrotome EM UC6/EM FC6	Leica Mikrosysteme GmbH, Vienna, Austria
Diamond cutting knife cryo immuno	Diatome AG, Biel, Switzerland
Diamond trimming knife cryotrim 45°	Diatome AG, Biel, Switzerland
DigestPro MS	Intavis AG, Cologne, Germany
Dynal MPC-1 Magnetic Particle Concentrator	Invitrogen Dynal AS, Oslo, Norway
EM 10 transmission electron microscope	Carl Zeiss, Göttingen, Germany
ESI-LTQ-Orbitrap mass spectrometer	Thermo Fisher Scientific Inc., Dreiech, Germany
FACSAria cell sorter	Becton Dickinson, Le Pont de Claix, France
FACSCalibur	Becton Dickinson, Le Pont de Claix, France
Function Line T12 Incubator	Heraeus, Hanau, Germany
Gel Doc 2000 Gel Documentation System	Bio-Rad Laboratories GmbH, Munich, Germany
HAAKE DC10 Water Bath	Thermo Fisher Scientific GmbH, Ulm, Germany
Heraeus Megafuge 40R	Thermo Fisher Scientific GmbH, Ulm, Germany
HERAsafe Microbiological Safety Cabinet	Thermo Fisher Scientific GmbH, Ulm, Germany
Inertsil C18 3 µm analytical column	LC Packings-Dionex GmbH, Idstein, Germany
Inertsil C18 trapping column	LC Packings-Dionex GmbH, Idstein, Germany
Kern 474 Balance	Gottl. Kern & Sohn GmbH, Albstadt, Germany
Liebisch evaporator and heating device	Liebisch GmbH & Co. KG, Bielefeld, Germany
LSM 510 Confocal Laser Scanning Microscope	Carl Zeiss, Göttingen, Germany

Magnetic Stirrers MR 3000 and 3001	Heidolph Instruments GmbH & Co. KG, Schwabach, Germany
Mini Trans-Blot System	Bio-Rad Laboratories GmbH, Munich, Germany
Mini-PROTEAN 3 Cell	Bio-Rad Laboratories GmbH, Munich, Germany
Multitron Incubator System	Infors GmbH, Einsbach, Germany
Nano-ESI emitter	New Objective Inc., Woburn, USA
NanoDrop ND-1000 Spectrophotometer	NanoDrop Technologies, Wilmington, USA
Nano-HPLC system	Eksigent, Axel Semrau GmbH, Sprockhövel, Germany
Odyssey Imaging System	LI-COR Biosciences, Bad Homburg, Germany
PH-Meter766 Calimatic	Knick GmbH, Egelsbach, Germany
PIPETBOY acu	INTEGRA Biosciences GmbH, Fernwald, Germany
Power Pac 200 and 300	Bio-Rad Laboratories GmbH, Munich, Germany
Promax 2020 Platform Shaker	Heidolph Instruments GmbH & Co. KG, Schwabach, Germany
Quattro II (triple quadrupole mass spectrometer)	Micromass, Manchester, UK
Sonorex ultrasonic bath	Bandelin Electronic, Berlin, Germany
Sorvall Evolution RC Centrifuge	Thermo Fisher Scientific, Kendro Laboratory Products, Hanau, Germany
Sorvall SLC-6000 rotor	Thermo Fisher Scientific, Kendro Laboratory Products, Hanau, Germany
SpeedVac vacuum centrifuge	Savant Instruments Inc., Holbrook, USA
Steri-Cycle CO_2 incubator	Thermo Fisher Scientific GmbH, Ulm, Germany
SW 60, SW 41 Ti and SW 32 Ti rotors	Beckman Coulter, Fullerton, USA
TC10 Automated Cell Counter	Bio-Rad Laboratories GmbH, Munich, Germany
Thermomixer 5436	Eppendorf AG, Hamburg, Germany
Thermomixer comfort and compact	Eppendorf AG, Hamburg, Germany
TLA-55 rotor	Beckman Coulter, Fullerton, USA
Ultracentrifuge Optima L-90K	Beckman Instruments GmbH, Munich, Germany
Ultracentrifuge Optima LE-80K	Beckman Instruments GmbH, Munich, Germany
Ultracentrifuge Optima MAX	Beckman Instruments GmbH, Munich, Germany
Ultracentrifuge Optima TLX	Beckman Instruments GmbH, Munich, Germany
Vortex mixer Reax control	Heidolph Instruments GmbH & Co. KG, Schwabach, Germany
XCell *SureLock* Mini-Cell Electrophoresis System	Invitrogen Ltd., Carlsbad, USA

6.2 Molecular biology methods

6.2.1 Digestion of DNA with restriction enzymes

Digestion of plasmid DNA with restriction endonucleases (New England Biolabs) was performed according to manufacturer's instructions, using 2-5 µg of DNA for preparative, and 500 ng for control digests, at 37°C, for 1.5-3 hours.

6.2.2 Agarose gel electrophoresis

DNA was separated in 1% agarose gels, prepared in 1x TAE (Tris-acetate-EDTA) buffer, with ethidium bromide added to the final concentration of 0.5 µg/ml. Samples were loaded in 1x sample buffer. 1 kb DNA Ladder (New England Biolabs) was used as a molecular weight marker. Electrophoretic separation was performed in 1x TAE buffer at 100 V for 30 minutes. Bands were visualized and documented using the gel documentation system Gel Doc 2000 (Bio-Rad).

TAE buffer (50x):
2 M Tris
2 M acetic acid
50 mM EDTA, pH 8.0

Sample buffer (5x):
0.25% (w/v) bromophenol blue
0.25% (w/v) xylene cyanol FF
30% (w/v) glycerol

6.2.3 Extraction of DNA from agarose gels

The DNA band of interest was cut out of the gel with a scalpel and processed using QIAquick Gel Extraction Kit (QIAGEN), according to manufacturer's instructions. In the last step the DNA was eluted from the column with 30 µl of elution buffer (EB).

6.2.4 Annealing of single-stranded oligonucleotides

Complementary single-stranded oligonucleotides (0.1 pmol/µl, in water) were mixed together (10 µl of each), incubated at 95°C for 10 minutes, and then slowly cooled down

to room temperature. The annealed oligonucleotide inserts were used in a ligation reaction.

Name	Sequence
Bam HASPB SH4-TEV Age For	gatccCGCCACCATGGGAAGTTCTTGTACAAAGGACTCCGCAAAGGAGCCCCAGAAGAGTGCTGAT**GAGAATTTGTATTTTCAGGGT**a
Bam HASPB SH4-TEV Age Rev	ccggt**ACCCTGAAAATACAAATTCTC**ATCAGCACTCTTCTGGGGCTCCTTTGCGGAGTCCTTTGTACAAGAACTTCCCATGGTGGCGg
Bam HASPB SH4 Δpal-TEV Age For	gatccCGCCACCATGGGAAGTTCTTCTACAAAGGACTCCGCAAAGGAGCCCCAGAAGAGTGCTGAT**GAGAATTTGTATTTTCAGGGT**a
Bam HASPB SH4 Δpal-TEV Age Rev	ccggt**ACCCTGAAAATACAAATTCTC**ATCAGCACTCTTCTGGGGCTCCTTTGCGGAGTCCTTTGTAGAAGAACTTCCCATGGTGGCGg
Bam Yes SH4-TEV Age For	gatccCGCCACCATGGGCTGCATTAAAAGTAAAGAAAACAAAAGTCCAGCCATTAAATACAGACCT**GAGAATTTGTATTTTCAGGGT**a
Bam Yes SH4-TEV Age Rev	ccggt**ACCCTGAAAATACAAATTCTC**AGGTCTGTATTTAATGGCTGGACTTTTGTTTTCTTTACTTTTAATGCAGCCCATGGTGGCGg

Table 2 Oligonucleotides used to generate constructs utilized in this study. Nucleotides which upon annealing of oligonucleotides form AgeI or BamHI sticky ends are represented by lower case letters. Nucleotides shown in bold type encode tobacco etch virus (TEV) protease cleavage site (amino acid residues ENLYFQG). Nucleotides encoding the mutated residue are highlighted in red.

6.2.5 Ligation of insert and vector

Ligations were performed at 16°C for 1 hour with the TaKaRa DNA Ligation Kit Ver.2.1 according to manufacturer's instructions, using 50 ng of vector DNA, with 1:1, 1:3 and 1:6 (or 1:10) molar ratios of vector to insert, and also without insert (vector self-ligation control).

6.2.6 Transformation of plasmid DNA into *Escherichia coli*

Chemocompetent *Escherichia coli* DH5α were mixed with DNA (an aliquot of ligation reaction or plasmid DNA in the case of retransformation). After a 30-minute incubation on ice, bacteria were subjected to a 20-second heat-shock at 37°C and further incubated on ice for 2 minutes, which was followed by the addition of LB (Luria-Bertani) medium (1% NaCl/1% tryptone/0.5% yeast extract; all w/v). Upon an 1-hour incubation at 37°C with shaking (600 rpm), cells were spread on LB agar plates containing appropriate antibiotics (100 µg/ml ampicillin or 30 µg/ml kanamycin), followed by overnight incubation at 37°C.

6.2.7 Small-scale isolation of plasmid DNA

5 ml of LB medium containing appropriate antibiotics was inoculated with a single colony and incubated overnight at 37°C with shaking (180 rpm). Plasmid DNA was isolated using the NucleoSpin Plasmid (Macherey-Nagel), according to manufacturer's instructions. Concentration of the isolated DNA was determined using the NanoDrop ND-1000 spectrophotometer.

6.2.8 Medium-scale isolation of plasmid DNA

LB medium containing appropriate antibiotics was inoculated with a single colony and incubated overnight at 37°C with shaking (180 rpm). Plasmid DNA was isolated from 125 ml of culture for low-copy and 40-50 ml for high-copy plasmids, with the use of the NucleoBond PC 100 (Macherey-Nagel) or QIAGEN Plasmid Midi (QIAGEN) kits, according to manufacturers' instructions. DNA was reconstituted in water and its concentration and quality determined using the NanoDrop ND-1000 spectrophotometer and agarose gel electrophoresis.

6.2.9 Sequencing of DNA

The correctness of the DNA constructs was confirmed by DNA sequencing performed by GATC Biotech AG, Konstanz (20 µl samples, DNA concentration 30-100 ng/µl), using pRevTRE2 For or GFP Rev primers for pRevTRE2/GFP constructs, and standard CMV For primer in the case of pEGFP-N1, pmRFP-N1, or pIRES2-based constructs.

6.3 Biochemical methods

6.3.1 Electrophoresis in polyacrylamide gels

Proteins were separated using sodium dodecyl sulfate polyacrylamide gel electrophoresis (SDS-PAGE) in the Laemmli system (Laemmli, 1970). Samples (in 1x concentrated sample buffer) were incubated at 95°C for 5 minutes, stacked in 4% polyacrylamide stacking gel at 100 V, and resolved in 12% separating gel at 200 V. As protein molecular weight markers, Prestained SDS-PAGE Standards, Broad Range (Bio-Rad) or PageRuler Prestained Protein Ladder (Fermentas) were used.

Sample buffer (4x):
240 mM Tris, pH 6.8
25% (v/v) glycerol
8% (w/v) SDS
0.04% (w/v) bromophenol blue
5% (v/v) β-mercaptoethanol

Stacking gel:
4% (w/v) acrylamide/bisacrylamide (37.5:1)
125 mM Tris, pH 6.8
0.1% (w/v) SDS
0.075% (w/v) APS
0.1% (v/v) TEMED

Separating gel:
12% (w/v) acrylamide/bisacrylamide (37.5:1)
375 mM Tris, pH 8.8
0.1% (w/v) SDS
0.075% (w/v) APS
0.05% (v/v) TEMED

Running buffer:
25 mM Tris, pH 8.3
192 mM glycine
0.1% (w/v) SDS

When a good separation of a broad range of protein sizes was desirable, precast NuPAGE Novex 4-12% Bis-Tris Gels (Life Technologies) were used, together with 1x MOPS SDS Running Buffer. Samples (in 1x concentrated NuPAGE LDS Sample Buffer, with NuPAGE Sample Reducing Agent added) were incubated at 70°C for 10 minutes. Lysate samples were instead boiled at 95°C for 10 minutes, followed by a 10-minute incubation in an ultrasonic bath. Samples were loaded onto a gel and resolved at 200 V for 50-60 minutes.

Samples to be analyzed by mass spectrometry were incubated at 70°C for 10 minutes in 1x concentrated NuPAGE LDS Sample Buffer, with NuPAGE Sample Reducing Agent added. Pelleted TEV eluates were first incubated in 1x concentrated NuPAGE LDS Sample Buffer (with NuPAGE Sample Reducing Agent added) at 37°C for 30-60 minutes with shaking, followed by incubation at 70°C as above. Samples were partially resolved in precast NuPAGE Novex 10% Bis-Tris Gels (1 mm thick) at 200 V for 7-8 minutes, using

1x MOPS SDS Running Buffer. Before electrophoresis, the gel running chamber was incubated overnight in 100 mM NaOH, and subsequently rinsed with ultrapure water.

6.3.2 Staining of polyacrylamide gels with Colloidal Coomassie

Gels were placed in 15 cm cell culture dishes, washed 2 times for 5 minutes in ultrapure water on a platform shaker, and then fixed for 30-45 minutes in 2% (v/v) acetic acid/4% (v/v) methanol (50 ml/gel). Gels were then stained for 1.5 hours in 1x Roti-Blue (Carl Roth)/20% (v/v) methanol (50 ml/gel) (first 10 ml of 5x Roti-Blue and 10 ml of methanol were mixed and vortexed, then water was added and the solution was vortexed again). Gels were destained in ultrapure water.

6.3.3 Western blotting

After protein separation by PAGE, proteins were transferred to polyvinylidene fluoride (PVDF) membrane (Immobilon-FL, Millipore) by wet blotting at 100 V for 60 minutes (for 0.75 mm and 1 mm gels) or 75 minutes (for 1.5 mm gels).

Blotting buffer:
25 mM Tris, pH 8.4
40 mM glycine
20% (v/v) methanol

After transfer, the membrane was blocked in 5% (w/v) milk in PBS (140 mM NaCl/2.7 mM KCl/1.2 mM KH_2PO_4/10 mM Na_2HPO_4) for 1 hour at room temperature or overnight in the cold room, and then washed 2 times for 5 minutes with PBST (0.05% (w/v) Tween 20 in PBS) on a platform shaker. After an 1-hour incubation at room temperature with primary antibody (diluted in PBST containing 1.5% (w/v) bovine serum albumin, BSA), the membrane was washed 4 times for 4 minutes with PBST, and then incubated with shaking with Alexa Fluor 680 or IRDye 800CW-coupled secondary antibody (in PBST containing 1.5% BSA) for 30 minutes at room temperature in the dark. After 4 washes for 4 minutes with PBST and one with PBS, the membrane was scanned and the signals quantified with the use of the Odyssey Imaging System (LI-COR).

6.3.4 Isolation of detergent-resistant membranes (DRMs)

A confluent 10 cm plate of HeLa or HeLa S3 cells was washed twice with cold PBS, and then scraped on ice with a cell scraper in 1-1.5 ml of PBS and transferred into a precooled Eppendorf tube. Cells were sedimented by centrifugation at 400 g at 4°C for 3 minutes, and resuspended in 400 µl of cold MBS TX^+ buffer. The cell suspension was incubated on ice for 45 minutes, while vortexing every 10 minutes, and then passed 10 times through a precooled 27G needle, using a 1 ml syringe. The lysate was centrifuged (800 g, 4°C, 5 minutes), the supernatant collected (post-nuclear supernatant, PNS), and an aliquot saved for Western blotting. 350 µl of PNS was loaded on the bottom of a SW 60 centrifuge tube and mixed with 700 µl of OptiPrep (i.e. 60% iodixanol), resulting in a final concentration of 40% iodixanol. 2.35 ml of 28% iodixanol (in MBS TX^+) was then layered on top, followed by 600 µl of MBS TX^+. The gradient was centrifuged at 35000 rpm at 4°C for 2 hours (SW 60 rotor, slow acceleration and deceleration). 8 fractions of 500 µl each were collected from the top of the gradient. Before collecting the last fraction the centrifuge tube was vortexed. Equal aliquots of each fraction were analyzed by Western blotting.

MBS TX^+ buffer:
20 mM MES, pH 6.5
150 mM NaCl
1% (w/v) Triton X-100
Complete Protease Inhibitor Cocktail (EDTA-free)

6.3.5 Disruption of human cells using nitrogen cavitation

Cell disruption chamber (4639 Cell Disruption Vessel, Parr) was placed on ice on a magnetic stirrer (1400 rpm), with the collection valve closed. Suspension of HeLa S3 cells in homogenization buffer (HB^+) was placed into the cell disruption chamber. Afterwards the chamber was attached to the filling hose, with the bomb inlet valve closed, and then the main valve was opened. The bomb inlet valve was gently opened until the desired pressure inside the chamber (2000 psi) was obtained. The nitrogen was allowed to dissolve within the cells during a 30-minute incubation, during which the bomb was repressurized several times in order to maintain the desired pressure level. A precooled

50 ml Falcon tube was placed at the base of the collection valve, which was then slowly opened to release the pressure and collect lysed cells. The pressure in the filling hose was then released by opening the bomb inlet valve. The lysate was rotated in the cold room to allow the foam to subside before centrifugation. Between different samples, the bomb was rinsed with water and then with homogenization buffer. After use the bomb was rinsed thoroughly with water and 70% ethanol.

HB^+ buffer:
10 mM Tris, pH 7.4
250 mM sucrose
0.5 mM magnesium acetate
Complete Protease Inhibitor Cocktail (EDTA-free)

6.3.6 Immunoaffinity purification of detergent-resistant membranes containing SH4 domain fusion proteins

HeLa S3 cells were grown on 10 cm plates in Dulbecco's modified Eagle's medium (DMEM). 4-5 days before immunoisolation, suspension culture was started: cells from 6-8 plates were trypsinized and transferred to 3 l Erlenmeyer cell culture flasks (Corning), filling them up to 400-500 ml with Roswell Park Memorial Institute (RPMI) medium, so as to obtain the concentration of $5x10^4$-$1x10^5$ cells/ml. The suspension was diluted after a couple of days, so as not to exceed the cell density of $8x10^5$/ml. Expression of SH4-TEV-GFP fusion proteins was induced with doxycycline (1 µg/ml, added from a stock solution of 1000 µg/ml in PBS) for 48 hours. Cells were harvested by centrifugation (1500 rpm, 4°C, 15 minutes, rotor SLC-6000), washed 3 times with 50 ml of PBS (each centrifugation: 500 g, 4°C, 5 minutes), followed by 3 washes with HB (500 g, 4°C, 5 minutes). Before the last centrifugation, cells were counted with trypan blue using a Bio-Rad TC10 automated cell counter. Pelleted cells were resuspended in HB^+ at a density of 4-$8x10^7$ cells/ml) and disrupted by nitrogen cavitation (as described in section 6.3.5). The lysates were subjected to differential centrifugation: at 3000 g at 4°C for 10 minutes, followed by 2 times at 15000 g at 4°C for 10 minutes. The resulting post-mitochondrial supernatants (PMS) were transferred to SW 32 centrifuge tubes,

filled up to 38 ml with MBS buffer, and centrifuged at 28000 rpm at 4°C for 60 minutes (rotor SW 32 Ti).

MBS buffer:
20 mM MES, pH 6.5
150 mM NaCl

Microsomal pellets were weighed, and 1 ml of MBS TX^+ was added for every 0.1 g of the pellet. Solubilization was carried out on ice for 60 minutes, while vortexing and pipetting every 10 minutes, and completed by passing 15 times through a precooled 27G needle, using a 1 ml syringe. Density gradients were prepared in SW 41 centrifuge tubes (1 or 2 gradients for each cell line): 800-1350 µl of solubilized microsomes were loaded on the bottom of the tube and mixed with an appropriate amount of 60% iodixanol to obtain a final concentration of 40% iodixanol. 6.15-7.80 ml of 28% iodixanol were then layered on top, followed by 1.8 ml of MBS TX^+. Gradients were centrifuged at 28000 rpm at 4°C overnight (14-16 hours, SW 41 Ti rotor, slow acceleration and deceleration). 8 fractions of 1.5 ml each were collected; before collecting the last fraction the centrifuge tube was vortexed. Protein G Dynabeads (Dynal) were washed 3 times with PBST (in a 15 ml Falcon tube, using Dynal MPC-1 magnet for retrieving beads), and incubated with affinity-purified anti-GFP antibodies (acidic fraction; Research Group Prof. Dr. Walter Nickel) in PBST, overnight in the cold room with rotation. The beads were then washed 2 times with PBST and 2 times with MBS. Fractions 2 from density gradients ('total DRMs') were incubated with the washed magnetic beads for 2 hours in the cold room with rotation. Afterwards, the beads were washed 2 times with MBS TX and 4 times with MBS (each wash: a 5-minute incubation in the cold room with rotation), and then incubated with tobacco etch virus (TEV) protease in MBS for 3-3.5 hours in the cold room with rotation. Beforehand, the protease had been spun down at 55000 rpm at 4°C for 20 minutes (rotor TLA55). After the incubation, supernatants (i.e. TEV eluates) were collected, and the magnetic beads were washed 3 times with MBS. Each TEV eluate was transferred to 1 or 2 SW 60 tubes, which were then filled up to 4 ml with MBS, and centrifuged at 37200 rpm at 4°C for 1.5 hours.

6.3.7 Lipid mass spectrometry

Lipid extractions were performed as described (Haag, 2010), with minor modifications: 1.9 ml of chloroform/methanol/37% HCl (40:80:0.6, v/v/v) and x µl of sample were added to Teflon-sealed glass vials containing lipid standards: PC mix (13:0/13:0, 14:0/14:0, 20:0/20:0, and 21:0/21:0), PE mix (14:1/14:1, 20:1/20:1, and 22:1/22:1), PS mix (14:1/14:1, 20:1/20:1, and 22:1/22:1), PG mix (14:1/14:1, 20:1/20:1, and 22:1/22:1), PI 37:4, PA 37:4, Cer mix (14:0, 19:0 and 25:0), HexCer mix (14:0, 19:0 and 25:0), and d6-cholesterol (CIS). PC and PI were purchased from Avanti Polar Lipids, all other standards were synthesized by Research Group Prof. Dr. Felix Wieland/Dr. Britta Brügger. Upon vortexing, water (500 µl – x µl of sample) was added. After vortexing again, 500 µl of chloroform and 500 µl of water were added, followed by vortexing and centrifugation (2000 rpm, room temperature, 2 minutes) to induce phase separation. The lower (chloroform) phase was transferred to a second vial, and then to both the aqueous phase and the chloroform phase 500 µl of chloroform and 500 µl of water were added, followed by vortexing and centrifugation. The chloroform phase of the second vial was transferred to a third vial. The chloroform phase of the first vial was transferred to the second vial (containing the aqueous phase), followed by re-extraction. After phase separation, the chloroform phase of the second vial was transferred to the third vial, followed by solvent evaporation by a gentle stream of argon at 37°C. Lipids were resuspended in 20 mM ammonium acetate in methanol. Nano-ESI-MS/MS analysis was performed using a Quattro II triple quadrupole mass spectrometer (Micromass), as described (Lorizate *et al.,* 2013). Quantitative analyses were performed as described (Brügger *et al*., 1997; Brügger *et al.,* 2000). Statistical significance of the differences in lipid composition between solubilized microsomes versus total DRMs, and total DRMs versus TEV eluates, was determined by a paired Student's t-test using Prism 5 software (version 5.0c; GraphPad Software Inc.).

6.3.8 Protein mass spectrometry

6.3.8.1 Sample preparation and liquid chromatography-tandem mass spectrometry (LC-MS/MS)

Proteins were partially resolved in a precast NuPAGE Novex 10% Bis-Tris Gel and stained

with Colloidal Coomassie as described (sections 6.3.1 and 6.3.2, respectively). Each lane was cut into 3 slices of about 4 mm in length, which were then subjected to reduction with DTT, alkylation with iodoacetamide, and digestion with trypsin (Catrein *et al.*, 2005), performed with the automated system DigestPro MS (Intavis). Tryptic peptides were eluted from the gel slices with 50% (v/v) acetonitrile/0.1% (v/v) trifluoroacetic acid (TFA). The eluate was evaporated nearly to dryness using a SpeedVac vacuum concentrator (Savant), and diluted to 50 µl with 0.1% (v/v) TFA. 25 µl of the sample were analyzed by a nano-HPLC system (Eksigent) coupled to a nano-ESI-LTQ-Orbitrap mass spectrometer (Thermo Fisher Scientific). The sample was injected onto an Inertsil C18 trapping column (LC Packings) using 0.1% TFA at a flow rate of 10 µl/min. Peptides were eluted, followed by separation on an Inertsil C18 3 µm analytical column (75 µm x 150 mm; LC Packings) at a flow rate of 200 nl/min using a gradient of buffer A (0.1% (v/v) formic acid in water) and buffer B (0.1% formic acid in acetonitrile): 0-6 min, 3% B; 6-60 min, 3-40% B; 60-65 min, 60-90% B. The column was connected to a nano-ESI emitter (New Objective). 1500 V were applied via liquid junction. One survey scan (resolution 60000) was followed by 5 information-dependent product ion scans in the LTQ. Only doubly and triply charged ions were selected for fragmentation.

6.3.8.2 Protein identification

MS/MS spectra were extracted by Mascot Daemon without grouping or smoothing and analyzed using Mascot software (version 2.2.04; Matrix Science; Perkins *et al.*, 1999). The database was set to Swiss-Prot (taxonomy filter: *Homo sapiens*), the protease was set to trypsin, and the allowed number of missed cleavages was set to 1. Fixed modification was set to carbamidomethylation of cysteine. Variable modifications were set to: deamidation of asparagine and glutamine, and oxidation of methionine. Peptide and fragment mass tolerance were set to 100 ppm and 0.5 Da, respectively. MS/MS-based peptide and protein identifications were validated using Scaffold (version Scaffold_3_00_08; Proteome Software Inc.; Searle, 2010). The cut-offs in Scaffold were set to: 95% protein identification probability as specified by the ProteinProphet algorithm (Nesvizhskii *et al.,* 2003), 95% peptide identification probability as assigned by the PeptideProphet algorithm (Keller *et al.,* 2002), and a minimum of two peptides. Common contaminants were excluded from protein identification lists. Proteins that

were indistinguishable given the available mass spectrometry data were reported together in a group. Peptides shared between proteins were assigned to the one with the most evidence according to the ProteinProphet algorithm. Each protein identification was assigned a subcellular localization based on information available from the Swiss-Prot database.

6.3.8.3 Quantification of relative protein amounts using exponentially modified protein abundance index (emPAI)

Relative amounts of proteins in TEV eluates, as compared with total DRMs, were quantified using a label-free approach, the exponentially modified protein abundance index (emPAI) method (Ishihama *et al*., 2005). EmPAI values were calculated according to the equation: $emPAI=10^{PAI}-1$, where PAI is the number of experimentally observed peptides per protein, normalized by the number of observable peptides per protein, $PAI=n_{observed}/n_{observable}$. Regarding the number of observed peptides per protein, unique parent ions (including different charge or modification states from the same peptide sequences) were counted, as this method was shown to give the best correlation between emPAI values and protein abundance (Ishihama *et al*., 2005). The number of observed unique parent ions (number of unique spectra) for each protein was exported from Scaffold 3. For each protein, the number of observable peptides in the mass range of 797-4060 Da was calculated using Protein Digestion Simulator (http://omics.pnl.gov/software/ProteinDigestionSimulator.php), by performing *in silico* a tryptic digest with no missed cleavages of a protein database in FASTA format (composed of the identified proteins, exported from Scaffold 3), and filtering the resulting peptides to exclude peptides outside the mass spectrometer scan range. The resulting emPAI values were normalized by amounts of total lipid in each sample to correct for unequal protein amounts, based on the assumption that the lipid/protein ratio is constant. For each protein, enrichment factor was calculated as the ratio between normalized emPAI value in TEV eluate and normalized emPAI value in the respective total DRMs. For those proteins that were only detected in a TEV eluate (and not in the respective total DRMs), the missing values were replaced before normalization by minimal emPAI values (calculated for 1 observed unique parent ion), allowing us to calculate minimal enrichment factors.

6.3.8.4 Quantification of relative protein amounts based on integrated areas of LC-MS peaks

Detection of peptide chromatographic peaks and quantification of the integrated peak area was performed using MaxQuant software, version 1.3.0.5 (Cox *et al.,* 2008), followed by a search against the human International Protein Index database (IPI; version 3.68) using Andromeda, a peptide search engine integrated into the MaxQuant software (Cox *et al.,* 2011). The protease was set to trypsin, the allowed number of missed cleavages was set to 1. Fixed modification was set to carbamidomethylation of cysteine. Variable modifications were set to: deamidation of asparagine and glutamine, and oxidation of methionine. The false discovery rate (FDR) was set to 0.05 for both peptides and proteins, the maximum peptide posterior error probability (PEP) to 0.01, the minimum peptide length was set to 7 amino acids, and the minimum score to 30. The 're-quantify' and 'label-free quantification' options were enabled. For each protein identified in both TEV eluate and the respective total DRMs, we chose 2 or 3 peptides with the highest intensity in TEV eluate. For each of the peptides, ratios between their peak areas in TEV eluate and the respective total DRMs were calculated and then averaged, to obtain protein ratios. Only peptides with the Andromeda peptide score above 80 were taken into account. When it was possible, only peptides unique for a protein were used for quantification. Otherwise, also peptides shared between proteins were used. Shared peptides were assigned to the protein with the most evidence according to Scaffold 3 (section 6.3.8.2). The averaged peak area ratios were normalized using data on the yield of total lipid in each sample, acquired using lipid MS.

6.4 Cell culture techniques

6.4.1 Maintenance of human cell lines

All cell lines were cultivated at 37°C in a humidified atmosphere containing 5% CO_2. HeLa (human epithelial carcinoma) cells and adherently grown HeLa S3 cells (a clonal derivative of HeLa cell line, capable of suspension growth) were cultivated in DMEM containing 10% (v/v) fetal calf serum (FCS), 2 mM L-glutamine and 100 µg/ml penicillin/streptomycin. HeLa S3 cells were grown in suspension in RPMI medium containing 10% (v/v) FCS, 2 mM L-glutamine and 100 µg/ml penicillin/streptomycin, with

shaking (42-46 rpm). Human embryonic kidney 293T (HEK 293T) cells were cultivated in DMEM containing the above supplements, on collagen-coated plates (rinsed with a 200 µg/ml collagen R solution in water and then left to dry). Adherent cells were passaged twice a week: the cultivation medium was aspirated, cells were washed with PBS and detached by trypsin/EDTA for 10 minutes at 37°C. Fresh medium was added, and then an aliquot of the cells was transferred into a new culture dish containing fresh growth medium.

6.4.2 Freezing and thawing of cells

Cells were grown on 10 cm dishes until subconfluency. Growth medium was discarded, cells washed with PBS and detached by incubation with trypsin/EDTA. Fresh medium was added, the cells were pelleted at 200 g for 3 minutes and resuspended in freezing medium at the density of 2-5x10^6 cells/ml, transferred into cryo tubes, and placed at -80°C for 24-48 hours in a Styrofoam box. For long-term storage, cells were transferred to liquid nitrogen.

Freezing medium:
20% (v/v) FCS
10% (v/v) DMSO
2 mM L-glutamine
100 µg/ml penicillin/streptomycin
in DMEM

To thaw the cells, cryo tubes were incubated in a water bath at 37°C, and the thawed cell suspension transferred to prewarmed growth medium. Cells were then sedimented and resuspended in fresh prewarmed growth medium. After thawing, the cells were incubated for a week with Mycoplasma Removal Agent (MP Biomedicals), added to the culture medium at the dilution of 1:100.

6.4.3 Generation of stable cell lines

6.4.3.1 Retroviral transduction

Stable cell lines were generated with the use of Moloney murine leukemia virus

(MMLV)-based retroviral expression vector pRevTRE2. The gene of interest (sequence encoding HASPB SH4-TEV-GFP, HASPB SH4 Δpal-TEV-GFP or Yes SH4-TEV-GFP) was located between the MMLV 5' and 3' long terminal repeat sequences (LTRs), under the control of the tetracycline-response element (TRE), to which reverse tetracycline-controlled transactivator protein, rtTA (Tet-On transactivator) can bind. The retroviral expression vector was transiently cotransfected into a packaging cell line, HEK 293T, together with pVPack-GP (*gag-pol*-expressing vector) and pVPack-Eco (*env*-expressing vector), with the use of MBS Mammalian Transfection Kit (Stratagene), according to manufacturer's instructions. Viral RNA encoding the gene of interest was encapsidated, and the resulting virus particles released into the supernatant of transfected cells. The supernatant was used to infect target cells - HeLa or HeLa S3 MCAT-TAM2 cells, i.e. stably expressing receptor for retroviral particles, mouse cationic amino acid transporter 1 (MCAT1), and an optimized form of rtTA protein (rtTA-M2). Upon infection of target cells, the viral RNA is reverse transcribed and the cDNA of interest, flanked by the LTRs, integrated into the host DNA.

6.4.3.2 Fluorescence-activated cell sorting

Upon infection of target cells, cells expressing the SH4-TEV-GFP fusion protein in a doxycycline-dependent manner were selected by several rounds of sorting using FACSAria flow cytometer (Becton Dickinson). During the first round of sorting ('bright sort'), transduced cells were selected (i.e. GFP-positive upon cultivation in the presence of doxycycline). After seven days, the second round of sorting was performed ('dark sort'), selecting for cells that do not express the fusion protein without having been induced with doxycycline (i.e. GFP-negative cells upon cultivation in the absence of doxycycline). And finally, the third round isolated pools and single cells, in which the transduced fragment was integrated into the genome (GFP-positive cells after induction with doxycycline).

Cells were cultivated in the presence of 1 µg/ml doxycycline for 48 hours ('bright sort'), or in its absence ('dark sort'), washed with PBS and detached by a 10-minute incubation at 37°C with Cell Dissociation Buffer (Invitrogen). Upon the addition of cold culture medium, cells were sedimented, resuspended in sorting medium, and the cell

suspension was passed through a 45 µm cell strainer cap into FACS tubes, which were then kept on ice until sorting. Cells were sorted into 6-well plates (pools during the three sorts) or 96-well plates (single cells during the last sort) containing DMEM or filtered conditioned DMEM (in the case of HeLa S3 cells).

Sorting medium:
5% (v/v) Cell Dissociation Buffer
0.2% (v/v) FCS
2 mM L-glutamine
100 µg/ml penicillin/streptomycin
in DMEM

6.4.4 Flow cytometry

To characterize the inducibility and levels of expression of SH4-TEV-GFP fusion proteins, stable HeLa and HeLa S3 cell lines were cultivated for 16 hours without or in the presence of 4 µg/ml doxycycline. The cells were washed once with PBS, detached in PBS/0.5 mM EDTA for 15 minutes at 37°C, and analyzed using flow cytometry (FACSCalibur, Becton Dickinson) by detecting GFP fluorescence. Autofluorescence of HeLa and HeLa S3 MCAT-TAM2 cells was adjusted to 10^1.

6.4.5 Transient transfection

6.4.5.1 Transient transfection with DNA using FuGENE HD transfection reagent

One day before transfection, HeLa cells were plated in 8-well Lab-Tek Chambered Coverglass plates, 2-well Lab-Tek II Coverglass plates, or 35 mm glass bottom dishes (µ-Dish 35 mm, ibidi). On the day of transfection, plasmid DNA was diluted in Opti-MEM medium to a concentration of 2 µg DNA/100 µl Opti-MEM. 6 µl of FuGENE were then added directly into the medium containing the diluted DNA. The transfection complex was mixed, incubated for 15 minutes at room temperature, and added to the cells (106 µl for a 35 mm plate). To prepare transfection complexes for smaller culture vessels, the quantity of all components was changed according to the surface area.

6.4.5.2 Transient transfection with DNA using jetPRIME transfection reagent

HeLa cells to be processed for electron microcopy (HeLa HASPB SH4-mCherry), were plated one day before transfection in 6 cm plates in DMEM with L-glutamine, without antibiotics. On the day of transfection, plasmid DNA (pIRES2-EGFP/Arf1 WT or Q71L) was diluted to a concentration of 1.5 µg DNA/500 µl jetPRIME buffer. 10 µl of jetPRIME were then added directly into the buffer containing the diluted DNA. The transfection complex was mixed, incubated for 10 minutes at room temperature, and added to the cells. Beforehand, the medium was changed to DMEM with L-glutamine and doxycycline (2 µg/ml), without antibiotics. 15 hours after transfection the cells were fixed, followed by further processing for electron microscopy, as described in section 6.5.2

6.4.5.3 Transient transfection with siRNA using Oligofectamine transfection reagent

HeLa cells to be imaged by live-cell confocal microscopy were plated one day before transfection in 8-well Lab-Tek Chambered Coverglass plates or 2-well Lab-Tek II Coverglass plates. For one well of a 2-well Lab-Tek II, 100 pmol of siRNA (2 µl of a 50 µM stock) was added to 88 µl of Opti-MEM, and mixed with 24 µl of 5x diluted Oligofectamine (in Opti-MEM). The siRNAs used were: Silencer Negative Control siRNA #1 (Ambion) and COPB1 Silencer Pre-designed siRNA (ID: 24546, Ambion). After a 20-minute incubation at room temperature, the transfection mixture was added to the cells. Beforehand, the medium was changed to Opti-MEM. 3-4 hours upon transfection, the medium was replaced by normal growth medium. To prepare transfection complexes for 8-well Lab-Tek Chambered Coverglass plates, the quantity of all components was changed according to the surface area. The cells were imaged by live-cell confocal microscopy 45-48 hours upon siRNA transfection, as described in section 6.5.1.

HeLa cells to be processed for electron microcopy (HeLa HASPB SH4-TEV-GFP, clone 4), were transfected with siRNAs in 6-well plates (2 wells per condition). For each condition, 600 pmol of siRNA (scrambled or COPB1) was added to 528 µl of Opti-MEM, and mixed with 72 µl of 5x diluted Oligofectamine. After a 20-minute incubation at room temperature, the transfection mixture was added to the cells. Beforehand, the medium

was changed to Opti-MEM. 3-4 hours upon transfection, the medium was replaced by normal growth medium. 24 hours after transfection, the cells were cells split onto two 6 cm plates, induced with doxycycline (2 µg/ml) and incubated for additional 24 hours, fixed, and processed for electron microscopy, as described in section 6.5.2.

6.4.6 Drug treatment

Synthesis of HASPB SH4-TEV-GFP, HASPB SH4 Δpal-TEV-GFP, Yes SH4-TEV-GFP or HASPB SH4-mCherry in stable cell lines, or HASPB SH4-mCherry transiently expressed from pRevTRE2/HASPB SH4-mCherry in HeLa MCAT-TAM2 cells, was induced with 1-4 µg/ml doxycycline for 16-48 hours. To inhibit protein synthesis, cells were incubated in the presence of 100 µg/ml cycloheximide for 4 hours. To inhibit guanine nucleotide exchange factors (GEFs) responsible for activating Arf1, cells were incubated in the presence of 0.1 µg/ml brefeldin A (BFA) for 16 hours.

6.5 Microscopy

6.5.1 Fluorescence microscopy

6.5.1.1 Live-cell confocal fluorescence microscopy

Cells were grown in 8-well Lab-Tek Chambered Coverglass plates, 2-well Lab-Tek II Coverglass plates, or 35 mm glass bottom dishes. Live-cell laser scanning confocal imaging was performed using a Zeiss LSM 510 laser scanning confocal microscope (Zeiss), using either a Plan-Neofluar 40x/1.3 Oil DIC or a Plan-Apochromat 63x/1.4 Oil DIC objective. GFP fluorescence was excited using a 488 nm argon laser, and detected through a band pass (BP) 505-530 nm emission filter. The fluorescence of mCherry or mRFP was excited using the 563 nm laser line of a helium-neon laser, and detected using a long pass (LP) 560 nm emission filter. 12-bit, 1240x1240 pixel Z stack images were collected using the 40x objective, with the Z-step size of 0.43 µm.

6.5.1.2 Intensity quantification of sum intensity projections of Z stack images

Intensity quantification was performed using ImageJ software (version 1.43u). First, Z stacks of confocal images were projected into a single image using a sum intensity projection (excluding the top- and bottom-most Z stack images). For quantification of

subcellular localization (perinuclear or intracellular accumulation), first the perinuclear or intracellular signal was quantified: the sum of the pixel values (integrated density) of perinuclear or intracellular area was measured, and then integrated density of background area of the same size was subtracted. Total signal per cell was quantified by measuring the integrated density of the whole cell, and subtracting from it the integrated density of background area of the same size. Perinuclear or intracellular accumulation per cell was quantified by dividing the perinuclear or intracellular signal by the total signal for a cell, and expressing it as a percentage. Statistical significance of the differences in the magnitude of perinuclear or intracellular accumulation was determined by an unpaired Student's t-test using Prism 5 software.

6.5.2 Immunogold electron microscopy

6.5.2.1 Fixation

Cells were grown on 6 cm dishes. Some of the growth medium was removed, leaving 2 ml per plate. An equal volume of fixative 1 was then added directly to the medium, followed by incubation for 1 hour at room temperature. The plates were drained, covered with 2 ml of fixative 2, wrapped with Parafilm and stored overnight at 4°C.

Fixative 1:
0.2 M PHEM buffer
8% (w/v) formaldehyde
0.2% (w/v) glutaraldehyde

Fixative 2:
0.1 M PHEM buffer
4% (w/v) formaldehyde

0.4 M PHEM buffer:
240 mM PIPES
100 mM HEPES
8 mM $MgCl_2$
40 mM EGTA
pH 6.9

6.5.2.2 Embedding in gelatin and sucrose infiltration

After fixation, cells were washed twice with PBS for 5 minutes, and then with PBS/50 mM glycine for 10 minutes. Cells were then covered with 2 ml of 1% (w/v) gelatin in PBS, scraped, transferred to 1.5 ml Eppendorf tubes and spun down for 5 minutes at 1000 rpm (Centrifuge 5804, Eppendorf). Supernatant was removed, the cells resuspended in 1 ml of 10-12% (w/v) gelatin in PBS (kept at 37°C to prevent it from solidifying), and incubated for 15 minutes at 37°C. Cells were spun down at full speed (14000 rpm) for 5 minutes, most of the supernatant removed, and the tube placed on ice for 45 minutes to 1.5 hours to solidify the gelatin. The pellet was pulled out of the tube with the use of a flattened toothpick, cut into slices, and then into cubic blocks of about 1 mm^3. The blocks were transferred to tubes containing 2.3 M sucrose in PBS, and rotated overnight in the cold room. Flat-head aluminum rivets were prepared to be mounting pins: the surface of the head was roughened by scratching with a file, and then the pins were cleaned with 100% ethanol. The next day, the blocks were taken out from the sucrose, and the excess of it removed, leaving enough to glue the blocks onto the mounting pins. The blocks mounted onto pins were frozen in liquid nitrogen.

6.5.2.3 Trimming and cutting

The block was trimmed with the use of EM UC6/EM FC6 cryo-ultramicrotome (Leica), equipped with a diamond trimming knife (Diatome), at a chamber temperature of -90°C. First, the face of the block was trimmed at a speed of 10 mm/s, with the section thickness of 250 nm and the ionizer on. Sections were picked up with the ionizer switched off, with a droplet of pick-up solution (1:1 mixture of 2.3 M sucrose in PBS and 2% (w/v) methyl cellulose) in a wire loop, transferred onto a glass slide, and stained with methylene blue to confirm the presence of cells in the sections using light microscopy. Afterwards, the block was trimmed at one side: 250 nm sections were cut at a speed of 10-80 mm/s. When the sectioning was deep enough (60 µm), the other side was trimmed. Then, the specimen was turned 90°, and the procedure was repeated until all sides of the block were trimmed, forming a rectangular 60 µm high prism. Cutting was performed at -110°C using a diamond cutting knife (Diatome), at a speed of 0.8-1 mm/s, with the section thickness of 60 nm and the ionizer on. Ribbon formed by cut ultrathin sections was kept straight during sectioning with the use of a brush (cat whisker glued to

the tip of a wooden stick). Sections were picked up with the ionizer switched off, with a droplet of pick-up solution in a wire loop. The wire loop with sections was withdrawn from the cryochamber and after thawing, the sections were placed on copper grids (Hexagonal 100 meshes, Plano), which had been coated with a Pioloform (polyvinyl butyral) film and a thin (2.6 nm) layer of carbon.

6.5.2.4 Double immunogold labeling of cryosections

Grids with sections were placed on gelatin plates (2% (w/v) gelatin/0.001% (w/v) NaN_3 in PBS), sections facing gelatin, and incubated at 37°C for 20 minutes. The grids were then washed on PBS at 37°C for 20 minutes, and blocked with 0.8% (w/v) BSA/0.1% (w/v) fish skin gelatin/50 mM glycine in PBS at room temperature for 30 minutes, by floating the grids on drops of the blocking solution placed on a Parafilm sheet, sections facing the drop. Then, the grids were labeled with primary antibody diluted in blocking solution, at room temperature for 30 minutes (7-10 µl for each grid). Afterwards, the grids were washed 5 times for 5 minutes in PBS/50 mM glycine at room temperature, and incubated for 30 minutes with 10 nm or 15 nm protein A-gold at room temperature, fixed for 5 minutes in 1% (w/v) glutaraldehyde in PBS, and washed in PBS/50 mM glycine as above. Then, the grids were blocked again, incubated with the second primary antibody, washed in PBS/50 mM glycine, incubated with 15 nm or 10 nm protein A-gold, fixed, and washed in PBS/50 mM glycine. After 10 washes for 2 minutes in water at room temperature, and 3 washes in water on ice, grids were passed over two drops of 3:2 mixture of 4% (w/v) watery uranyl acetate and 2% (w/v) methyl cellulose on ice, and then incubated on fresh drops of this mixture for 10 minutes on ice. The grids were picked up with wire loops, the excess of uranyl acetate/methyl cellulose was removed by slowly dragging along filter paper, and the grids were dried at room temperature for 10 minutes.

6.5.2.5 Electron microscopy

Grids were examined at 60 kV using a Zeiss EM10 electron microscope. Pictures were taken at magnifications of 20000-50000x.

7 Appendix

7.1 Abbreviations

1D-PAGE	1-dimensional polyacrylamide gel electrophoresis
ADP	adenosine diphosphate
AMPA	α-amino-3-hydroxy-5-methyl-4-isoxazolepropionic acid
APs	adaptor protein complexes
APT1	acyl-protein thioesterase 1
Arf1	ADP-ribosylation factor 1
ATP	adenosine triphosphate
BARS	brefeldin A-ribosylated substrate
BASP1	brain acid soluble protein 1
BCR	B cell antigen receptor
BFA	brefeldin A
BHK	baby hamster kidney
Bis-Tris	bis(2-hydroxyethyl)amino-tris(hydroxymethyl)methane
BP	band pass
BSA	bovine serum albumin
cAMP	cyclic adenosine monophosphate
cDNA	complementary DNA
Cer	ceramide
CHO	Chinese hamster ovary
Chol	cholesterol
COP	coat protein complex
COPB	coat protein complex, subunit β
CR	cysteine-rich
Da	dalton
DHHC	aspartate-histidine-histidine-cysteine
DIC	differential interference contrast
DMEM	Dulbecco's modified Eagle's medium
DMSO	dimethyl sulfoxide
DNA	deoxyribonucleic acid
DRMs	detergent-resistant membranes
DTT	dithiothreitol
EDTA	ethylenediaminetetraacetic acid
EGFP	enhanced green fluorescent protein
EGTA	ethylene glycol-bis(2-aminoethylether)-N,N,N',N'-tetraacetic acid
emPAI	exponentially modified protein abundance index

eNOS	endothelial nitric-oxide synthase
ER	endoplasmic reticulum
ERGIC	ER-Golgi intermediate compartment
ESI	electrospray ionization
FACS	fluorescence-activated cell sorting
FCS	fetal calf serum
FRET	fluorescence resonance energy transfer
GalCer	galactosylceramide
GAP	GTPase-activating protein
GBF1	Golgi-specific brefeldin A-resistance guanine nucleotide exchange factor 1
GDP	guanosine diphosphate
GEF	guanine nucleotide exchange factor
GFP	green fluorescent protein
GGAs	Golgi-localized, γ-ear-containing, Arf-binding proteins
GlcCer	glucosylceramide
$GlcNH_2$	glucosamine
GPCR	G protein-coupled receptor
GPI	glycosyl-phosphatidylinositol
GPI-APs	glycosyl-phosphatidylinositol-anchored proteins
GPMVs	giant plasma membrane vesicles
GTP	guanosine triphosphate
GTPase	guanosine triphosphatase
HA	influenza hemagglutinin
HASP	hydrophilic acylated surface protein
HASPB	hydrophilic acylated surface protein B
HB	homogenization buffer
HEK	human embryonic kidney
HEPES	4-(2-hydroxyethyl)piperazine-1-ethanesulfonic acid
HexCer	hexosylceramide
HIV-1	human immunodeficiency virus type 1
HPLC	high-performance liquid chromatography
IQGAP1	Ras GTPase-activating-like protein
IRES	internal ribosome entry site
LB	Luria-Bertani
LC	liquid chromatography
l_d	liquid-disordered
LDS	lithium dodecyl sulfate
l_o	liquid-ordered
LP	long pass
LSM	laser scanning microscope
LTQ	linear trap quadrupole

LTRs	long terminal repeat sequences
m/z	mass-to-charge ratio
Man	mannose
MARCKS	myristoylated alanine-rich C kinase substrate
MBS	MES buffered saline
MBS	modified bovine serum
MCAT1	mouse cationic amino acid transporter 1
MDCK	Madin-Darby canine kidney
MES	2-(N-morpholino)ethanesulfonic acid (MES)
MMLV	Moloney murine leukemia virus
MOPS	3-(N-morpholino)propanesulfonic acid
MVD	mevalonate-diphospho-dehydrogenase
mRFP	monomeric red fluorescent protein
MS	mass spectrometry
MS/MS	tandem mass spectrometry
MβCD	methyl-β-cyclodextrin
NMT	N-myristoyltransferase
NONO	non-POU domain-containing octamer-binding protein
NRK	normal rat kidney
ns	not significant
PA	phosphatidic acid
PAGE	polyacrylamide gel electrophoresis
PAI	protein abundance index
PAT	palmitoyl transferase
PBS	phosphate buffered saline
PBST	PBS/Tween
PC	phosphatidylcholine
PE	phosphatidylethanolamine
PI	phosphatidylinositol
PIP	phosphatidylinositol-4-monophosphate
PIP_2	phosphatidylinositol-4,5-bisphosphate
PIPES	piperazine-N,N'-bis(2-ethanesulfonic acid)
PKD	protein kinase D
PLAP	placental alkaline phosphatase
PMS	post-mitochondrial supernatant
PMS	plasma membrane spheres
PNS	post-nuclear supernatant
PP	protein phosphatase
ppm	parts per million
PrP	prion protein
PS	phosphatidylserine

psi	pound-force per square inch
PVDF	polyvinylidene fluoride
RNA	ribonucleic acid
RNAi	RNA interference
rpm	revolutions per minute
RPMI	Roswell Park Memorial Institute medium
rtTA	reverse tetracycline-controlled transactivator protein
SD	standard deviation
SDS	sodium dodecyl sulfate
SFKs	Src family kinases
SFPQ	splicing factor, proline- and glutamine-rich
SH	Src homology
SILAC	stable isotope labeling with amino acids in cell culture
siRNA	small interfering RNA
SM	sphingomyelin
SNARE	soluble N-ethylmaleimide-sensitive factor attachment protein receptor
SP	spacer
SR	signal recognition particle receptor
SRP	signal recognition particle
TAE	Tris-acetate-EDTA
TCR	T cell antigen receptor
TEV	tobacco etch virus
TFA	trifluoroacetic acid
TGN	*trans*-Golgi network
TRE	tetracycline-response element
Tris	tris(hydroxymethyl)aminomethane
VP4	viral protein 4
VSVG	vesicular stomatitis virus glycoprotein
VTCs	vesicular-tubular clusters
WT	wild-type

7.2 Supplementary tables

Table S1 Proteins identified in Triton X-100 detergent-resistant membranes (DRMs) isolated from HeLa S3 cells. DRMs were isolated from HeLa S3 cell lines stably expressing HASPB SH4-TEV-GFP or Yes SH4-TEV-GFP, as well as from HeLa S3 cells that do not express any SH4-TEV-GFP fusion protein. Listed are proteins identified in at least 3 out of 6 DRM preparations (2 experiments for the 3 cell lines each, considered together), their Swiss-Prot accession numbers, primary subcellular localizations, and classification according to Foster *et al.,* 2003. Not identified - the protein was not identified in Triton X-100 DRMs from HeLa cells in the study by Foster *et al.*; unable to quantify - the protein was identified in Triton X-100 DRMs from HeLa cells in the study by Foster *et al.*, but was not quantifiable and thus was not classified.

Protein name	Swiss-Prot accession number	Subcellular localization	Classification by Foster *et al.*, 2003
116 kDa U5 small nuclear ribonucleoprotein component	U5S1_HUMAN	nucleus	not identified
40S ribosomal protein S11	RS11_HUMAN	cytosol	not identified
40S ribosomal protein S13	RS13_HUMAN	cytosol	unable to quantify
40S ribosomal protein S3	RS3_HUMAN	cytosol	unable to quantify
40S ribosomal protein S3a	RS3A_HUMAN	cytosol	unable to quantify
40S ribosomal protein S4, X isoform	RS4X_HUMAN	cytosol	not identified
40S ribosomal protein S7	RS7_HUMAN	cytosol	not identified
40S ribosomal protein S8	RS8_HUMAN	cytosol	raft
40S ribosomal protein SA	RSSA_HUMAN	cytosol	nonspecific
5'-nucleotidase	5NTD_HUMAN	plasma membrane	raft
60S acidic ribosomal protein P0	RLA0_HUMAN	cytosol	raft
60S acidic ribosomal protein P2	RLA2_HUMAN	cytosol	unable to quantify
60S ribosomal protein L10a	RL10A_HUMAN	cytosol	not identified
60S ribosomal protein L11	RL11_HUMAN	cytosol	not identified
60S ribosomal protein L12	RL12_HUMAN	cytosol	nonspecific
60S ribosomal protein L13	RL13_HUMAN	cytosol	unable to quantify
60S ribosomal protein L18	RL18_HUMAN	cytosol	unable to quantify
60S ribosomal protein L18a	RL18A_HUMAN	cytosol	not identified
60S ribosomal protein L21	RL21_HUMAN	cytosol	not identified
60S ribosomal protein L22	RL22_HUMAN	cytosol	not identified
60S ribosomal protein L3	RL3_HUMAN	cytosol	unable to quantify
60S ribosomal protein L4	RL4_HUMAN	cytosol	nonspecific
60S ribosomal protein L5	RL5_HUMAN	cytosol	not identified
60S ribosomal protein L6	RL6_HUMAN	cytosol	nonspecific
60S ribosomal protein L7a	RL7A_HUMAN	cytosol	raft
60S ribosomal protein L8	RL8_HUMAN	cytosol	unable to quantify
60S ribosomal protein L9	RL9_HUMAN	cytosol	not identified
Actin, cytoplasmic 2	ACTG_HUMAN	cytoskeleton	raft-associated
ADP/ATP translocase 2	ADT2_HUMAN	mitochondrion	not identified
ADP/ATP translocase 3	ADT3_HUMAN	mitochondrion	nonspecific
Aldehyde dehydrogenase family 3 member B1	AL3B1_HUMAN	cytosol	unable to quantify
Annexin A2	ANXA2_HUMAN	plasma membrane	raft-associated
AP-2 complex subunit alpha-1	AP2A1_HUMAN	plasma membrane	not identified
ATP synthase subunit alpha, mitochondrial	ATPA_HUMAN	mitochondrion	nonspecific
ATP synthase subunit beta, mitochondrial	ATPB_HUMAN	mitochondrion	nonspecific
ATP-binding cassette sub-family D member 3	ABCD3_HUMAN	peroxisome	raft
ATP-binding cassette sub-family G member 2	ABCG2_HUMAN	plasma membrane	not identified
ATP-dependent RNA helicase A	DHX9_HUMAN	nucleus	not identified
ATP-dependent RNA helicase DDX3X	DDX3X_HUMAN	nucleus	not identified
B-cell receptor-associated protein 31	BAP31_HUMAN	endoplasmic reticulum	nonspecific
Basigin	BASI_HUMAN	plasma membrane	nonspecific

Table S1 - continued. Caption on page 117.

Protein name	Swiss-Prot accession number	Subcellular localization	Classification by Foster *et al.*, 2003
Bone marrow stromal antigen 2	BST2_HUMAN	plasma membrane	raft
Brain acid soluble protein 1	BASP1_HUMAN	plasma membrane	unable to quantify
Canalicular multispecific organic anion transporter 1	MRP2_HUMAN	plasma membrane	not identified
Caprin-1	CAPR1_HUMAN	cytosol	not identified
Carboxypeptidase M	CBPM_HUMAN	plasma membrane	raft
CD109 antigen	CD109_HUMAN	plasma membrane	raft
CD44 antigen	CD44_HUMAN	plasma membrane	raft
CD59 glycoprotein	CD59_HUMAN	plasma membrane	raft
Complement decay-accelerating factor	DAF_HUMAN	plasma membrane	raft
Cytospin-B	CYTSB_HUMAN	nucleus	raft
Desmoglein-2	DSG2_HUMAN	plasma membrane	raft
DNA-dependent protein kinase catalytic subunit	PRKDC_HUMAN	nucleus	nonspecific
Dolichyl-diphosphooligosaccharide-protein glycosyltransferase 48 kDa subunit	OST48_HUMAN	endoplasmic reticulum	nonspecific
Dolichyl-diphosphooligosaccharide-protein glycosyltransferase subunit 1	RPN1_HUMAN	endoplasmic reticulum	nonspecific
Elongation factor 1-alpha 1	EF1A1_HUMAN	cytosol	raft-associated
Elongation factor 2	EF2_HUMAN	cytosol	unable to quantify
Epidermal growth factor receptor	EGFR_HUMAN	plasma membrane	not identified
Epiplakin	EPIPL_HUMAN	cytoskeleton	not identified
Erythrocyte band 7 integral membrane protein	STOM_HUMAN	plasma membrane	raft-associated
Eukaryotic initiation factor 4A-III	IF4A3_HUMAN	nucleus	not identified
Ezrin	EZRI_HUMAN	plasma membrane	not identified
Flotillin-1	FLOT1_HUMAN	plasma membrane	raft
Flotillin-2	FLOT2_HUMAN	plasma membrane	raft
Folate receptor alpha	FOLR1_HUMAN	plasma membrane	raft
Fructose-bisphosphate aldolase A	ALDOA_HUMAN	cytosol	raft-associated
Glyceraldehyde-3-phosphate dehydrogenase	G3P_HUMAN	cytosol	raft
Glypican-1	GPC1_HUMAN	plasma membrane	raft
Guanine nucleotide-binding protein G(i) subunit alpha-2	GNAI2_HUMAN	plasma membrane	raft
Guanine nucleotide-binding protein G(I)/G(S)/G(O) subunit gamma-12	GBG12_HUMAN	plasma membrane	raft
Guanine nucleotide-binding protein G(I)/G(S)/G(T) subunit beta-2	GBB2_HUMAN	plasma membrane	raft
Guanine nucleotide-binding protein G(k) subunit alpha	GNAI3_HUMAN	plasma membrane	raft
Guanine nucleotide-binding protein G(s) subunit alpha isoforms short	GNAS2_HUMAN	plasma membrane	raft
HEAT repeat-containing protein 1	HEAT1_HUMAN	nucleus	not identified
Heat shock 70 kDa protein 1A/1B	HSP71_HUMAN	cytosol	raft
Heat shock cognate 71 kDa protein	HSP7C_HUMAN	cytosol	raft-associated
Heat shock protein HSP 90-beta	HS90B_HUMAN	cytosol	raft-associated
Heterogeneous nuclear ribonucleoprotein A1	ROA1_HUMAN	nucleus	not identified
Heterogeneous nuclear ribonucleoprotein D0	HNRPD_HUMAN	nucleus	not identified
Heterogeneous nuclear ribonucleoprotein H	HNRH1_HUMAN	nucleus	not identified
Heterogeneous nuclear ribonucleoprotein M	HNRPM_HUMAN	nucleus	nonspecific
Heterogeneous nuclear ribonucleoprotein Q	HNRPQ_HUMAN	nucleus	not identified
Heterogeneous nuclear ribonucleoprotein U	HNRPU_HUMAN	nucleus	unable to quantify
Heterogeneous nuclear ribonucleoproteins A2/B1	ROA2_HUMAN	nucleus	unable to quantify
Heterogeneous nuclear ribonucleoproteins C1/C2	HNRPC_HUMAN	nucleus	unable to quantify
Histone H2A type 1-H	H2A1H_HUMAN	nucleus	not identified
Histone H2B type 1-C/E/F/G/I	H2B1C_HUMAN	nucleus	unable to quantify
Histone H4	H4_HUMAN	nucleus	nonspecific
HLA class I histocompatibility antigen, A-2 alpha chain	1A02_HUMAN	plasma membrane	not identified
Inositol 1,4,5-trisphosphate receptor type 3	ITPR3_HUMAN	endoplasmic reticulum	unable to quantify
Integrin alpha-3	ITA3_HUMAN	plasma membrane	unable to quantify
Integrin beta-1	ITB1_HUMAN	plasma membrane	raft-associated
Interleukin enhancer-binding factor 2	ILF2_HUMAN	nucleus	not identified
Junction plakoglobin	PLAK_HUMAN	plasma membrane	raft
Kinase D-interacting substrate of 220 kDa	KDIS_HUMAN	plasma membrane	raft-associated
LIM domain and actin-binding protein 1	LIMA1_HUMAN	cytoskeleton	not identified
Matrin-3	MATR3_HUMAN	nucleus	not identified
Mitochondrial inner membrane protein	IMMT_HUMAN	mitochondrion	nonspecific
Moesin	MOES_HUMAN	plasma membrane	raft
Monocarboxylate transporter 1	MOT1_HUMAN	plasma membrane	unable to quantify
Monocarboxylate transporter 4	MOT4_HUMAN	plasma membrane	unable to quantify

Table S1 - continued. Caption on page 117.

Protein name	Swiss-Prot accession number	Subcellular localization	Classification by Foster *et al.*, 2003
Mucin-1	MUC1_HUMAN	plasma membrane	raft
Multidrug resistance-associated protein 4	MRP4_HUMAN	plasma membrane	not identified
Myb-binding protein 1A	MBB1A_HUMAN	nucleus	not identified
Myoferlin	MYOF_HUMAN	plasma membrane	raft
Myosin-9	MYH9_HUMAN	cytoskeleton	raft
Myosin-Ib	MYO1B_HUMAN	plasma membrane	unable to quantify
Myosin-Ic	MYO1C_HUMAN	plasma membrane	unable to quantify
Myosin-Ie	MYO1E_HUMAN	cytoskeleton	not identified
Myosin-Ig	MYO1G_HUMAN	plasma membrane	not identified
Myosin-VI	MYO6_HUMAN	plasma membrane	not identified
N-acetyltransferase 10	NAT10_HUMAN	nucleus	not identified
Neuroblast differentiation-associated protein AHNAK	AHNK_HUMAN	nucleus	raft
Non-POU domain-containing octamer-binding protein	NONO_HUMAN	nucleus	not identified
Nuclease-sensitive element-binding protein 1	YBOX1_HUMAN	cytosol	not identified
Nucleolar RNA helicase 2	DDX21_HUMAN	nucleus	not identified
Nucleolin	NUCL_HUMAN	nucleus	raft
Nucleophosmin	NPM_HUMAN	nucleus	nonspecific
Phosphate carrier protein, mitochondrial	MPCP_HUMAN	mitochondrion	nonspecific
Pinin	PININ_HUMAN	nucleus	not identified
Plasminogen activator inhibitor 1 RNA-binding protein	PAIRB_HUMAN	cytosol	unable to quantify
Plectin	PLEC_HUMAN	cytoskeleton	raft
Poly [ADP-ribose] polymerase 1	PARP1_HUMAN	nucleus	unable to quantify
Polypyrimidine tract-binding protein 1	PTBP1_HUMAN	nucleus	not identified
Pre-mRNA-processing-splicing factor 8	PRP8_HUMAN	nucleus	not identified
Prelamin-A/C	LMNA_HUMAN	nucleus	raft-associated
Probable ATP-dependent RNA helicase DDX27	DDX27_HUMAN	nucleus	not identified
Probable ATP-dependent RNA helicase DDX5	DDX5_HUMAN	nucleus	unable to quantify
Prohibitin	PHB_HUMAN	mitochondrion	nonspecific
Prohibitin-2	PHB2_HUMAN	mitochondrion	nonspecific
Proliferation-associated protein 2G4	PA2G4_HUMAN	nucleus	not identified
Prostaglandin F2 receptor negative regulator	FPRP_HUMAN	endoplasmic reticulum	unable to quantify
Protein EFR3 homolog A	EFR3A_HUMAN	plasma membrane	raft
Protein kinase C and casein kinase substrate in neurons protein 3	PACN3_HUMAN	plasma membrane	raft
Putative pre-mRNA-splicing factor ATP-dependent RNA helicase DHX15	DHX15_HUMAN	nucleus	not identified
Putative ribosomal RNA methyltransferase NOP2	NOP2_HUMAN	nucleus	not identified
Pyruvate kinase isozymes M1/M2	KPYM_HUMAN	cytosol	raft-associated
Ras GTPase-activating protein-binding protein 1	G3BP1_HUMAN	cytosol	raft
Ras GTPase-activating-like protein IQGAP1	IQGA1_HUMAN	plasma membrane	raft-associated
Ras-related C3 botulinum toxin substrate 1	RAC1_HUMAN	plasma membrane	raft-associated
Ras-related protein Rap-1b	RAP1A_HUMAN	plasma membrane	raft-associated
Retinoic acid-induced protein 3	RAI3_HUMAN	plasma membrane	raft
Ribosomal L1 domain-containing protein 1	RL1D1_HUMAN	nucleus	not identified
Signal peptidase complex catalytic subunit SEC11A	SC11A_HUMAN	endoplasmic reticulum	not identified
Sodium/potassium-transporting ATPase subunit alpha-1	AT1A1_HUMAN	plasma membrane	unable to quantify
Sodium/potassium-transporting ATPase subunit beta-3	AT1B3_HUMAN	plasma membrane	not identified
Solute carrier family 12 member 3	S12A3_HUMAN	plasma membrane	not identified
Solute carrier family 2, facilitated glucose transporter member 1	GTR1_HUMAN	plasma membrane	raft-associated
Spectrin alpha chain, brain	SPTA2_HUMAN	cytoskeleton	unable to quantify
Spectrin beta chain, brain 1	SPTB2_HUMAN	cytoskeleton	unable to quantify
Splicing factor, proline- and glutamine-rich	SFPQ_HUMAN	nucleus	raft
Sterol O-acyltransferase 1	SOAT1_HUMAN	plasma membrane	unable to quantify
T-complex protein 1 subunit gamma	TCPG_HUMAN	cytosol	raft-associated
Trans-2,3-enoyl-CoA reductase	TECR_HUMAN	endoplasmic reticulum	raft-associated
Transferrin receptor protein 1	TFR1_HUMAN	plasma membrane	nonspecific
Trifunctional enzyme subunit alpha, mitochondrial	ECHA_HUMAN	mitochondrion	raft
tRNA (cytosine(34)-C(5))-methyltransferase	NSUN2_HUMAN	nucleus	not identified
Tubulin alpha-1B chain	TBA1B_HUMAN	cytoskeleton	nonspecific
Tubulin beta chain	TBB5_HUMAN	cytoskeleton	nonspecific
Tubulin beta-2C chain	TBB2C_HUMAN	cytoskeleton	nonspecific
Tyrosine-protein kinase Lyn	LYN_HUMAN	plasma membrane	raft

Table S1 - continued. Caption on page 117.

Protein name	Swiss-Prot accession number	Subcellular localization	Classification by Foster *et al.*, 2003
Tyrosine-protein kinase Yes	YES_HUMAN	plasma membrane	raft
U5 small nuclear ribonucleoprotein 200 kDa helicase	U520_HUMAN	nucleus	not identified
Ubiquitin-60S ribosomal protein L40/ Ubiquitin-40S ribosomal protein S27a/ Polyubiquitin-B/ Polyubiquitin-C *	RL40_HUMAN/ RS27A_HUMAN/ UBB_HUMAN/ UBC_HUMAN	cytosol	nonspecific
V-type proton ATPase 116 kDa subunit a isoform 1	VPP1_HUMAN	plasma membrane	raft-associated
V-type proton ATPase 116 kDa subunit a isoform 2	VPP2_HUMAN	plasma membrane	raft-associated
V-type proton ATPase 116 kDa subunit a isoform 3	VPP3_HUMAN	plasma membrane	raft-associated
V-type proton ATPase subunit d 1	VA0D1_HUMAN	lysosome	raft-associated
V-type proton ATPase subunit S1	VAS1_HUMAN	lysosome	raft-associated
Vesicle-associated membrane protein-associated protein A	VAPA_HUMAN	endoplasmic reticulum	unable to quantify
Vimentin	VIME_HUMAN	cytoskeleton	raft
Voltage-dependent anion-selective channel protein 1	VDAC1_HUMAN	mitochondrion	nonspecific
Voltage-dependent anion-selective channel protein 2	VDAC2_HUMAN	mitochondrion	nonspecific
Voltage-dependent calcium channel subunit alpha-2/delta-1	CA2D1_HUMAN	plasma membrane	raft
X-ray repair cross-complementing protein 5	XRCC5_HUMAN	nucleus	not identified
X-ray repair cross-complementing protein 6	XRCC6_HUMAN	nucleus	raft-associated
Zinc transporter 1	ZNT1_HUMAN	plasma membrane	not identified

*all four proteins were identified with exactly the same set of peptides

Caption for table on pages 121-122. Table S2 Proteins identified in TEV eluates. TEV eluates were obtained following the procedure for immunoisolation of detergent-resistant membranes (DRMs) containing SH4 domain fusion proteins. As input for immunoprecipitation served Triton X-100 DRMs prepared from HeLa S3 cell lines stably expressing HASPB SH4-TEV-GFP (denoted as HASPB), Yes SH4-TEV-GFP (denoted as Yes), or from control cells (HeLa S3 cells that do not express any SH4-TEV-GFP fusion protein, denoted as ctrl). Listed are proteins that were identified in at least one TEV eluate sample (i.e. that met criteria for positive protein identification specified in Scaffold 3: 95% protein identification probability, 95% peptide identification probability, and a minimum of two peptides), their Swiss-Prot accession numbers, primary subcellular localizations, and classification according to Foster *et al.,* 2003. The table lists also the number of unique spectra identified in TEV eluates and in total DRMs, the number of observable peptides, normalized exponentially modified protein abundance index (emPAI) values, and enrichment factors of proteins in TEV eluates relative to the respective total DRMs, calculated by the comparison of normalized emPAI values, and by the comparison of integrated areas of liquid chromatography-mass spectrometry (LC-MS) peptide peaks between samples. For those proteins that were only detected in a TEV eluate (and not in the respective total DRMs), the missing emPAI values were replaced by minimal emPAI values (calculated for 1 observed unique spectrum; underlined), allowing us to calculate minimal enrichment factors (underlined). Blank cells indicate normalized emPAI values that equal zero (no unique spectra identified), or they indicate that enrichment factors could not be calculated. Not identified - the protein was not identified in Triton X-100 DRMs from HeLa cells in the study by Foster *et al.*; unable to quantify - the protein was identified, but was not quantifiable and thus was not classified.

Table S2 Caption on page 120.

Protein name	Swiss-Prot accession number	Subcellular localization	Classification by Foster *et al.*, 2003	No. of unique spectra												No. of observable peptides
				ctrl				HASPB				Yes				
				Total DRMs		TEV eluate		Total DRMs		TEV eluate		Total DRMs		TEV eluate		
				Experiment No.												
				1	2	1	2	1	2	1	2	1	2	1	2	
Actin, cytoplasmic 2	ACTG_HUMAN	cytoskeleton	raft-associated	31	35	3	0	31	36	22	22	33	32	30	18	19
Alkaline phosphatase, placental type	PPB1_HUMAN	plasma membrane	raft	0	0	0	0	0	0	0	0	5	4	2	0	28
ATP-binding cassette sub-family F member 1	ABCF1_HUMAN	cytosol	not identified	0	0	0	0	0	0	0	8	0	3	0	0	40
ATP-dependent RNA helicase DDX1	DDX1_HUMAN	nucleus	not identified	0	0	0	0	0	0	0	0	0	2	0	2	37
Basigin	BASI_HUMAN	plasma membrane	nonspecific	11	15	0	0	11	15	2	8	10	15	2	6	16
Bone marrow stromal antigen 2	BST2_HUMAN	plasma membrane	raft	5	3	0	0	3	3	0	0	3	3	0	2	9
Brain acid soluble protein 1	BASP1_HUMAN	plasma membrane	unable to quantify	20	16	0	0	14	21	0	6	15	19	0	0	10
Caprin-1	CAPR1_HUMAN	cytosol	not identified	0	5	0	0	0	6	0	2	2	4	0	3	20
Carboxypeptidase M	CBPM_HUMAN	plasma membrane	raft	9	14	0	0	5	11	0	4	4	9	0	4	22
CCR4-NOT transcription complex subunit 7	CNOT7_HUMAN	nucleus	not identified	0	0	0	0	0	0	0	0	0	0	0	2	15
CD109 antigen	CD109_HUMAN	plasma membrane	raft	0	24	0	0	9	19	0	4	17	20	0	0	65
Complement decay-accelerating factor	DAF_HUMAN	plasma membrane	raft	10	11	0	0	5	10	3	0	8	11	6	3	20
Desmoglein-2	DSG2_HUMAN	plasma membrane	raft	5	31	0	0	22	30	0	2	16	29	0	3	48
Eukaryotic translation initiation factor 2 subunit 2	IF2B_HUMAN	cytosol	not identified	0	2	0	0	0	0	0	5	0	0	0	0	20
Eukaryotic translation initiation factor 2 subunit 3	IF2G_HUMAN	cytosol	not identified	0	5	0	0	0	0	2	12	0	3	4	9	22
Flotillin-1	FLOT1_HUMAN	plasma membrane	raft	18	20	0	0	16	21	0	3	15	19	0	0	27
Flotillin-2	FLOT2_HUMAN	plasma membrane	raft	13	14	0	0	12	16	0	2	12	12	0	0	25
Folate receptor alpha	FOLR1_HUMAN	plasma membrane	raft	3	5	0	0	4	5	0	3	2	2	0	2	14
Guanine nucleotide-binding protein G(k) subunit alpha	GNAI3_HUMAN	plasma membrane	raft	16	15	0	0	14	20	0	4	10	18	0	3	17
Guanine nucleotide-binding protein G(s) subunit alpha isoforms short	GNAS2_HUMAN	plasma membrane	raft	2	7	0	0	2	8	0	2	0	6	0	0	19
Heat shock cognate 71 kDa protein	HSP7C_HUMAN	cytosol	raft-associated	4	16	0	0	4	17	0	0	2	15	0	3	31
Heterogeneous nuclear ribonucleoproteins A2/B1	ROA2_HUMAN	nucleus	unable to quantify	3	0	0	0	2	2	0	2	4	5	0	2	17
Interleukin enhancer-binding factor 2	ILF2_HUMAN	nucleus	not identified	0	2	0	0	0	3	0	2	0	3	0	0	19
Junction plakoglobin	PLAK_HUMAN	plasma membrane	raft	13	31	0	0	7	24	0	0	7	30	4	3	41
KH domain-containing, RNA-binding, signal transduction-associated protein 1	KHDR1_HUMAN	nucleus	not identified	0	0	0	0	0	0	0	2	0	0	0	0	13
LIM domain and actin-binding protein 1	LIMA1_HUMAN	cytoskeleton	not identified	3	16	0	0	5	17	0	0	13	13	4	0	43
Moesin	MOES_HUMAN	plasma membrane	raft	17	25	0	0	9	20	4	4	6	24	2	13	35
Myoferlin	MYOF_HUMAN	plasma membrane	raft	3	46	0	0	4	61	0	4	10	19	0	0	116
Myosin-9	MYH9_HUMAN	cytoskeleton	raft	0	23	0	0	2	68	0	6	24	20	0	0	103
Myosin-Ic	MYO1C_HUMAN	plasma membrane	unable to quantify	18	44	0	0	33	52	6	0	49	38	0	0	55
Neuroblast differentiation-associated protein AHNAK	AHNK_HUMAN	nucleus	raft	3	26	0	0	0	51	0	5	9	37	0	0	230
Non-POU domain-containing octamer-binding protein	NONO_HUMAN	nucleus	not identified	0	14	0	0	0	13	5	20	0	10	9	17	20
Nucleolin	NUCL_HUMAN	nucleus	raft	10	19	0	0	12	23	0	4	11	26	2	5	26
Nucleophosmin	NPM_HUMAN	nucleus	nonspecific	10	15	0	0	9	13	2	0	14	14	0	0	11
Plasminogen activator inhibitor 1 RNA-binding protein	PAIRB_HUMAN	cytosol	unable to quantify	3	8	0	0	4	4	0	3	4	7	0	2	19
Probable ATP-dependent RNA helicase DDX5	DDX5_HUMAN	nucleus	unable to quantify	0	10	0	0	0	6	0	7	0	5	2	6	31
Pyruvate kinase isozymes M1/M2	KPYM_HUMAN	cytosol	raft-associated	11	19	0	0	5	23	0	7	11	20	0	2	28
Ras GTPase-activating protein-binding protein 1	G3BP1_HUMAN	cytosol	raft	0	9	0	0	0	9	0	6	0	6	0	2	19
Ras GTPase-activating-like protein IQGAP1	IQGA1_HUMAN	plasma membrane	raft-associated	3	17	0	0	28	32	0	45	29	34	5	18	81
Retinoic acid-induced protein 3	RAI3_HUMAN	plasma membrane	raft	8	7	0	0	6	7	3	2	5	4	3	2	13
Sodium/potassium-transporting ATPase subunit alpha-1	AT1A1_HUMAN	plasma membrane	unable to quantify	18	42	0	0	29	41	0	0	29	46	0	7	44
Spectrin alpha chain, brain	SPTA2_HUMAN	cytoskeleton	unable to quantify	2	55	0	0	0	100	0	50	19	36	11	0	148
Spectrin beta chain, brain 1	SPTB2_HUMAN	cytoskeleton	unable to quantify	0	55	0	0	0	71	0	32	18	30	2	0	137
Splicing factor, proline- and glutamine-rich	SFPQ_HUMAN	nucleus	raft	0	14	0	0	3	8	2	3	2	12	4	15	26
tRNA-splicing ligase RtcB homolog	RTCB_HUMAN	cytosol	not identified	0	0	0	0	0	0	0	0	0	0	0	2	25
Tubulin alpha-1B chain 1	TBA1B_HUMAN	cytoskeleton	nonspecific	15	25	0	0	13	27	3	10	16	21	2	5	20
Tubulin beta chain	TBB5_HUMAN	cytoskeleton	nonspecific	19	30	0	0	21	32	5	12	19	23	4	5	21
Tyrosine-protein kinase Lyn	LYN_HUMAN	plasma membrane	raft	0	9	0	0	0	8	0	2	0	10	0	0	27
Ubiquitin-60S ribosomal protein L40/ Ubiquitin-40S ribosomal protein S27a/ Polyubiquitin-B/ Polyubiquitin-C *	RL40_HUMAN/ RS27A_HUMAN/ UBB_HUMAN/ UBC_HUMAN	cytosol	nonspecific	3	3	0	0	4	5	0	0	3	4	2	0	6 6 5 6
V-type proton ATPase catalytic subunit A	VATA_HUMAN	lysosome	raft-associated	0	0	0	0	0	0	0	0	0	0	0	5	33
V-type proton ATPase subunit B, brain isoform	VATB2_HUMAN	lysosome	raft-associated	0	0	0	0	0	0	0	0	0	0	2	0	25
Vimentin	VIME_HUMAN	cytoskeleton	raft	6	34	0	0	4	33	0	7	3	18	0	3	32

*all four proteins were identified with exactly the same set of peptides; emPAI values were calculated for each one of them and then averaged

Table S2 - continued. Caption on page 120.

Protein name	Normalized emPAI												Enrichment factor TEV eluate/ total DRMs (emPAI)						Enrichment factor TEV eluate/ total DRMs (peak area)					
	ctrl				HASPB				Yes				ctrl		HASPB		Yes		ctrl		HASPB		Yes	
	Total DRMs		TEV eluate		Total DRMs		TEV eluate		Total DRMs		TEV eluate													
	Experiment No.												Experiment No.						Experiment No.					
	1	2	1	2	1	2	1	2	1	2	1	2	1	2	1	2	1	2	1	2	1	2	1	2
Actin, cytoplasmic 2	94.9	87.8	14.3		89.3	77.5	78.6	96.5	151.9	72.9	326.7	242.3	0.2		0.9	1.2	2.2	3.3						
Alkaline phosphatase, placental type									1.4	0.6	1.6						1.1						1.1	4.5
ATP-binding cassette sub-family F member 1						0.1		4.2		0.3						71.2					7.3			
ATP-dependent RNA helicase DDX1										0.2		4.1						20.0						9.7
Basigin	8.8	9.8			8.3	7.7	2.0	15.6	9.1	11.8	3.0	42.3			0.2	2.0	0.3	3.6			1.0		0.3	1.9
Bone marrow stromal antigen 2	5.9	1.5			2.5	1.2			3.3	1.8		20.6						11.6					0.2	7.5
Brain acid soluble protein 1	224.7	49.7			51.5	124.9		21.5	86.9	120.8						0.2					0.7			
Caprin-1		1.0				1.0		1.9	0.7	0.9		12.7				1.9		14.1			0.4			1.6
Carboxypeptidase M	3.6	4.3			1.5	2.2		3.7	1.5	2.4		16.0				1.7		6.6			1.2		0.7	2.6
CCR4-NOT transcription complex subunit 7										0.3		11.1						43.4						
CD109 antigen		1.7			0.8	1.0		1.1	2.3	1.6						1.1					2.2			2.3
Complement decay-accelerating factor	4.9	3.3			1.7	2.2	2.4		4.3	3.9	8.8	12.7			1.5		2.1	3.2			1.2	2.1	1.5	4.7
Desmoglein-2	0.6	4.4			4.0	3.2		0.7	3.3	4.7		4.8				0.2		1.0			1.1			2.8
Eukaryotic translation initiation factor 2 subunit 2		0.3				0.1		5.6								46.0					2.4			
Eukaryotic translation initiation factor 2 subunit 3		0.9			0.2	0.1	1.4	18.1	0.3	0.6	4.6	48.2			5.8	164.1	14.7	84.9			4.9			18.9
Flotillin-1	8.3	5.8			6.2	5.0		2.1	7.4	6.2						0.4					0.7			
Flotillin-2	5.2	3.4			4.3	3.4		1.5	5.7	3.1						0.4					0.7			
Folate receptor alpha	1.4	1.6			2.0	1.3		4.6	1.1	0.6		12.0				3.6		20.0			1.3		3.2	4.6
Guanine nucleotide-binding protein G(k) subunit alpha	17.6	8.5			12.1	14.0		5.2	8.2	16.1		15.5				0.4		1.0		0.3	0.7			3.5
Guanine nucleotide-binding protein G(s) subunit alpha isoforms short	0.6	1.7			0.6	1.6		2.0		1.6						1.2					0.8			
Heat shock cognate 71 kDa protein	0.8	2.9			0.7	2.5			0.5	3.2		7.7						2.4						12.8
Heterogeneous nuclear ribonucleoproteins A2/B1	1.1				0.7	0.3		2.2	2.0	1.5		9.6				7.2		6.4			3.7			8.6
Interleukin enhancer-binding factor 2		0.4				0.4		2.0		0.7						4.5								
Junction plakoglobin	2.4	6.0			1.0	2.8			1.4	6.8	2.2	5.7					1.6	0.8			0.5		1.3	2.1
KH domain-containing, RNA-binding, signal transduction-associated protein 1						0.2		3.1								15.8								
LIM domain and actin-binding protein 1	0.4	1.7			0.7	1.5			2.9	1.5	2.1						0.7						1.0	
Moesin	4.7	5.4			1.7	2.7	1.8	2.2	1.4	5.9	1.2	41.7			1.0	0.8	0.9	7.0			2.0		1.4	10.2
Myoferlin	0.1	1.9			0.2	2.4		0.6	0.6	0.7						0.3					0.4			
Myosin-9		0.9			0.1	3.6		1.0	2.0	0.9						0.3					0.4			
Myosin-Ic	2.6	6.8			6.4	7.8	1.7		19.2	6.0					0.3					0.2		0.3		0.5
Neuroblast differentiation-associated protein AHNAK	0.1	0.4				0.7		0.4	0.3	0.7						0.6					1.0			
Non-POU domain-containing octamer-binding protein		5.1			0.3	3.5	4.6	64.9	0.3	3.3	16.1	187.4			17.5	18.7	46.5	56.3			15.0		6.2	26.9
Nucleolin	3.2	5.6			4.0	6.7		3.1	4.7	13.9	1.7	17.2				0.5	0.4	1.2			1.5		1.6	3.4
Nucleophosmin	16.1	28.3			11.9	14.2	3.1		50.3	27.3					0.3					0.4	0.7			
Plasminogen activator inhibitor 1 RNA-binding protein	1.0	2.1			1.3	0.6		3.2	1.8	2.1		8.5				5.1		4.1			2.1			3.5
Probable ATP-dependent RNA helicase DDX5		1.4				0.6		4.9	0.2	0.7	1.4	17.3				8.8	6.5	25.0			4.2			12.6
Pyruvate kinase isozymes M1/M2	3.3	4.8			1.1	5.6		5.6	4.2	6.4		5.5				1.0		0.9			0.9			3.0
Ras GTPase-activating protein-binding protein 1		2.5				2.0		7.7		1.6		8.5				3.9		5.1			2.0			4.6
Ras GTPase-activating-like protein IQGAP1	0.2	0.8			2.6	1.5		18.7	3.6	2.5	1.4	20.6				12.6	0.4	8.2			0.9	13.3	1.7	5.7
Retinoic acid-induced protein 3	7.1	3.1			4.0	2.5	4.1	3.1	4.0	1.6	6.2	13.1			1.0	1.2	1.5	8.3			0.8	3.3	7.1	7.5
Sodium/potassium-transporting ATPase subunit alpha-1	3.6	10.3			7.6	7.5			10.1	15.6		13.6						0.9					0.3	2.9
Spectrin alpha chain, brain	0.1	1.7				3.7		8.5	1.0	1.2	1.7					2.3	1.7				1.9		2.6	
Spectrin beta chain, brain 1		1.9				2.3		5.1	1.0	1.0	0.3					2.2	0.3				1.5		1.6	
Splicing factor, proline- and glutamine-rich		3.1			0.7	1.0	1.1	2.2	0.5	2.9	3.8	85.5			1.8	2.1	6.8	29.3			1.7		5.2	24.7
tRNA-splicing ligase RtcB homolog										0.1		6.2						42.0						
Tubulin alpha-1B chain 1	10.5	21.5			7.4	21.4	2.4	15.6	15.1	15.7	2.3	24.0			0.3	0.7	0.2	1.5						
Tubulin beta chain	16.0	33.1			19.2	32.4	4.3	19.7	19.9	17.6	4.9	22.5			0.2	0.6	0.2	1.3			0.4	1.7	0.5	2.4
Tyrosine-protein kinase Lyn		1.5				1.0		1.3		2.1						1.4					0.9			
Ubiquitin-60S ribosomal protein L40/ Ubiquitin-40S ribosomal protein S27a/ Polyubiquitin-B/ Polyubiquitin-C *	5.4	3.0			8.7	6.6			6.7	6.3	11.0						1.6				1.1		2.3	1.7
V-type proton ATPase catalytic subunit A										0.1		12.9						115.6						10.6
V-type proton ATPase subunit B, brain isoform									0.3		1.8						6.5							
Vimentin	1.2	13.5			0.7	9.7		4.7	0.7	4.1		7.4				0.5		1.8			0.9			2.4

*all four proteins were identified with exactly the same set of peptides; emPAI values were calculated for each one of them and then averaged

8 References

Abrami, L., S.H. Leppla, and F.G. van der Goot. 2006. Receptor palmitoylation and ubiquitination regulate anthrax toxin endocytosis. *J Cell Biol*. 172:309-320.

Ahmed, S.N., D.A. Brown, and E. London. 1997. On the origin of sphingolipid/cholesterol-rich detergent-insoluble cell membranes: physiological concentrations of cholesterol and sphingolipid induce formation of a detergent-insoluble, liquid-ordered lipid phase in model membranes. *Biochemistry*. 36:10944-10953.

Alce, T.M., S. Gokool, D. McGhie, S. Stager, and D.F. Smith. 1999. Expression of hydrophilic surface proteins in infective stages of *Leishmania donovani*. *Mol Biochem Parasitol*. 102:191-196.

Alland, L., S.M. Peseckis, R.E. Atherton, L. Berthiaume, and M.D. Resh. 1994. Dual myristylation and palmitylation of Src family member p59fyn affects subcellular localization. *J Biol Chem*. 269:16701-16705.

Anitei, M., and B. Hoflack. 2011. Exit from the *trans*-Golgi network: from molecules to mechanisms. *Curr Opin Cell Biol*. 23:443-451.

Antonny, B., S. Beraud-Dufour, P. Chardin, and M. Chabre. 1997. N-terminal hydrophobic residues of the G-protein ADP-ribosylation factor-1 insert into membrane phospholipids upon GDP to GTP exchange. *Biochemistry*. 36:4675-4684.

Apolloni, A., I.A. Prior, M. Lindsay, R.G. Parton, and J.F. Hancock. 2000. H-ras but not K-ras traffics to the plasma membrane through the exocytic pathway. *Mol Cell Biol*. 20:2475-2487.

Barlowe, C. 2000. Traffic COPs of the early secretory pathway. *Traffic*. 1:371-377.

Barlowe, C. 2003. Signals for COPII-dependent export from the ER: what's the ticket out? *Trends Cell Biol*. 13:295-300.

Baumgart, T., A.T. Hammond, P. Sengupta, S.T. Hess, D.A. Holowka, B.A. Baird, and W.W. Webb. 2007. Large-scale fluid/fluid phase separation of proteins and lipids in giant plasma membrane vesicles. *Proc Natl Acad Sci U S A*. 104:3165-3170.

Beck, R., M. Rawet, F.T. Wieland, and D. Cassel. 2009. The COPI system: molecular mechanisms and function. *FEBS Lett*. 583:2701-2709.

Bhamre, S., H.Y. Wang, and E. Friedman. 1998. Serotonin-mediated palmitoylation and depalmitoylation of G alpha proteins in rat brain cortical membranes. *J Pharmacol Exp Ther*. 286:1482-1489.

Bielli, A., C.J. Haney, G. Gabreski, S.C. Watkins, S.I. Bannykh, and M. Aridor. 2005. Regulation of Sar1 NH2 terminus by GTP binding and hydrolysis promotes membrane deformation to control COPII vesicle fission. *J Cell Biol*. 171:919-924.

Bijlmakers, M.J., M. Isobe-Nakamura, L.J. Ruddock, and M. Marsh. 1997. Intrinsic signals in the unique domain target p56(lck) to the plasma membrane independently of CD4. *J Cell Biol*. 137:1029-1040.

Bijlmakers, M.J., and M. Marsh. 1999. Trafficking of an acylated cytosolic protein: newly synthesized p56(lck) travels to the plasma membrane via the exocytic pathway. *J Cell Biol*. 145:457-468.

Blom, T., P. Somerharju, and E. Ikonen. 2011. Synthesis and biosynthetic trafficking of membrane lipids. *Cold Spring Harb Perspect Biol*. 3:a004713.

Bremser, M., W. Nickel, M. Schweikert, M. Ravazzola, M. Amherdt, C.A. Hughes, T.H. Sollner, J.E. Rothman, and F.T. Wieland. 1999. Coupling of coat assembly and vesicle budding to packaging of putative cargo receptors. *Cell*. 96:495-506.

Brown, D.A., B. Crise, and J.K. Rose. 1989. Mechanism of membrane anchoring affects polarized expression of two proteins in MDCK cells. *Science*. 245:1499-1501.

Brown, D.A., and J.K. Rose. 1992. Sorting of GPI-anchored proteins to glycolipid-enriched membrane subdomains during transport to the apical cell surface. *Cell*. 68:533-544.

Brügger, B., G. Erben, R. Sandhoff, F.T. Wieland, and W.D. Lehmann. 1997. Quantitative analysis of biological membrane lipids at the low picomole level by nano-electrospray ionization tandem mass spectrometry. *Proc Natl Acad Sci U S A*. 94:2339-2344.

Brügger, B., C. Graham, I. Leibrecht, E. Mombelli, A. Jen, F. Wieland, and R. Morris. 2004. The membrane domains occupied by glycosylphosphatidylinositol-anchored prion protein and Thy-1 differ in lipid composition. *J Biol Chem*. 279:7530-7536.

Brügger, B., R. Sandhoff, S. Wegehingel, K. Gorgas, J. Malsam, J.B. Helms, W.D. Lehmann, W. Nickel, and F.T. Wieland. 2000. Evidence for segregation of sphingomyelin and cholesterol during formation of COPI-coated vesicles. *J Cell Biol*. 151:507-518.

Casey, P.J., and M.C. Seabra. 1996. Protein prenyltransferases. *J Biol Chem*. 271:5289-5292.

Catrein, I., R. Herrmann, A. Bosserhoff, and T. Ruppert. 2005. Experimental proof for a signal peptidase I like activity in *Mycoplasma pneumoniae*, but absence of a gene encoding a conserved bacterial type I SPase. *FEBS J*. 272:2892-2900.

Chege, N.W., and S.R. Pfeffer. 1990. Compartmentation of the Golgi complex: brefeldin-A distinguishes *trans*-Golgi cisternae from the *trans*-Golgi network. *J Cell Biol*. 111:893-899.

Cheong, K.H., D. Zacchetti, E.E. Schneeberger, and K. Simons. 1999. VIP17/MAL, a lipid raft-associated protein, is involved in apical transport in MDCK cells. *Proc Natl Acad Sci U S A*. 96:6241-6248.

Chow, M., J.F. Newman, D. Filman, J.M. Hogle, D.J. Rowlands, and F. Brown. 1987. Myristylation of picornavirus capsid protein VP4 and its structural significance. *Nature*. 327:482-486.

Connolly, T., P.J. Rapiejko, and R. Gilmore. 1991. Requirement of GTP hydrolysis for dissociation of the signal recognition particle from its receptor. *Science*. 252:1171-1173.

Cox, J., and M. Mann. 2008. MaxQuant enables high peptide identification rates, individualized p.p.b.-range mass accuracies and proteome-wide protein quantification. *Nat Biotechnol*. 26:1367-1372.

Cox, J., N. Neuhauser, A. Michalski, R.A. Scheltema, J.V. Olsen, and M. Mann. 2011. Andromeda: a peptide search engine integrated into the MaxQuant environment. *J Proteome Res*. 10:1794-1805.

Dalbey, R.E., and G. Von Heijne. 1992. Signal peptidases in prokaryotes and eukaryotes - a new protease family. *Trends Biochem Sci*. 17:474-478.

Daleke, D.L. 2003. Regulation of transbilayer plasma membrane phospholipid asymmetry. *J Lipid Res*. 44:233-242.

Dascher, C., and W.E. Balch. 1994. Dominant inhibitory mutants of ARF1 block endoplasmic reticulum to Golgi transport and trigger disassembly of the Golgi apparatus. *J Biol Chem*. 269:1437-1448.

De Matteis, M.A., and A. Luini. 2008. Exiting the Golgi complex. *Nat Rev Mol Cell Biol*. 9:273-284.

Delacour, D., V. Gouyer, J.P. Zanetta, H. Drobecq, E. Leteurtre, G. Grard, O. Moreau-Hannedouche, E. Maes, A. Pons, S. Andre, A. Le Bivic, H.J. Gabius, A. Manninen, K. Simons, and G. Huet. 2005. Galectin-4 and sulfatides in apical membrane trafficking in enterocyte-like cells. *J Cell Biol*. 169:491-501.

Delaunay, J.L., M. Breton, G. Trugnan, and M. Maurice. 2008. Differential solubilization of inner plasma membrane leaflet components by Lubrol WX and Triton X-100. *Biochim Biophys Acta*. 1778:105-112.

Denny, P.W., S. Gokool, D.G. Russell, M.C. Field, and D.F. Smith. 2000. Acylation-dependent protein export in *Leishmania*. *J Biol Chem*. 275:11017-11025.

Dietrich, C., L.A. Bagatolli, Z.N. Volovyk, N.L. Thompson, M. Levi, K. Jacobson, and E. Gratton. 2001a. Lipid rafts reconstituted in model membranes. *Biophys J*. 80:1417-1428.

Dietrich, C., Z.N. Volovyk, M. Levi, N.L. Thompson, and K. Jacobson. 2001b. Partitioning of Thy-1, GM1, and cross-linked phospholipid analogs into lipid rafts reconstituted in supported model membrane monolayers. *Proc Natl Acad Sci U S A*. 98:10642-10647.

Donaldson, J.G., and C.L. Jackson. 2011. ARF family G proteins and their regulators: roles in membrane transport, development and disease. *Nat Rev Mol Cell Biol*. 12:362-375.

Donaldson, J.G., R.A. Kahn, J. Lippincott-Schwartz, and R.D. Klausner. 1991. Binding of ARF and beta-COP to Golgi membranes: possible regulation by a trimeric G protein. *Science*. 254:1197-1199.

Donaldson, J.G., J. Lippincott-Schwartz, G.S. Bloom, T.E. Kreis, and R.D. Klausner. 1990. Dissociation of a 110-kD peripheral membrane protein from the Golgi apparatus is an early event in brefeldin A action. *J Cell Biol*. 111:2295-2306.

Duden, R. 2003. ER-to-Golgi transport: COP I and COP II function. *Mol Membr Biol*. 20:197-207.

Duncan, J.A., and A.G. Gilman. 1998. A cytoplasmic acyl-protein thioesterase that removes palmitate from G protein alpha subunits and p21(RAS). *J Biol Chem*. 273:15830-15837.

Elazar, Z., L. Orci, J. Ostermann, M. Amherdt, G. Tanigawa, and J.E. Rothman. 1994. ADP-ribosylation factor and coatomer couple fusion to vesicle budding. *J Cell Biol*. 124:415-424.

Farazi, T.A., G. Waksman, and J.I. Gordon. 2001. The biology and enzymology of protein N-myristoylation. *J Biol Chem*. 276:39501-39504.

Ferrell, J.E., Jr., J.A. Noble, G.S. Martin, Y.V. Jacques, and D.F. Bainton. 1990. Intracellular localization of pp60c-src in human platelets. *Oncogene*. 5:1033-1036.

Fishburn, C.S., P. Herzmark, J. Morales, and H.R. Bourne. 1999. Gbetagamma and palmitate target newly synthesized Galphaz to the plasma membrane. *J Biol Chem*. 274:18793-18800.

Flinn, H.M., D. Rangarajan, and D.F. Smith. 1994. Expression of a hydrophilic surface protein in infective stages of *Leishmania major*. *Mol Biochem Parasitol*. 65:259-270.

Fölsch, H. 2008. Regulation of membrane trafficking in polarized epithelial cells. *Curr Opin Cell Biol*. 20:208-213.

Foster, L.J., C.L. De Hoog, and M. Mann. 2003. Unbiased quantitative proteomics of lipid rafts reveals high specificity for signaling factors. *Proc Natl Acad Sci U S A*. 100:5813-5818.

Fujita, M., and T. Kinoshita. 2010. Structural remodeling of GPI anchors during biosynthesis and after attachment to proteins. *FEBS Lett*. 584:1670-1677.

Galbiati, F., F. Guzzi, A.I. Magee, G. Milligan, and M. Parenti. 1994. N-terminal fatty acylation of the alpha-subunit of the G-protein Gi1: only the myristoylated protein is a substrate for palmitoylation. *Biochem J*. 303 (Pt 3):697-700.

Gauld, S.B., and J.C. Cambier. 2004. Src-family kinases in B-cell development and signaling. *Oncogene*. 23:8001-8006.

Gerber, L.D., K. Kodukula, and S. Udenfriend. 1992. Phosphatidylinositol glycan (PI-G) anchored membrane proteins. Amino acid requirements adjacent to the site of cleavage and PI-G attachment in the COOH-terminal signal peptide. *J Biol Chem*. 267:12168-12173.

Glaichenhaus, N., N. Shastri, D.R. Littman, and J.M. Turner. 1991. Requirement for association of p56lck with CD4 in antigen-specific signal transduction in T cells. *Cell*. 64:511-520.

Glick, B.S., and V. Malhotra. 1998. The curious status of the Golgi apparatus. *Cell*. 95:883-889.

Goldberg, J. 1998. Structural basis for activation of ARF GTPase: mechanisms of guanine nucleotide exchange and GTP-myristoyl switching. *Cell*. 95:237-248.

Greaves, J., and L.H. Chamberlain. 2007. Palmitoylation-dependent protein sorting. *J Cell Biol*. 176:249-254.

Greaves, J., and L.H. Chamberlain. 2011. DHHC palmitoyl transferases: substrate interactions and (patho)physiology. *Trends Biochem Sci*. 36:245-253.

Griffiths, G., and K. Simons. 1986. The *trans* Golgi network: sorting at the exit site of the Golgi complex. *Science*. 234:438-443.

Guo, Y., V. Punj, D. Sengupta, and A.D. Linstedt. 2008. Coat-tether interaction in Golgi organization. *Mol Biol Cell*. 19:2830-2843.

Haag, M. 2010. Development of mass spectrometric methods for the quantification of membrane lipids - studies on mitochondria, T Cells, Golgi membranes and COPI vesicles. PhD thesis. University of Heidelberg.

Hagmann, J., and P.H. Fishman. 1982. Detergent extraction of cholera toxin and gangliosides from cultured cells and isolated membranes. *Biochim Biophys Acta*. 720:181-187.

Halic, M., and R. Beckmann. 2005. The signal recognition particle and its interactions during protein targeting. *Curr Opin Struct Biol*. 15:116-125.

Hancock, J.F., A.I. Magee, J.E. Childs, and C.J. Marshall. 1989. All ras proteins are polyisoprenylated but only some are palmitoylated. *Cell*. 57:1167-1177.

Harder, T., P. Scheiffele, P. Verkade, and K. Simons. 1998. Lipid domain structure of the plasma membrane revealed by patching of membrane components. *J Cell Biol*. 141:929-942.

Harder, T., and K. Simons. 1999. Clusters of glycolipid and glycosylphosphatidylinositol-anchored proteins in lymphoid cells: accumulation of actin regulated by local tyrosine phosphorylation. *Eur J Immunol*. 29:556-562.

Härri, E., W. Loeffler, H.P. Sigg, H. Stähelin, and Ch. Tamm. 1963. Über die Isolierung neuer Stoffwechselprodukte aus *Penicillium brefeldianum* DODGE. *Helv. Chim. Acta*. 46:1235-1243.

Hayashi, T., G. Rumbaugh, and R.L. Huganir. 2005. Differential regulation of AMPA receptor subunit trafficking by palmitoylation of two distinct sites. *Neuron*. 47:709-723.

Hermida-Matsumoto, L., and M.D. Resh. 1999. Human immunodeficiency virus type 1 protease triggers a myristoyl switch that modulates membrane binding of Pr55(gag) and p17MA. *J Virol*. 73:1902-1908.

Holthuis, J.C., and T.P. Levine. 2005. Lipid traffic: floppy drives and a superhighway. *Nat Rev Mol Cell Biol*. 6:209-220.

Hooper, N.M., and A.J. Turner. 1988. Ectoenzymes of the kidney microvillar membrane. Differential solubilization by detergents can predict a glycosyl-phosphatidylinositol membrane anchor. *Biochem J*. 250:865-869.

Hughes, H., and D.J. Stephens. 2008. Assembly, organization, and function of the COPII coat. *Histochem Cell Biol*. 129:129-151.

Ipsen, J.H., G. Karlstrom, O.G. Mouritsen, H. Wennerstrom, and M.J. Zuckermann. 1987. Phase equilibria in the phosphatidylcholine-cholesterol system. *Biochim Biophys Acta*. 905:162-172.

Ishihama, Y., Y. Oda, T. Tabata, T. Sato, T. Nagasu, J. Rappsilber, and M. Mann. 2005. Exponentially modified protein abundance index (emPAI) for estimation of absolute protein amount in proteomics by the number of sequenced peptides per protein. *Mol Cell Proteomics*. 4:1265-1272.

Jacob, R., M. Heine, J. Eikemeyer, N. Frerker, K.P. Zimmer, U. Rescher, V. Gerke, and H.Y. Naim. 2004. Annexin II is required for apical transport in polarized epithelial cells. *J Biol Chem*. 279:3680-3684.

Johnson, A.E., and M.A. van Waes. 1999. The translocon: a dynamic gateway at the ER membrane. *Annu Rev Cell Dev Biol*. 15:799-842.

Johnson, D.R., R.S. Bhatnagar, L.J. Knoll, and J.I. Gordon. 1994. Genetic and biochemical studies of protein N-myristoylation. *Annu Rev Biochem*. 63:869-914.

Johnson, S.A., B.M. Stinson, M.S. Go, L.M. Carmona, J.I. Reminick, X. Fang, and T. Baumgart. 2010. Temperature-dependent phase behavior and protein partitioning in giant plasma membrane vesicles. *Biochim Biophys Acta*. 1798:1427-1435.

Jungnickel, B., T.A. Rapoport, and E. Hartmann. 1994. Protein translocation: common themes from bacteria to man. *FEBS Lett*. 346:73-77.

Kabouridis, P.S., A.I. Magee, and S.C. Ley. 1997. S-acylation of LCK protein tyrosine kinase is essential for its signalling function in T lymphocytes. *EMBO J*. 16:4983-4998.

Kaplan, K.B., J.R. Swedlow, H.E. Varmus, and D.O. Morgan. 1992. Association of p60c-src with endosomal membranes in mammalian fibroblasts. *J Cell Biol*. 118:321-333.

Kasahara, K., Y. Nakayama, K. Ikeda, Y. Fukushima, D. Matsuda, S. Horimoto, and N. Yamaguchi. 2004. Trafficking of Lyn through the Golgi caveolin involves the charged residues on alphaE and alphaI helices in the kinase domain. *J Cell Biol*. 165:641-652.

Kasahara, K., Y. Nakayama, A. Kihara, D. Matsuda, K. Ikeda, T. Kuga, Y. Fukumoto, Y. Igarashi, and N. Yamaguchi. 2007. Rapid trafficking of c-Src, a non-palmitoylated Src-family kinase, between the plasma membrane and late endosomes/lysosomes. *Exp Cell Res*. 313:2651-2666.

Keller, A., A.I. Nesvizhskii, E. Kolker, and R. Aebersold. 2002. Empirical statistical model to estimate the accuracy of peptide identifications made by MS/MS and database search. *Anal Chem*. 74:5383-5392.

Keller, P., D. Toomre, E. Diaz, J. White, and K. Simons. 2001. Multicolour imaging of post-Golgi sorting and trafficking in live cells. *Nat Cell Biol*. 3:140-149.

Khan, T.K., B. Yang, N.L. Thompson, S. Maekawa, R.M. Epand, and K. Jacobson. 2003. Binding of NAP-22, a calmodulin-binding neuronal protein, to raft-like domains in model membranes. *Biochemistry*. 42:4780-4786.

Kiessling, V., J.M. Crane, and L.K. Tamm. 2006. Transbilayer effects of raft-like lipid domains in asymmetric planar bilayers measured by single molecule tracking. *Biophys J*. 91:3313-3326.

Klausner, R.D., J.G. Donaldson, and J. Lippincott-Schwartz. 1992. Brefeldin A: insights into the control of membrane traffic and organelle structure. *J Cell Biol*. 116:1071-1080.

Klemm, R.W., C.S. Ejsing, M.A. Surma, H.J. Kaiser, M.J. Gerl, J.L. Sampaio, Q. de Robillard, C. Ferguson, T.J. Proszynski, A. Shevchenko, and K. Simons. 2009. Segregation of sphingolipids and sterols during formation of secretory vesicles at the *trans*-Golgi network. *J Cell Biol*. 185:601-612.

Klumperman, J. 2000. Transport between ER and Golgi. *Curr Opin Cell Biol*. 12:445-449.

Koegl, M., P. Zlatkine, S.C. Ley, S.A. Courtneidge, and A.I. Magee. 1994. Palmitoylation of multiple Src-family kinases at a homologous N-terminal motif. *Biochem J*. 303 (Pt 3):749-753.

Kornfeld, R., and S. Kornfeld. 1985. Assembly of asparagine-linked oligosaccharides. *Annu Rev Biochem*. 54:631-664.

Ladinsky, M.S., and K.E. Howell. 1992. The *trans*-Golgi network can be dissected structurally and functionally from the cisternae of the Golgi complex by brefeldin A. *Eur J Cell Biol*. 59:92-105.

Laemmli, U.K. 1970. Cleavage of structural proteins during the assembly of the head of bacteriophage T4. *Nature*. 227:680-685.

Lafont, F., S. Lecat, P. Verkade, and K. Simons. 1998. Annexin XIIIb associates with lipid microdomains to function in apical delivery. *J Cell Biol*. 142:1413-1427.

Ledesma, M.D., K. Simons, and C.G. Dotti. 1998. Neuronal polarity: essential role of protein-lipid complexes in axonal sorting. *Proc Natl Acad Sci U S A*. 95:3966-3971.

Lee, M.C., E.A. Miller, J. Goldberg, L. Orci, and R. Schekman. 2004. Bi-directional protein transport between the ER and Golgi. *Annu Rev Cell Dev Biol*. 20:87-123.

Levental, I., M. Grzybek, and K. Simons. 2010a. Greasing their way: lipid modifications determine protein association with membrane rafts. *Biochemistry*. 49:6305-6316.

Levental, I., D. Lingwood, M. Grzybek, U. Coskun, and K. Simons. 2010b. Palmitoylation regulates raft affinity for the majority of integral raft proteins. *Proc Natl Acad Sci U S A*. 107:22050-22054.

Linder, M.E., and R.J. Deschenes. 2007. Palmitoylation: policing protein stability and traffic. *Nat Rev Mol Cell Biol*. 8:74-84.

Linder, M.E., P. Middleton, J.R. Hepler, R. Taussig, A.G. Gilman, and S.M. Mumby. 1993. Lipid modifications of G proteins: alpha subunits are palmitoylated. *Proc Natl Acad Sci U S A*. 90:3675-3679.

Lingwood, D., J. Ries, P. Schwille, and K. Simons. 2008. Plasma membranes are poised for activation of raft phase coalescence at physiological temperature. *Proc Natl Acad Sci U S A*. 105:10005-10010.

Lippincott-Schwartz, J., L. Yuan, C. Tipper, M. Amherdt, L. Orci, and R.D. Klausner. 1991. Brefeldin A's effects on endosomes, lysosomes, and the TGN suggest a general mechanism for regulating organelle structure and membrane traffic. *Cell*. 67:601-616.

Lippincott-Schwartz, J., L.C. Yuan, J.S. Bonifacino, and R.D. Klausner. 1989. Rapid redistribution of Golgi proteins into the ER in cells treated with brefeldin A: evidence for membrane cycling from Golgi to ER. *Cell*. 56:801-813.

Lisanti, M.P., I.W. Caras, M.A. Davitz, and E. Rodriguez-Boulan. 1989. A glycophospholipid membrane anchor acts as an apical targeting signal in polarized epithelial cells. *J Cell Biol*. 109:2145-2156.

London, E., and D.A. Brown. 2000. Insolubility of lipids in triton X-100: physical origin and relationship to sphingolipid/cholesterol membrane domains (rafts). *Biochim Biophys Acta*. 1508:182-195.

Lorizate, M., T. Sachsenheimer, B. Glass, A. Habermann, M.J. Gerl, H.G. Krausslich, and B. Brügger. 2013. Comparative lipidomics analysis of HIV-1 particles and their producer cell membrane in different cell lines. *Cell Microbiol*. 15:292-304.

Malsam, J., D. Gommel, F.T. Wieland, and W. Nickel. 1999. A role for ADP ribosylation factor in the control of cargo uptake during COPI-coated vesicle biogenesis. *FEBS Lett*. 462:267-272.

Marrari, Y., M. Crouthamel, R. Irannejad, and P.B. Wedegaertner. 2007. Assembly and trafficking of heterotrimeric G proteins. *Biochemistry*. 46:7665-7677.

McCabe, J.B., and L.G. Berthiaume. 1999. Functional roles for fatty acylated amino-terminal domains in subcellular localization. *Mol Biol Cell*. 10:3771-3786.

McConville, M.J., and M.A. Ferguson. 1993. The structure, biosynthesis and function of glycosylated phosphatidylinositols in the parasitic protozoa and higher eukaryotes. *Biochem J*. 294 (Pt 2):305-324.

Melkonian, K.A., A.G. Ostermeyer, J.Z. Chen, M.G. Roth, and D.A. Brown. 1999. Role of lipid modifications in targeting proteins to detergent-resistant membrane rafts. Many raft proteins are acylated, while few are prenylated. *J Biol Chem*. 274:3910-3917.

Mellman, I., and G. Warren. 2000. The road taken: past and future foundations of membrane traffic. *Cell*. 100:99-112.

Miller, J.D., H. Wilhelm, L. Gierasch, R. Gilmore, and P. Walter. 1993. GTP binding and hydrolysis by the signal recognition particle during initiation of protein translocation. *Nature*. 366:351-354.

Miller, S.G., L. Carnell, and H.H. Moore. 1992. Post-Golgi membrane traffic: brefeldin A inhibits export from distal Golgi compartments to the cell surface but not recycling. *J Cell Biol*. 118:267-283.

Mishra, R., M. Grzybek, T. Niki, M. Hirashima, and K. Simons. 2010. Galectin-9 trafficking regulates apical-basal polarity in Madin-Darby canine kidney epithelial cells. *Proc Natl Acad Sci U S A*. 107:17633-17638.

Misumi, Y., K. Miki, A. Takatsuki, G. Tamura, and Y. Ikehara. 1986. Novel blockade by brefeldin A of intracellular transport of secretory proteins in cultured rat hepatocytes. *J Biol Chem*. 261:11398-11403.

Moffett, S., D.A. Brown, and M.E. Linder. 2000. Lipid-dependent targeting of G proteins into rafts. *J Biol Chem*. 275:2191-2198.

Mumby, S.M., C. Kleuss, and A.G. Gilman. 1994. Receptor regulation of G-protein palmitoylation. *Proc Natl Acad Sci U S A*. 91:2800-2804.

Müsch, A., H. Xu, D. Shields, and E. Rodriguez-Boulan. 1996. Transport of vesicular stomatitis virus G protein to the cell surface is signal mediated in polarized and nonpolarized cells. *J Cell Biol*. 133:543-558.

Nadolski, M.J., and M.E. Linder. 2009. Molecular recognition of the palmitoylation substrate Vac8 by its palmitoyltransferase Pfa3. *J Biol Chem*. 284:17720-17730.

Nesvizhskii, A.I., A. Keller, E. Kolker, and R. Aebersold. 2003. A statistical model for identifying proteins by tandem mass spectrometry. *Anal Chem*. 75:4646-4658.

Ohno, Y., A. Kihara, T. Sano, and Y. Igarashi. 2006. Intracellular localization and tissue-specific distribution of human and yeast DHHC cysteine-rich domain-containing proteins. *Biochim Biophys Acta*. 1761:474-483.

Orci, L., M. Stamnes, M. Ravazzola, M. Amherdt, A. Perrelet, T.H. Sollner, and J.E. Rothman. 1997. Bidirectional transport by distinct populations of COPI-coated vesicles. *Cell*. 90:335-349.

Paige, L.A., M.J. Nadler, M.L. Harrison, J.M. Cassady, and R.L. Geahlen. 1993. Reversible palmitoylation of the protein-tyrosine kinase p56lck. *J Biol Chem*. 268:8669-8674.

Palmer, D.J., J.B. Helms, C.J. Beckers, L. Orci, and J.E. Rothman. 1993. Binding of coatomer to Golgi membranes requires ADP-ribosylation factor. *J Biol Chem*. 268:12083-12089.

Parenti, M., M.A. Vigano, C.M. Newman, G. Milligan, and A.I. Magee. 1993. A novel N-terminal motif for palmitoylation of G-protein alpha subunits. *Biochem J*. 291 (Pt 2):349-353.

Pepperkok, R., J.A. Whitney, M. Gomez, and T.E. Kreis. 2000. COPI vesicles accumulating in the presence of a GTP restricted arf1 mutant are depleted of anterograde and retrograde cargo. *J Cell Sci*. 113 (Pt 1):135-144.

Perkins, D.N., D.J. Pappin, D.M. Creasy, and J.S. Cottrell. 1999. Probability-based protein identification by searching sequence databases using mass spectrometry data. *Electrophoresis*. 20:3551-3567.

Petäjä-Repo, U.E., M. Hogue, T.T. Leskela, P.M. Markkanen, J.T. Tuusa, and M. Bouvier. 2006. Distinct subcellular localization for constitutive and agonist-modulated palmitoylation of the human delta opioid receptor. *J Biol Chem*. 281:15780-15789.

Peyroche, A., B. Antonny, S. Robineau, J. Acker, J. Cherfils, and C.L. Jackson. 1999. Brefeldin A acts to stabilize an abortive ARF-GDP-Sec7 domain protein complex: involvement of specific residues of the Sec7 domain. *Mol Cell*. 3:275-285.

Pike, L.J. 2006. Rafts defined: a report on the Keystone Symposium on Lipid Rafts and Cell Function. *J Lipid Res*. 47:1597-1598.

Pike, L.J., X. Han, and R.W. Gross. 2005. Epidermal growth factor receptors are localized to lipid rafts that contain a balance of inner and outer leaflet lipids: a shotgun lipidomics study. *J Biol Chem*. 280:26796-26804.

Popoff, V., F. Adolf, B. Brügger, and F. Wieland. 2011. COPI budding within the Golgi stack. *Cold Spring Harb Perspect Biol*. 3:a005231.

Prior, I.A., A. Harding, J. Yan, J. Sluimer, R.G. Parton, and J.F. Hancock. 2001. GTP-dependent segregation of H-ras from lipid rafts is required for biological activity. *Nat Cell Biol*. 3:368-375.

Putilina, T., P. Wong, and S. Gentleman. 1999. The DHHC domain: a new highly conserved cysteine-rich motif. *Mol Cell Biochem*. 195:219-226.

Rajendran, L., and K. Simons. 2005. Lipid rafts and membrane dynamics. *J Cell Sci*. 118:1099-1102.

Rapiejko, P.J., and R. Gilmore. 1992. Protein translocation across the ER requires a functional GTP binding site in the alpha subunit of the signal recognition particle receptor. *J Cell Biol*. 117:493-503.

Resh, M.D. 1993. Interaction of tyrosine kinase oncoproteins with cellular membranes. *Biochim Biophys Acta*. 1155:307-322.

Resh, M.D. 1994. Myristylation and palmitylation of Src family members: the fats of the matter. *Cell*. 76:411-413.

Resh, M.D. 1999. Fatty acylation of proteins: new insights into membrane targeting of myristoylated and palmitoylated proteins. *Biochim Biophys Acta*. 1451:1-16.

Resh, M.D. 2006. Palmitoylation of ligands, receptors, and intracellular signaling molecules. *Sci STKE*. 2006:re14.

Ritzerfeld, J. 2009. Identification of components of the intracellular transport machinery of acylated proteins by a genome-wide RNAi screen. PhD thesis. University of Heidelberg.

Ritzerfeld, J., S. Remmele, T. Wang, K. Temmerman, B. Brügger, S. Wegehingel, S. Tournaviti, J.R. Strating, F.T. Wieland, B. Neumann, J. Ellenberg, C. Lawerenz, J. Hesser, H. Erfle, R. Pepperkok, and W. Nickel. 2011. Phenotypic profiling of the human genome reveals gene products involved in plasma membrane targeting of SRC kinases. *Genome Res*. 21:1955-1968.

Robertson, J.D. 1981. Membrane structure. *J Cell Biol*. 91:189s-204s.

Rocks, O., M. Gerauer, N. Vartak, S. Koch, Z.P. Huang, M. Pechlivanis, J. Kuhlmann, L. Brunsveld, A. Chandra, B. Ellinger, H. Waldmann, and P.I. Bastiaens. 2010. The palmitoylation machinery is a spatially organizing system for peripheral membrane proteins. *Cell*. 141:458-471.

Rocks, O., A. Peyker, M. Kahms, P.J. Verveer, C. Koerner, M. Lumbierres, J. Kuhlmann, H. Waldmann, A. Wittinghofer, and P.I. Bastiaens. 2005. An acylation cycle regulates localization and activity of palmitoylated Ras isoforms. *Science*. 307:1746-1752.

Romano, J.D., W.K. Schmidt, and S. Michaelis. 1998. The *Saccharomyces cerevisiae* prenylcysteine carboxyl methyltransferase Ste14p is in the endoplasmic reticulum membrane. *Mol Biol Cell*. 9:2231-2247.

Saitoh, A., H.W. Shin, A. Yamada, S. Waguri, and K. Nakayama. 2009. Three homologous ArfGAPs participate in coat protein I-mediated transport. *J Biol Chem*. 284:13948-13957.

Sato, I., Y. Obata, K. Kasahara, Y. Nakayama, Y. Fukumoto, T. Yamasaki, K.K. Yokoyama, T. Saito, and N. Yamaguchi. 2009. Differential trafficking of Src, Lyn, Yes and Fyn is specified by the state of palmitoylation in the SH4 domain. *J Cell Sci*. 122:965-975.

Schatz, G., and B. Dobberstein. 1996. Common principles of protein translocation across membranes. *Science*. 271:1519-1526.

Schmidt, W.K., A. Tam, K. Fujimura-Kamada, and S. Michaelis. 1998. Endoplasmic reticulum membrane localization of Rce1p and Ste24p, yeast proteases involved in carboxyl-terminal CAAX protein processing and amino-terminal a-factor cleavage. *Proc Natl Acad Sci U S A*. 95:11175-11180.

Schroeder, R., E. London, and D. Brown. 1994. Interactions between saturated acyl chains confer detergent resistance on lipids and glycosylphosphatidylinositol (GPI)-anchored proteins: GPI-anchored proteins in liposomes and cells show similar behavior. *Proc Natl Acad Sci U S A*. 91:12130-12134.

Schuck, S., M. Honsho, K. Ekroos, A. Shevchenko, and K. Simons. 2003. Resistance of cell membranes to different detergents. *Proc Natl Acad Sci U S A*. 100:5795-5800.

Schuck, S., and K. Simons. 2004. Polarized sorting in epithelial cells: raft clustering and the biogenesis of the apical membrane. *J Cell Sci*. 117:5955-5964.

Schuck, S., and K. Simons. 2006. Controversy fuels trafficking of GPI-anchored proteins. *J Cell Biol*. 172:963-965.

Sciaky, N., J. Presley, C. Smith, K.J. Zaal, N. Cole, J.E. Moreira, M. Terasaki, E. Siggia, and J. Lippincott-Schwartz. 1997. Golgi tubule traffic and the effects of brefeldin A visualized in living cells. *J Cell Biol*. 139:1137-1155.

Searle, B.C. 2010. Scaffold: a bioinformatic tool for validating MS/MS-based proteomic studies. *Proteomics*. 10:1265-1269.

Sevier, C.S., and C.A. Kaiser. 2002. Formation and transfer of disulphide bonds in living cells. *Nat Rev Mol Cell Biol*. 3:836-847.

Shahinian, S., and J.R. Silvius. 1995. Doubly-lipid-modified protein sequence motifs exhibit long-lived anchorage to lipid bilayer membranes. *Biochemistry*. 34:3813-3822.

Sharma, P., R. Varma, R.C. Sarasij, Ira, K. Gousset, G. Krishnamoorthy, M. Rao, and S. Mayor. 2004. Nanoscale organization of multiple GPI-anchored proteins in living cell membranes. *Cell*. 116:577-589.

Shenoy-Scaria, A.M., D.J. Dietzen, J. Kwong, D.C. Link, and D.M. Lublin. 1994. Cysteine3 of Src family protein tyrosine kinase determines palmitoylation and localization in caveolae. *J Cell Biol*. 126:353-363.

Shenoy-Scaria, A.M., L.K. Gauen, J. Kwong, A.S. Shaw, and D.M. Lublin. 1993. Palmitylation of an amino-terminal cysteine motif of protein tyrosine kinases p56lck and p59fyn mediates interaction with glycosyl-phosphatidylinositol-anchored proteins. *Mol Cell Biol*. 13:6385-6392.

Sicheri, F., I. Moarefi, and J. Kuriyan. 1997. Crystal structure of the Src family tyrosine kinase Hck. *Nature*. 385:602-609.

Sigal, C.T., W. Zhou, C.A. Buser, S. McLaughlin, and M.D. Resh. 1994. Amino-terminal basic residues of Src mediate membrane binding through electrostatic interaction with acidic phospholipids. *Proc Natl Acad Sci U S A*. 91:12253-12257.

Silverman, L., M. Sudol, and M.D. Resh. 1993. Members of the src family of nonreceptor tyrosine kinases share a common mechanism for membrane binding. *Cell Growth Differ*. 4:475-482.

Simons, K., and M.J. Gerl. 2010. Revitalizing membrane rafts: new tools and insights. *Nat Rev Mol Cell Biol*. 11:688-699.

Simons, K., and E. Ikonen. 1997. Functional rafts in cell membranes. *Nature*. 387:569-572.

Simons, K., and G. van Meer. 1988. Lipid sorting in epithelial cells. *Biochemistry*. 27:6197-6202.

Simons, K., and W.L. Vaz. 2004. Model systems, lipid rafts, and cell membranes. *Annu Rev Biophys Biomol Struct*. 33:269-295.

Singer, S.J., and G.L. Nicolson. 1972. The fluid mosaic model of the structure of cell membranes. *Science*. 175:720-731.

Smotrys, J.E., and M.E. Linder. 2004. Palmitoylation of intracellular signaling proteins: regulation and function. *Annu Rev Biochem*. 73:559-587.

Sprong, H., P. van der Sluijs, and G. van Meer. 2001. How proteins move lipids and lipids move proteins. *Nat Rev Mol Cell Biol*. 2:504-513.

Stechly, L., W. Morelle, A.F. Dessein, S. Andre, G. Grard, D. Trinel, M.J. Dejonghe, E. Leteurtre, H. Drobecq, G. Trugnan, H.J. Gabius, and G. Huet. 2009. Galectin-4-regulated delivery of glycoproteins to the brush border membrane of enterocyte-like cells. *Traffic*. 10:438-450.

Stegmayer, C., A. Kehlenbach, S. Tournaviti, S. Wegehingel, C. Zehe, P. Denny, D.F. Smith, B. Schwappach, and W. Nickel. 2005. Direct transport across the plasma membrane of mammalian cells of *Leishmania* HASPB as revealed by a CHO export mutant. *J Cell Sci*. 118:517-527.

Straus, D.B., and A. Weiss. 1992. Genetic evidence for the involvement of the lck tyrosine kinase in signal transduction through the T cell antigen receptor. *Cell*. 70:585-593.

Styers, M.L., A.K. O'Connor, R. Grabski, E. Cormet-Boyaka, and E. Sztul. 2008. Depletion of beta-COP reveals a role for COP-I in compartmentalization of secretory compartments and in biosynthetic transport of caveolin-1. *Am J Physiol Cell Physiol*. 294:C1485-1498.

Tanigawa, G., L. Orci, M. Amherdt, M. Ravazzola, J.B. Helms, and J.E. Rothman. 1993. Hydrolysis of bound GTP by ARF protein triggers uncoating of Golgi-derived COP-coated vesicles. *J Cell Biol*. 123:1365-1371.

Taniguchi, H., and S. Manenti. 1993. Interaction of myristoylated alanine-rich protein kinase C substrate (MARCKS) with membrane phospholipids. *J Biol Chem*. 268:9960-9963.

Teal, S.B., V.W. Hsu, P.J. Peters, R.D. Klausner, and J.G. Donaldson. 1994. An activating mutation in ARF1 stabilizes coatomer binding to Golgi membranes. *J Biol Chem*. 269:3135-3138.

Thomas, S.M., and J.S. Brugge. 1997. Cellular functions regulated by Src family kinases. *Annu Rev Cell Dev Biol*. 13:513-609.

Tisdale, E.J., J.R. Bourne, R. Khosravi-Far, C.J. Der, and W.E. Balch. 1992. GTP-binding mutants of rab1 and rab2 are potent inhibitors of vesicular transport from the endoplasmic reticulum to the Golgi complex. *J Cell Biol*. 119:749-761.

Tournaviti, S., S. Hannemann, S. Terjung, T.M. Kitzing, C. Stegmayer, J. Ritzerfeld, P. Walther, R. Grosse, W. Nickel, and O.T. Fackler. 2007. SH4-domain-induced plasma membrane dynamization promotes bleb-associated cell motility. *J Cell Sci*. 120:3820-3829.

Tournaviti, S., E.S. Pietro, S. Terjung, T. Schafmeier, S. Wegehingel, J. Ritzerfeld, J. Schulz, D.F. Smith, R. Pepperkok, and W. Nickel. 2009. Reversible phosphorylation as a molecular switch to regulate plasma membrane targeting of acylated SH4 domain proteins. *Traffic*. 10:1047-1060.

Turner, J.M., M.H. Brodsky, B.A. Irving, S.D. Levin, R.M. Perlmutter, and D.R. Littman. 1990. Interaction of the unique N-terminal region of tyrosine kinase p56lck with cytoplasmic domains of CD4 and CD8 is mediated by cysteine motifs. *Cell*. 60:755-765.

Valdez-Taubas, J., and H. Pelham. 2005. Swf1-dependent palmitoylation of the SNARE Tlg1 prevents its ubiquitination and degradation. *EMBO J*. 24:2524-2532.

van't Hof, W., and M.D. Resh. 1997. Rapid plasma membrane anchoring of newly synthesized p59fyn: selective requirement for NH2-terminal myristoylation and palmitoylation at cysteine-3. *J Cell Biol*. 136:1023-1035.

Vidugiriene, J., and A.K. Menon. 1993. Early lipid intermediates in glycosyl-phosphatidylinositol anchor assembly are synthesized in the ER and located in the cytoplasmic leaflet of the ER membrane bilayer. *J Cell Biol*. 121:987-996.

Vitetta, E.S., E.A. Boyse, and J.W. Uhr. 1973. Isolation and characterization of a molecular complex containing Thy-1 antigen from the surface of murine thymocytes and T cells. *Eur J Immunol*. 3:446-453.

Voyksner, R.D., and H. Lee. 1999. Investigating the use of an octupole ion guide for ion storage and high-pass mass filtering to improve the quantitative performance of electrospray ion trap mass spectrometry. *Rapid Commun Mass Spectrom*. 13:1427-1437.

Walter, P., and A.E. Johnson. 1994. Signal sequence recognition and protein targeting to the endoplasmic reticulum membrane. *Annu Rev Cell Biol*. 10:87-119.

Wang, T.Y., R. Leventis, and J.R. Silvius. 2001. Partitioning of lipidated peptide sequences into liquid-ordered lipid domains in model and biological membranes. *Biochemistry*. 40:13031-13040.

Wedegaertner, P.B., and H.R. Bourne. 1994. Activation and depalmitoylation of Gs alpha. *Cell*. 77:1063-1070.

Welker, R., M. Harris, B. Cardel, and H.G. Krausslich. 1998. Virion incorporation of human immunodeficiency virus type 1 Nef is mediated by a bipartite membrane-targeting signal: analysis of its role in enhancement of viral infectivity. *J Virol*. 72:8833-8840.

Wennerberg, K., K.L. Rossman, and C.J. Der. 2005. The Ras superfamily at a glance. *J Cell Sci*. 118:843-846.

Wilcox, C., J.S. Hu, and E.N. Olson. 1987. Acylation of proteins with myristic acid occurs cotranslationally. *Science*. 238:1275-1278.

Wolven, A., H. Okamura, Y. Rosenblatt, and M.D. Resh. 1997. Palmitoylation of p59fyn is reversible and sufficient for plasma membrane association. *Mol Biol Cell*. 8:1159-1173.

Xu, W., S.C. Harrison, and M.J. Eck. 1997. Three-dimensional structure of the tyrosine kinase c-Src. *Nature*. 385:595-602.

Yanai, A., K. Huang, R. Kang, R.R. Singaraja, P. Arstikaitis, L. Gan, P.C. Orban, A. Mullard, C.M. Cowan, L.A. Raymond, R.C. Drisdel, W.N. Green, B. Ravikumar, D.C. Rubinsztein, A. El-Husseini, and M.R. Hayden. 2006. Palmitoylation of huntingtin by HIP14 is essential for its trafficking and function. *Nat Neurosci*. 9:824-831.

Yeh, D.C., J.A. Duncan, S. Yamashita, and T. Michel. 1999. Depalmitoylation of endothelial nitric-oxide synthase by acyl-protein thioesterase 1 is potentiated by Ca^{2+}-calmodulin. *J Biol Chem*. 274:33148-33154.

Yoshimori, T., P. Keller, M.G. Roth, and K. Simons. 1996. Different biosynthetic transport routes to the plasma membrane in BHK and CHO cells. *J Cell Biol*. 133:247-256.

Yu, J., D.A. Fischman, and T.L. Steck. 1973. Selective solubilization of proteins and phospholipids from red blood cell membranes by nonionic detergents. *J Supramol Struct*. 1:233-248.

Zacharias, D.A., J.D. Violin, A.C. Newton, and R.Y. Tsien. 2002. Partitioning of lipid-modified monomeric GFPs into membrane microdomains of live cells. *Science*. 296:913-916.

Zamoyska, R., P. Derham, S.D. Gorman, P. von Hoegen, J.B. Bolen, A. Veillette, and J.R. Parnes. 1989. Inability of CD8 alpha' polypeptides to associate with p56lck correlates with impaired function in vitro and lack of expression in vivo. *Nature*. 342:278-281.

Zapun, A., C.A. Jakob, D.Y. Thomas, and J.J. Bergeron. 1999. Protein folding in a specialized compartment: the endoplasmic reticulum. *Structure*. 7:R173-182.

Zhang, C.J., A.G. Rosenwald, M.C. Willingham, S. Skuntz, J. Clark, and R.A. Kahn. 1994. Expression of a dominant allele of human ARF1 inhibits membrane traffic in vivo. *J Cell Biol*. 124:289-300.

Zhang, G., B.M. Ueberheide, S. Waldemarson, S. Myung, K. Molloy, J. Eriksson, B.T. Chait, T.A. Neubert, and D. Fenyo. 2010. Protein quantitation using mass spectrometry. *Methods Mol Biol*. 673:211-222.

Zhao, X., T.K. Lasell, and P. Melancon. 2002. Localization of large ADP-ribosylation factor-guanine nucleotide exchange factors to different Golgi compartments: evidence for distinct functions in protein traffic. *Mol Biol Cell*. 13:119-133.

Zheng, J., D.R. Knighton, N.H. Xuong, S.S. Taylor, J.M. Sowadski, and L.F. Ten Eyck. 1993. Crystal structures of the myristylated catalytic subunit of cAMP-dependent protein kinase reveal open and closed conformations. *Protein Sci*. 2:1559-1573.

Zhou, W., L.J. Parent, J.W. Wills, and M.D. Resh. 1994. Identification of a membrane-binding domain within the amino-terminal region of human immunodeficiency virus type 1 Gag protein which interacts with acidic phospholipids. *J Virol*. 68:2556-2569.

Acknowledgements

I would like to express my gratitude to Prof. Dr. Walter Nickel for giving me the opportunity to perform my PhD work in his laboratory, for his patience and encouragement.

I want to thank Dr. Britta Brügger for performing lipid mass spectrometry and subsequent data analysis, and Iris Leibrecht for carrying out lipid extractions.

I would like to thank Dr. Thomas Ruppert and Sabine Merker from the ZMBH Core Facility for Mass Spectrometry and Proteomics for performing protein mass spectrometry.

I am grateful to Dr. Jacomine Krijnse-Locker and Brita Heck from the Electron Microscopy Core Facility for their invaluable assistance.

I would like to thank Prof. Dr. Thomas Söllner for being my second referee.

I am grateful to Dr. Vytaute Starkuviene-Erfle and Prof. Dr. Oliver Fackler for agreeing to be members of my examination committee.

I want to thank all current and former members of the Nickel laboratory for a pleasant and friendly working atmosphere: Helena Andreas, Eleni Dimou, Mareike Laußmann, Giuseppe La Venuta, Hans-Michael Müller, Julia Ritzerfeld, Christina Sendlmeier, Julia Steringer, Tao Wang, Sabine Wegehingel, Georg Weidmann, Sonja Zacherl and Marcel Zeitler. In particular, I would like to thank Julia Ritzerfeld for all her experimental help and Hans-Michael Müller for translating the summary of this thesis into German. A special thank goes to Tao Wang for all her help, support and friendship.

A great thank goes to Vedrana Mijošek for always being there for me, for her support and friendship, and for making my stay in Heidelberg so much more enjoyable.

I would like to thank Simeon Simeonov for all his optimism, encouragement and understanding.

And lastly but most importantly, I would like to thank my family for all the care, love and support they have been giving me throughout all these years.